

The Messenger



No. 132 – June 2008

10th anniversary of VLT First Light
The ground layer seeing on Paranal
HAWK-I Science Verification
The emission nebula around Antares



The Perfect Machine

Tim de Zeeuw
(ESO Director General)

This issue of the Messenger marks the tenth anniversary of first light of the Very Large Telescope. It is an excellent occasion to look at the broader implications of the VLT's success and to consider the next steps.

Mission

ESO's mission is to enable scientific discoveries by constructing and operating powerful observational facilities that are beyond the capabilities of individual member states. This principle was understood right at the start in 1962, when Belgium, France, Germany, Sweden and the Netherlands created ESO (with Denmark joining in 1967) to build a large telescope in the South. The main motivation was the need to be able to compete scientifically with astronomers in California who had access to large private telescopes, most notably the 5-m Hale telescope on Mount Palomar, known as the 'Big Eye', and considered by many to be 'The Perfect Machine' of its time. In the United States of America, the same motivation had already led in 1957 to the creation of AURA, the Association of Universities for Research in Astronomy, which resulted in the Kitt Peak and Cerro Tololo Observatories, each including a 4-m telescope and supported by the National Science Foundation. In Europe the ESO mission resulted in the construction of the La Silla Observatory north of La Serena in Chile, operating a fleet of telescopes, with the 3.6-m as flagship.

The Very Large Telescope

By the early 1980's there were half-a-dozen observatories with 4-m-class telescopes available to astronomers worldwide, La Silla being one of them. Plans were being drawn-up to construct much more powerful telescopes with primary mirrors in the 8–10-m range. The Keck Foundation enabled the California Institute of Technology and the University of California to build twin 10-m telescopes on Mauna Kea, obtaining first light in the early nineties, providing, in particular,

a ground-based spectroscopic complement to the Hubble Space Telescope. Italy and Switzerland had joined ESO in 1981, enabling the construction of the 3.5-m New Technology Telescope with pioneering advances in active optics, crucial for the next step: the construction of the Very Large Telescope, which received the green light from Council in 1987 and was built on Cerro Paranal in the Atacama desert between Antofagasta and Taltal in Northern Chile. The 8.1-m Gemini telescopes and the 8.3-m Subaru telescope were constructed on a similar time scale, while the Large Binocular Telescope and the Gran Telescopio Canarias are now starting operations.

The VLT was designed from the start as an integrated system of four 8.2-m telescopes, including the possibility to combine the light from individual telescopes for optical interferometry, enabling stupendous spatial resolution. First light on Antu occurred in May 1998, with Kueyen, Melipal and Yepun following soon after. Most of the VLT and VLTI instruments were built in close collaboration with institutes in the member states. The entire first-generation instrument suite was completed in 2007 with the commissioning of CRIRES. The Paranal arsenal includes turnkey adaptive optics systems and a rapid-response mode to react to fast transient events. Recently, the near-infrared imager HAWK-I was added as a 'generation-1.5' instrument.

The VLT and VLTI have contributed to all areas of astronomy, including the nature of dark matter and dark energy, the extreme physics of gamma-ray bursts and supernovae, the formation, structure and evolution of galaxies, the properties of super-massive black holes in galactic nuclei, in particular the one in the Galactic Centre, of star clusters and stellar populations, of the interstellar and intergalactic medium, the formation of stars and planets, the properties of exoplanets, and of Solar System objects. The output in terms of refereed research papers was 469 in 2007 alone, bringing the total since first light to over 2200, with the annual rate still increasing.

The total number of observing proposals for ESO facilities has doubled in the past decade, and now approaches nearly a

thousand each semester, 800 of which are for Paranal. The User Portal has about 4000 registered users and the archive contains 74 TB of data and advanced data products.

Winning strategy

The VLT opened for business some five years after the Keck telescopes, but the decision to take the time to build a fully integrated system, consisting of four 8.2-m telescopes and providing a dozen foci for a carefully thought-out complement of instruments together with four 1.8-m Auxiliary Telescopes for the interferometer, was the right one. The combination of a long-term adequately-funded instrument and technology development plan, with an approach where most of the instruments were built in collaboration with institutions in the member states, with in-kind contributions in labour compensated by guaranteed observing time, has created the most advanced ground-based optical observatory in the world. The operations model distinguishes visitor and service mode, and provides world-leading observing efficiency on a site where nearly 90% of the nights are clear. All of this was made possible by the motivation of ESO staff members to build, operate and support the best possible observatory. As a result, the VLT is arguably the natural successor of the 'Perfect Machine' on Mount Palomar. Our 2007 Visiting Committee, chaired by Professor Günther Hasinger, stated it thus: "ESO has become the premier observatory for optical-infrared astronomy on a worldwide basis."

The stunning scientific success of the VLT attracted new member states to ESO. In the past decade Portugal joined (after a ten-year associate status), followed by the United Kingdom, Finland, Spain and the Czech Republic. At the time of writing it looks likely that Austria will join later this year (see text of Press Release on page 5). These countries are drawn to ESO because of the unique observing opportunities and by the possibility to be involved in a coherent long-term programme involving the design, construction and operation of future world-class ground-based facilities for astronomy. As their annual contribution and entrance



The VLT as it is today with four Unit Telescopes and four Auxiliary Telescopes.

fee is added to ESO's income, the accession of new member states also enables new projects.

The next steps

The VLT will continue to increase in power over the next decade. X-Shooter will come on line this year, with KMOS, SPHERE and MUSE to follow, together with multiple laser guide stars, an adaptive secondary mirror on Yepun, and one or more third-generation instruments, including an ultra-stable high-resolution spectrograph at the combined focus (as foreseen in the original VLT design). The VLTI will be equipped with the second-generation instruments GRAVITY and MATISSE, to be followed by VSI, the latter perhaps with two additional Auxiliary Telescopes, if external funding can be found.

VISTA and the VST are expected to start regular operations next year with a five-year programme of coherent public surveys led by international teams. These surveys are performed together with data centres in the member states, coordinated by ESO. This collaboration builds a European survey capability which will deliver eminent science, provides crucial ground-based data in support of future space missions, and prepares the way for the next step in surveys.

The Atacama Large Millimeter/submillimeter Array is being constructed at

5 050-m altitude on Chajnantor east of San Pedro de Atacama in northern Chile. ALMA evolved from separate regional plans to a global partnership between Europe, North America (USA and Canada) and East Asia (Japan and Taiwan), with ESO representing Europe. Participation in ALMA expands ESO's activities into a wavelength regime often associated with radio astronomy. The first step has already been taken: ESO operates APEX, a single-dish 12-m antenna for sub-millimetre astronomy located on Chajnantor, in a partnership with Sweden and the Max-Planck-Gesellschaft.

ALMA construction is well underway. ESO has delivered key components, including the Technical Building for the Observing Support Facility at 2 950 m, and two antenna transporters (see the article on page 23). Institutes in the member states are providing the Band 7 and Band 9 high-frequency receivers and front-end integration for the 66 ALMA antennas. The 25 12-m antennas to be delivered by European industry are behind schedule, with the first one arriving in Chile in the first half of 2009, where Japan and North America already have four antennas each at the OSF being readied for acceptance. The hope is that the schedule slip can be recovered through a speedy delivery of the later antennas. The creation of the ALMA European Regional Centre, with nodes in many of the member states, will help prepare the European astronomical community for leadership in ALMA sci-

ence exploitation, building on expertise with existing sub-millimetre telescopes, including APEX, and on science to be done with the 3.5-m Herschel Space Observatory, which ESA expects to launch in 2009.

The next world-class ground-based facility is the European Extremely Large Telescope for the visible/infrared wavelength regime. ESO is undertaking the design study, in close collaboration with industry and institutes in the member states. The baseline design consists of a 42-m segmented primary mirror, an innovative five-mirror design, and adaptive optics built into the telescope. The study draws on the entire expertise built up in ESO and the member states over the past decades, including lessons learned from ALMA construction. The aim is to be ready for a construction start in 2010, so that there is an opportunity for overlap with the James Webb Space Telescope, which is the next NASA/ESA/CSA flagship facility.

This combined programme is ambitious, but achievable by building on the 'VLT model' in which high-quality staff carries out a coherent programme in close collaboration with scientists and institutions in the member states, with long-term planning enabled by the security of an intergovernmental treaty.

ESO continues to attract and train high-quality staff both in Chile and in Garching. In the past eight months I spent a fair

amount of time at our sites in Chile, and after each visit I came away impressed by the dedication and motivation of our personnel in all areas of expertise. The same is true for our staff members in Garching, who provide general user support, develop critical software, coordinate the construction of new instrumentation, and follow developments in technology (both of which include in-house activities). The astronomers have a fraction of their time available for personal research, as this is

crucial for ESO's ability to deliver the best observing facilities for the member states.

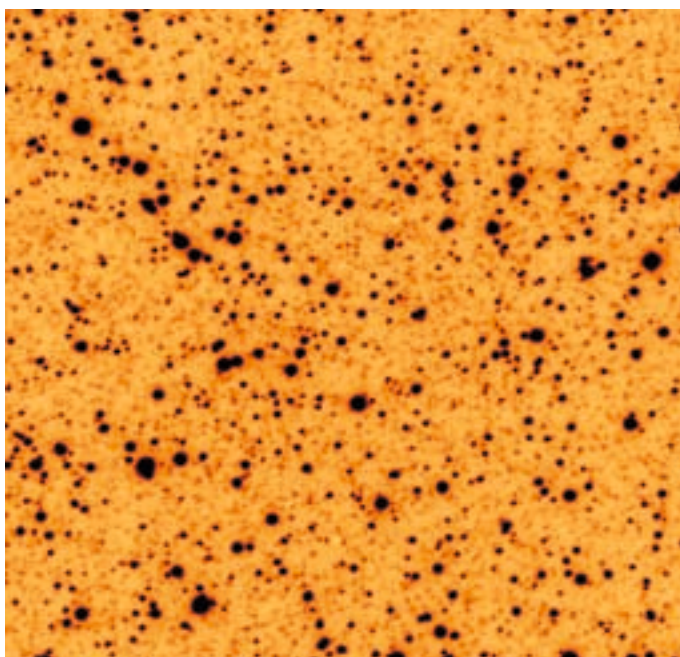
ESO's Fellowship programme deserves special mention. It also has grown over the past decade. A remarkable statistic is that 92 % of all former ESO Fellows are still active in astronomy, many in institutions in the member states. This strengthens the partnership between ESO and the member states in a natural way, contributing to the long-term success of the entire programme.

When the VLT turns 15 in five years time, the medium-sized telescopes on La Silla will be focused on unique long-term science, the VLT and VLTI will be nearing their full potential, and ALMA will be operational. If all goes well, the Extremely Large Telescope will be in construction, and ESO and the member states will already be planning for another world-class ground-based facility. This entire prospect is very exciting and I look forward to being a part of this.

10th Anniversary of First Light of the VLT

On 16 May 1998, 'First Light', in the sense of imaging with active optics and telescope tracking, was obtained with the VLT Test Camera for Unit Telescope 1. The First Light image, which originally appeared in *The Messenger*, No. 92 is reproduced here and shows a 10-min *R*-band image of the globular cluster Omega Centauri. The image was actually obtained before the mirror was coated but has measured image quality (Full Width at Half Maximum) of 0.43 arcsec. The accompanying photograph taken during that period shows the three key staff – Massimo Tarenghi, then director of the Paranal Observatory, Roberto Gilmozzi and Jason Spyromilio – in the VLT control room. All three are still with ESO: Massimo has been ALMA Director, Roberto succeeded Massimo as director of the Paranal Observatory and was himself succeeded by Jason. Both are now working on ESO's next large telescope project – the European Extremely Large Telescope (E-ELT). The understated sense of jubilation at the meeting of performance criteria is well caught in the quotation from the article "The First Steps of UT1" by Tarenghi, Gray, Spyromilio and Gilmozzi, which appeared in *The Messenger* No. 93, printed here.

To mark this anniversary a poster has been produced by the ESO Public Affairs Department (PAD) group and is enclosed with this issue.



VLT UT1 First Light image of Omega Centauri.



Massimo Tarenghi, Roberto Gilmozzi and Jason Spyromilio in the VLT control room in May 1998.

“Although first light was specified for the night of the 25th of May, the internal planning target date was the 15th of May. By this time we had moved out of the hut in the enclosure and were operating the telescope from the relative comfort of the control room. On the night of the 15th of May we decided that we should meet all specifications laid out in the integration plan for the telescope. The target was to be ω Cen. Conditions were excellent:

low wind and good seeing. We started a 10-minute exposure on target with the test camera. We had never tried anything as long as this. Krister Wirenstrand anxiously waited for the test camera CCD to read out. This was to be the first true image taken with the telescope on a scientific CCD. When the image was transferred to the Real Time Display, we quickly measured the image quality. Great jubilation again as the stars ap-

peared at 0.48 arcseconds. A series of other measurements on tracking stability and image quality verified the telescope had met all the performance criteria for first light.”

Tarengi, M., Gray, P., Spyromilio, J. & Gilmozzi, R. 1998, *The Messenger*, 93, 4

Austria Declares Intent to Join ESO

At a press conference held at the University of Vienna Observatory on 24 April 2008, the Austrian Science Minister Johannes Hahn announced the decision by the Austrian Government to seek membership of ESO from 1 July of this year.

Said Minister Hahn: “With membership of ESO, Austria’s scientists will receive direct access to the world’s leading infrastructure in astronomy. This strengthens Austria as a place for research and provides an opportunity for young researchers to continue their work from here. With this move, Austria takes an important step in the reinforcement of Europe’s science and research infrastructure.”

The ESO Director General Tim de Zeeuw responded: “ESO welcomes the Austrian bid to join our organisation. I salute the Austrian Government for taking this important step and look forward to working closely with our Austrian friends and colleagues in the years to come.”

The decision constitutes a major breakthrough for Austrian astronomers who have argued for joining ESO for many years. Membership would mean not only unrestricted access to ESO’s world-leading observational facilities, including the Very Large Telescope and full participation in the international ALMA project, but also the possibility to participate in future projects, including the realisation of the European Extremely Large Telescope (E-ELT), which is currently in its design phase.



All these projects require some of the most advanced technologies in key areas such as optics, detectors, lightweight structures, etc. Austrian participation in ESO opens the door for Austrian industry and major research institutes to take part in the development of such technologies, with their associated potential for industrial spin off.

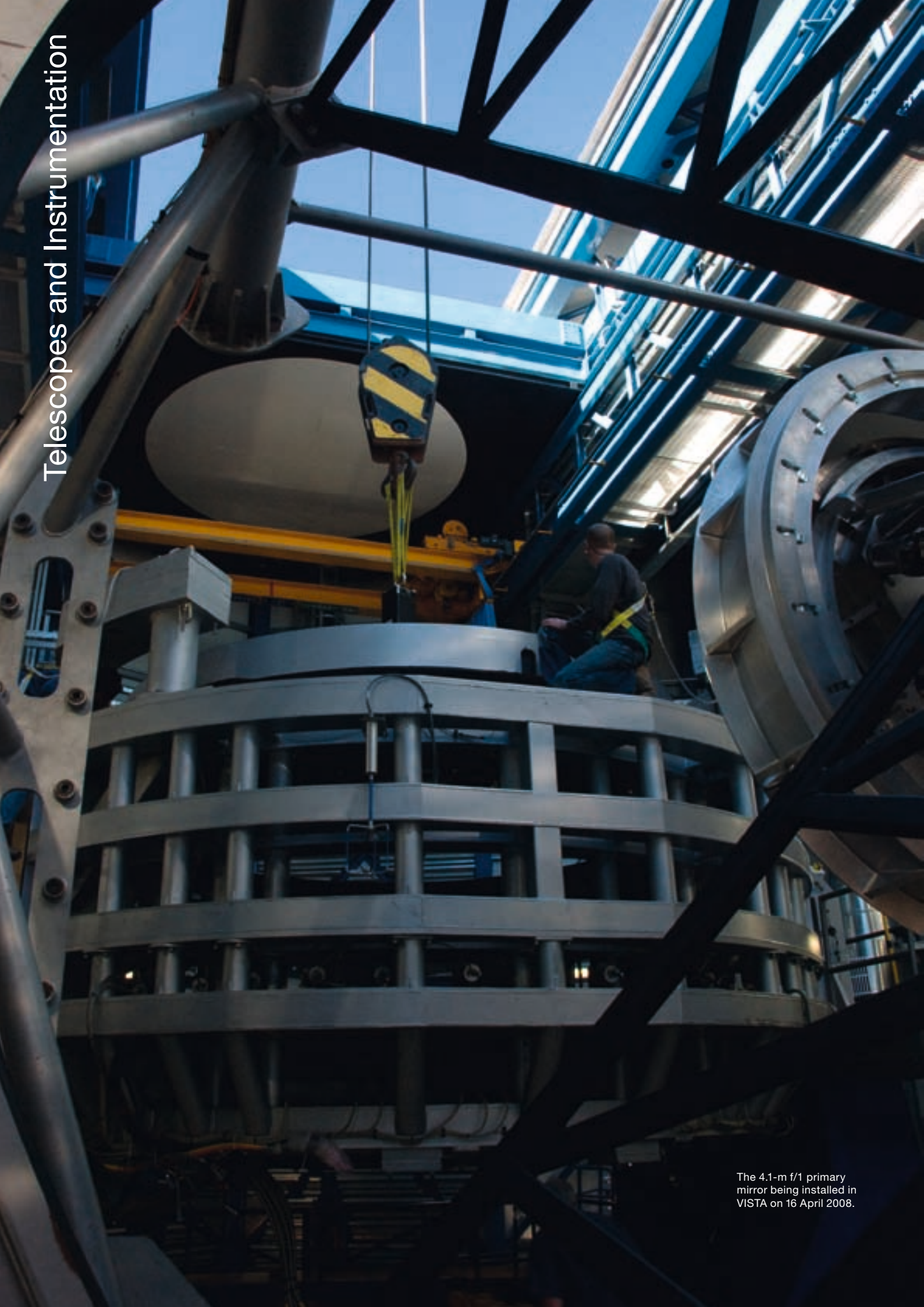
The main centres for astronomical research in Austria are at the Universities of Graz, Innsbruck and Vienna. Furthermore, scientists in the area of mathematics, applied physics and computer science have already expressed their

From left to right: Prof. Tim de Zeeuw, ESO Director General, Prof. Sabine Schindler, the President of the Austrian Society for Astronomy and Astrophysics, and Dr. Johannes Hahn, the Austrian Science Minister.

interest in contributing to the development of the advanced technologies required for ESO’s future projects.

The Austrian bid for ESO membership was formally approved by the ESO Council at its meeting on 3–4 June and is now subject to ratification by the Austrian Parliament.

(Adapted from ESO Press Release 11/08)



The 4.1-m f/1 primary mirror being installed in VISTA on 16 April 2008.

Hawk-I – First Results from Science Verification

Markus Kissler-Patig¹

Andrea Fontana²

Bram Venemans³

Jean-Paul Kneib⁴

Michelle Doherty¹

Christopher Lidman¹

Harald Kuntschner⁵

Mark Norris⁶

Soeren Larsen⁷

Mark Gieles¹

Alcione Mora Fernandes⁸

Mark McCaughrean⁹

Thomas Preibisch¹⁰

Andreas Seifahrt¹¹

Jon Willis¹²

Elizabeth Wehner¹³

¹ ESO

² INAF – Osservatorio Astronomico di Roma, Italy

³ Institute of Astronomy, University of Cambridge, United Kingdom

⁴ OAMP, Laboratoire d'Astrophysique de Marseille, France

⁵ ST-ECF, ESO

⁶ Department of Physics, University of Durham, United Kingdom

⁷ Astronomical Institute, University of Utrecht, the Netherlands

⁸ Departamento de Física Teórica C-XI, Universidad Autónoma de Madrid, Spain

⁹ School of Physics, University of Exeter, United Kingdom

¹⁰ Max-Planck-Institut für Radioastronomie, Bonn, Germany

¹¹ Institut für Astrophysik, Georg-August-Universität, Göttingen, Germany

¹² Department of Physics and Astronomy, University of Victoria, Canada

¹³ Department of Physics and Astronomy, McMaster University, Hamilton, Canada

The VLT wide-field near-infrared imager HAWK-I was commissioned in 2007 and Science Verification (SV) programmes were conducted in August 2007. A selection of results from among the twelve Science Verification proposals are summarised.

HAWK-I is the new wide-field infrared imager on the VLT. We reported previously in *The Messenger* on its capabilities (Casali et al., 2005) and refer to Kissler-Patig et al. (2008) for a recent description

of the instrument. Here we briefly describe a selection among the twelve accepted Science Verification programmes and highlight some of the first spectacular results in the areas of distant galaxies, clusters of galaxies, star clusters and star formation.

The science verification (SV) for HAWK-I was interleaved with the commissioning activities that took place in three runs between October 2007 and February 2008. The goal of SV was to demonstrate the capabilities of the new instrument in a wide variety of research fields. More details on SV, the selected programmes and all the data, together with a description of how they were acquired, can be found on the HAWK-I SV web pages (<http://www.eso.org/sci/activities/vltsv/hawkisv/>). HAWK-I was offered to the community in Period 81 for regular service and visitor mode observing.

Distant galaxies

HAWK-I observations in the GOODS-S field were designed to obtain a self-consistent sample of galaxies at redshift about 7, providing a new view on the Universe at the end of the epoch of re-ionisation. The extraordinary efficiency of HAWK-I was used to detect $z > 6.5$ candidates in the Y-filter (centred at $1.021 \mu\text{m}$) through an appropriate recasting of the Lyman-break technique: candidates are selected as “Z-drop”, i.e. their colours satisfy the following criteria: $(Z-Y) > 1.0 \text{ mag.}$ and $(Y-K) < 1.5 \text{ mag.}$ 333 frames

were obtained, for a grand total of 27 hours of integration. The final mosaic provides the deepest image ever obtained in the Y-band. Thanks also to the excellent image quality ($< 0.5''$), it enables the detection of galaxies as faint as $m(\text{AB}) = 26.8$. The preliminary photometric analysis has identified a set of 25 high-redshift candidates. Extensive simulations are underway to assess the completeness and reliability of the selected sample.

This programme was complemented by HAWK-I observations in the NB1060 filter as an alternative method to search for star-forming galaxies at $z = 7.7$, thus demonstrating the potential of HAWK-I in directly probing the epoch of re-ionisation. The SV observations alone will form a sufficiently complete dataset to put a constraint on the number of luminous star-forming galaxies at $z = 7.7$. Preliminary analysis of 8.3 hours of narrowband data indicates that HAWK-I is capable of reaching a limiting depth of $7.5 \times 10^{-18} \text{ erg s}^{-1} \text{ cm}^{-2} \text{ arcsec}^{-2}$ (5 sigma). By measuring the colours of the candidate line emitters in the available HST/ACS images of the field, the line which has caused the narrowband excess can be determined. Figure 1 shows a colour-magnitude diagram of detected sources and an example image of a low-redshift emission-line galaxy.

A programme with similar aims, but using a different technique, aimed at detecting high-redshift ($z \sim 7.7$) Ly- α emitters amplified by the strong lensing of a massive

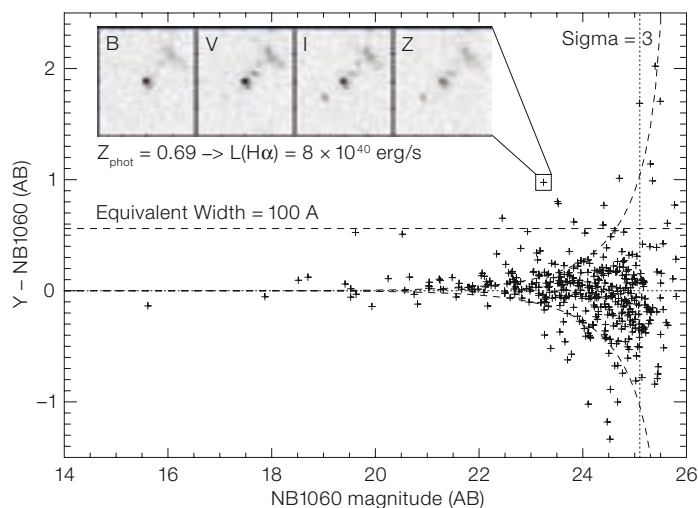


Figure 1. Colour-magnitude diagram showing objects detected in one of the four HAWK-I chips. Candidate emission-line galaxies are objects with a significant flux excess in the narrow-band filter. The inset shows ACS images of an example low-redshift line emitter, detected through H α redshifted to $z = 0.69$.

cluster. The massive cluster MS0451-03 was observed with the NB1060 filter of HAWK-I. The magnification of background galaxies ranges from 0.3 to 3 mag. The NB image provides an effective test for the presence of gravitationally lensed $z \sim 7.7$ galaxies. Many interloping $z < 7$ galaxies are detected in this image and will be of wider interest for follow-up studies.

Galaxy clusters

There is now strong evidence that galaxy evolution is closely linked to environment and that the oldest, reddest galaxies locally are found in large clusters. Hence to study the early stages of galaxy evolution we need to study the highest redshift (proto-)clusters. The number of these currently known is small but one of the most promising ways to locate them is by characterising the environment of high-redshift radio galaxies which lie at the centres of proto-clusters. HAWK-I was used to image the radio galaxy MRC0030-219 at $z = 2.168$ in the J -, K - and NB1190-filters (see Figure 2 for the K -band image). At this redshift the narrowband filter traces [OII] 3727 Å emission: the aim is to search for an overdensity of star-forming galaxies and at the same time for redder, evolved galaxies using $J-K$ colours. Initial analysis seems to indicate no evidence for an over-density but this is still to be verified. If true, it will allow interesting limits to be placed on the properties of a radio galaxy required for a forming proto-cluster.

A ubiquitous feature in rich galaxy clusters at all redshifts is the tight sequence of red, passively-evolving early-type galaxies in the colour-magnitude diagram. HAWK-I is well suited for studying the formation of the red sequence and of rich galaxy clusters in general, since such clusters form over regions that are several Mpc in size. In the concordance cosmology, 5 Mpc corresponds to $10'$ on the sky at a redshift of 1.5. The aim of this SV programme was to image the galaxy cluster XMMU J2235.3-2557 at $z = 1.39$, one of the most distant X-ray luminous clusters known. The resulting images were superb (see Figure 3). In K_s , the image quality of the final stack reached $0.32''$, and, in some of the individual im-

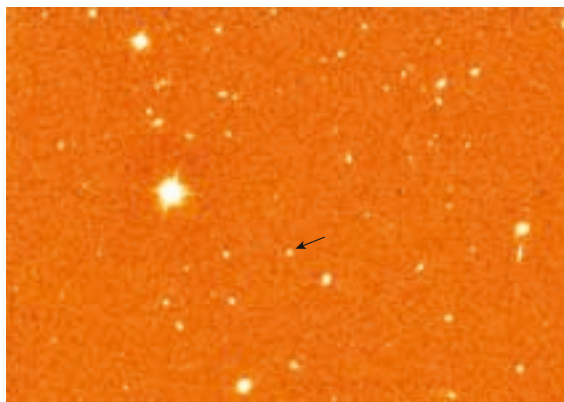


Figure 2. A $\sim 2.5' \times 2'$ section of a HAWK-I K_s -band image containing the radio galaxy MRC0030-219, which is marked with an arrow.

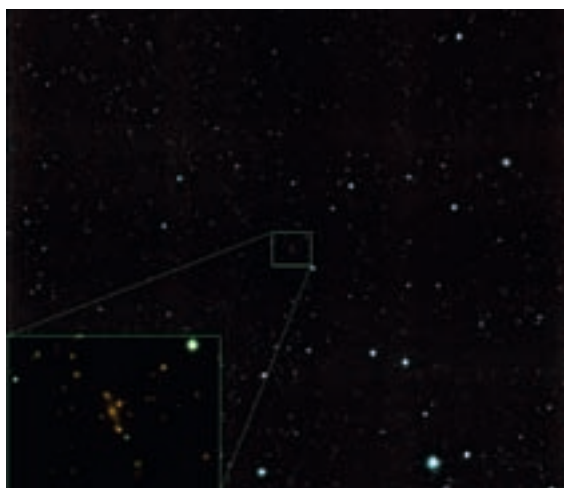


Figure 3. Colour composite of four HAWK-I pointings in both J and K_s , covering $13.5'$ on a side, of the galaxy cluster XMMU J2235.3-2557. The cluster is in the middle of the frame and a blow-up centred on the cluster is shown in the inset. The centre of XMMU J2235.3-2557 is dominated by red galaxies with very similar colours.

ages, the image quality reached $0.2''$, which approaches that obtainable with NICMOS on HST, but with the advantage of a much larger field of view.

Star clusters

Globular clusters provide important tools to distinguish between competing models for the formation of their host galaxies. The combination of optical and IR photometry is a very powerful tool to investigate the age distribution of globular clusters in a given system. However, currently available samples are severely limited by the spatial coverage of the IR data. With HAWK-I, wide field J -, H -, K_s -band imaging was obtained of the nearest S0 galaxy NGC 3115. A preliminary colour-colour plot, obtained using archival FORS2 imaging and the HAWK-I SV data (filled black circles), is shown in Figure 4, and compared with previous measurements (open blue circles) by Puzia et al. (2002) who used ISAAC and HST/WFPC2 imag-

ing. Overplotted are Maraston et al. (2003) SSP models for ages 3–15 Gyr and $[Z/H] = -2.25$ to 0.67. The depth of the HAWK-I data allows exploration of the interesting blue end (intermediate ages?) of the colour distribution in $V-K_s$.

In a similar programme HAWK-I was used to study the star cluster system of the intermediate-age (~ 3 Gyr) merger remnant NGC 1316. This galaxy has a substantial number of star clusters, some of which have ages corresponding to the merger. However, it is not clear what fraction were formed during this most recent merger event. The new, deep K_s -band imaging (Figure 5) has already revealed an extensive system of star clusters and, along with archival VIMOS optical imaging and spectroscopy, will allow the various cluster populations in NGC 1316 to be clearly separated and their ages and metallicities to be constrained.

The spiral galaxy NGC 7793 was also observed with HAWK-I to complement

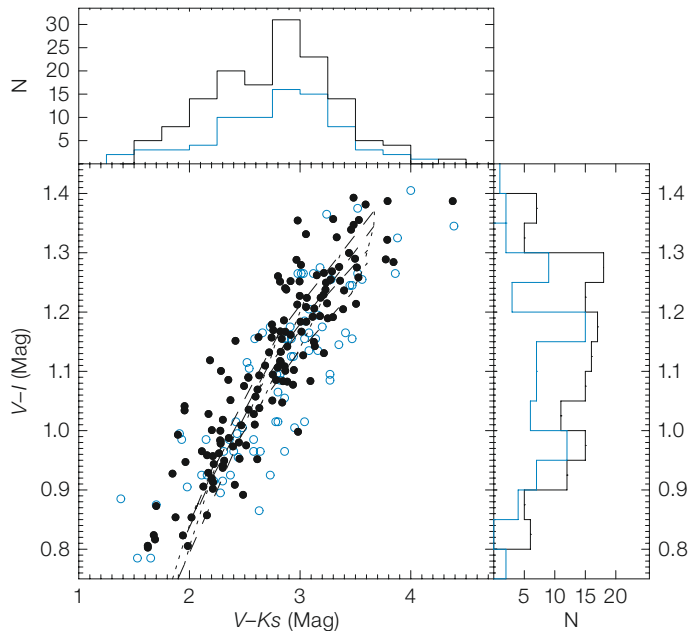


Figure 4. *V-I versus V-Ks* colour-colour diagram, with associated projections of the axes, of globular clusters in NGC 3115. The black points refer to data taken with FORS2 and HAWK-I, the blue points to data from HST WF/PC2 and ISAAC.

tions are surprising, NGC 602 was observed with HAWK-I, taking advantage of its high spatial resolution and sensitivity, in order to analyse the association of IRAC protostars and their suggested optical counterparts. Figure 6 shows the spectacular HAWK-I composite *JHKs* image of the young stellar population and the nebulosity in NGC 602/N 90. The 0.5–8 μm SED was computed, using the preliminary HAWK-I fluxes, of three previously suggested Class I protostellar objects in the region (see Figure 7). It is apparent that the near-IR data are essential to determine the true nature of these objects.

High spatial resolution H_2 2.122 micron images of the highly symmetric protostellar jet HH 212 were made with HAWK-I. Since the jet fits within a single quadrant of the HAWK-I field of view, these data provide a stable, precision astrometric template to which the archival mosaiced ISAAC images of HH 212, taken from 2001–2006, can be aligned. The scientific aim is to measure transverse motions in the outflow down to 20 km/s to trace the dynamical history of the jet and thus the accretion history of the underlying protostar. The HAWK-I observations also extend the proper-motion monitoring baseline from five to seven years, further improving the velocity resolution.

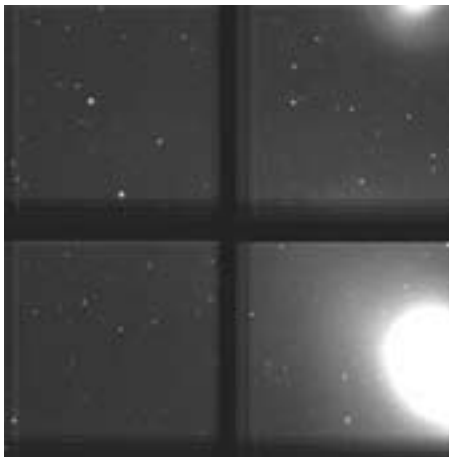


Figure 5. A deep HAWK-I *Ks*-band image of NGC 1316 showing many star clusters. The interchip gaps are apparent on this combined image.

existing wide-field optical HST/ACS data and to study its star cluster population. The combination of NIR and optical data and the large field of view of HAWK-I allow construction of the cluster luminosity function, the cluster initial mass function and the cluster age distribution of the entire cluster population, and for different environments within the disc. This will shed light into how cluster masses depend on the star formation rate of the host galaxy and how the early disruption due to the removal of natal gas, or ‘infant mortality’ of clusters, depends on local variables.

Star formation

NGC 602/N 90 in the Small Magellanic Cloud (SMC) hosts a cluster of Young Stellar Objects (YSOs) including pre-main-sequence (PMS) stars detected by HST/ACS and Class 0-I protostars detected by Spitzer/IRAC. Some protostellar objects are apparently related to optical PMS stars. Since the Spitzer/IRAC beam is relatively large and such associa-

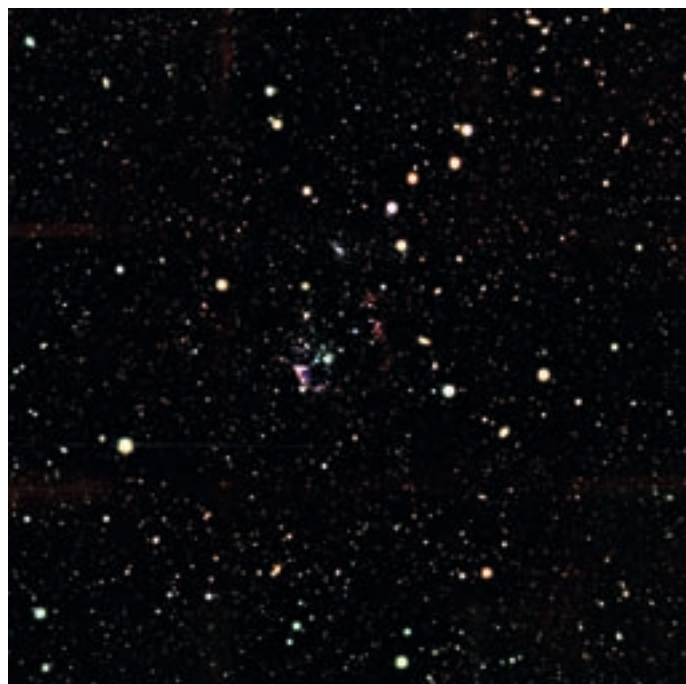


Figure 6. *JHKs* colour composite of the central region of NGC 602/N90. Reflection nebulae and a rich stellar population, mainly grouped in clusters, are distinguished, together with many background galaxies.

A deep wide-field near-IR survey of the Carina Nebula was performed with HAWK-I, in order to study the physics of violent massive star formation and the resulting feedback effects, including cloud dispersal and triggered star formation. The survey reveals all young stars in the region through extinction of up to $A_V < 25$ mag and brown dwarfs down to 35 Jupiter masses through 10 mag of extinction. In combination with recent observations at other wavelengths, the survey will allow mass, age, and circumstellar disc fraction distributions to be ascertained for the entire young stellar population as a function of environment within the Carina Nebula.

Deep HAWK-I images (5 sigma K-band limit approx. 19.5 mag in 12-min on-sky) were collected in two sub-fields of the Chamaeleon I star-forming region. The observations are complete down to at least 5 Jupiter masses, according to the theoretical isochrones for the typical distance and age of Chamaeleon I. The internal astrometric precision is better than 25 mas (root-mean-squared error – see

Figure 8). Given the typical proper motions of Chamaeleon members, a second epoch after three years will reveal all members of this region down to the free-floating planetary mass objects (planemos) regime. The astrometric performance is further backed up by the high number of background galaxies identified in the deep HAWK-I frames. These galaxies form the astrometric reference frame of the planned second epoch. The current data of this programme will be made accessible as an Advanced Data Product.

Prospects

HAWK-I is currently the most performant near-infrared imager on an 8-m-class telescope. It has proven its very high throughput and exceptional image quality during the SV observations. In period 81, HAWK-I has been scheduled for 21 runs and will, without doubt, deliver further stunning images. Given its performance, it is on the path to becoming a work-horse instrument at the VLT. We are look-

ing forward to seeing many more spectacular HAWK-I results reported in the Messenger and elsewhere.

Acknowledgements

Many thanks to the SV team who enabled all these first science results: Nancy Ageorges, Mark Casali, Yves Jung, Jorge Melnick, Alan Moorwood, Monika Petr-Gotzens, John Pritchard and Masayuki Tanaka.

References

- Casali, M., Piraud, J.-F., Kissler-Patig, M., et al. 2005, *The Messenger*, 119, 6
 Kissler-Patig, M., et al. 2008, *A&A*, accepted
 Maraston, C., et al. 2003, *A&A*, 400, 823
 Puzia, T. H., et al. 2002, *A&A*, 391, 453

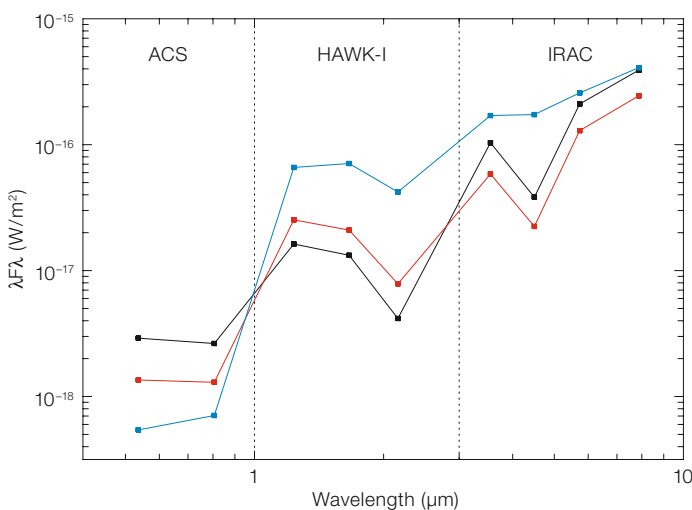


Figure 7. Spectral energy distribution for selected objects identified as protostars in Spitzer/IRAC images of NGC 602/N 90 having tentative optical counterparts observed with HST/ACS.

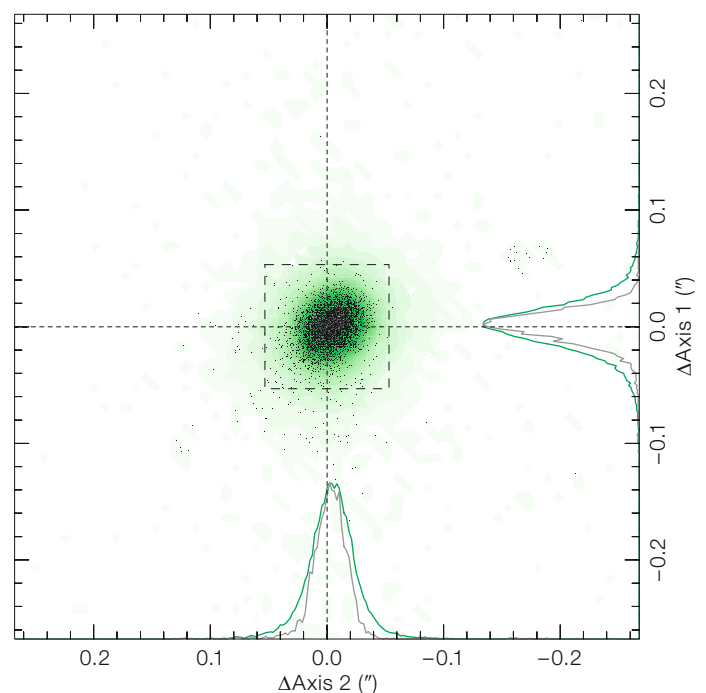


Figure 8. The X and Y astrometric errors corresponding to the HAWK-I astrometry in the Chamaeleon I star-forming region.

Seeing is Believing: New Facts about the Evolution of Seeing on Paranal

Marc Sarazin¹
 Jorge Melnick¹
 Julio Navarrete¹
 Gianluca Lombardi^{1,2,3}

¹ ESO

² National Institute for Astrophysics,
 Bologna Astronomical Observatory, Italy

³ Department of Astronomy, University
 of Bologna, Italy

Since the commissioning of the VLT it has been known that the image quality delivered by the telescopes is better, and often much better, than predicted by the seeing monitor. The advent of new sensitive instruments to measure the optical turbulence profile of the atmosphere over Paranal has finally allowed us to understand the origin of this discrepancy: the presence of a highly turbulent layer so close to the ground that it is seen by the seeing monitor, but not by the VLT unit telescopes. In this article we tell the story of this elusive surface layer.

The inconvenient discrepancy

It has been known since the commissioning of the VLT that the image quality delivered by the UT's is at times significantly better than the seeing measured by the Differential Image Motion Monitor (DIMM). The difference is not subtle. Already in 1999 the careful observations made with

the test camera during the commissioning of UT2 revealed an alarming discrepancy between the UT2 image quality and the DIMM seeing, with an average DIMM-UT2 difference of $\sim 0.2''$. During these tests that lasted several nights, UT2 was pointing at the same region of the sky and through the same filter as the DIMM, so there was no straightforward explanation for the lack of agreement. A dramatic manifestation of the discrepancy between the DIMM and the UT's is given by the time evolution of seeing on Paranal. Figure 1, shows in the left panel, a plot of the evolution of DIMM seeing since 1989 taken from the ESO astro-climatology web pages (<http://www.eso.org/astclim/paranal/seeing/>). The DIMM seeing has degraded considerably over the past 17 years from a median value of $0.65''$ in 1990 to more than $1.1''$ in 2007. On the other hand, the right panel of Figure 1 shows that the image quality delivered by FORS2 and ISAAC seem to have improved with time, at least since the instrument values have been systematically logged through the quality control process! This result could however be a selection effect since some of the PI's requested special seeing conditions. We note in passing that the La Silla seeing has also slightly degraded in a similar period (<http://www.eso.org/astclim/paranal/seeing/>).

We have been puzzling for a long time about the origin of this rather *inconvenient discrepancy*, but it has not been until recently, with the deployment of new

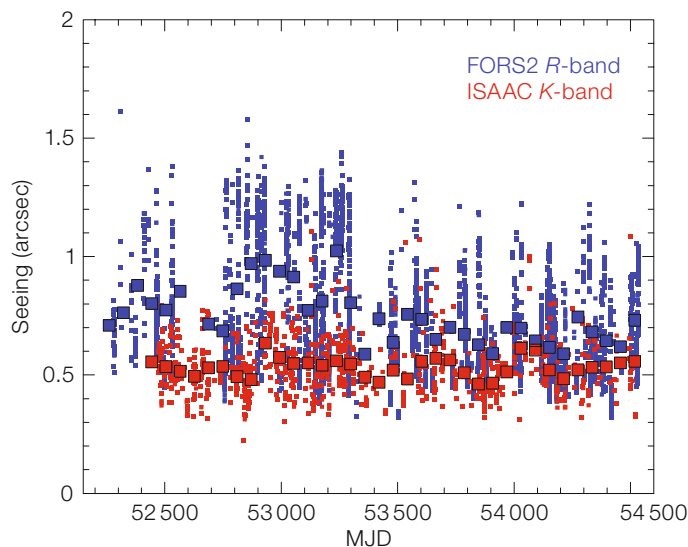
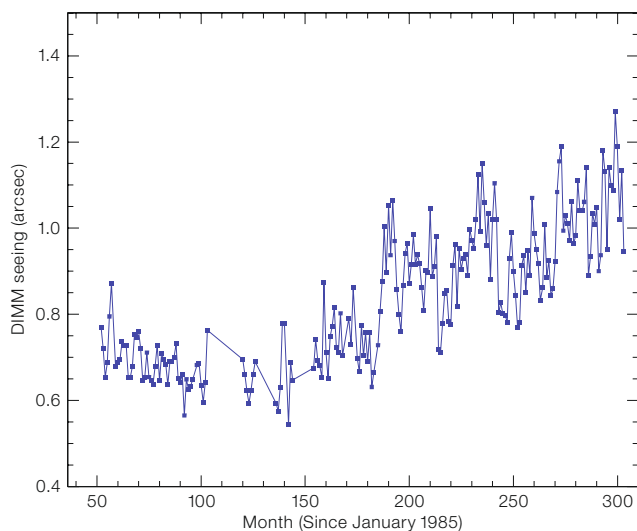
sensitive instruments in the context of the ELT site testing campaign, that we have finally been able to draw a coherent picture. This article tells the story of the seeing on Paranal.

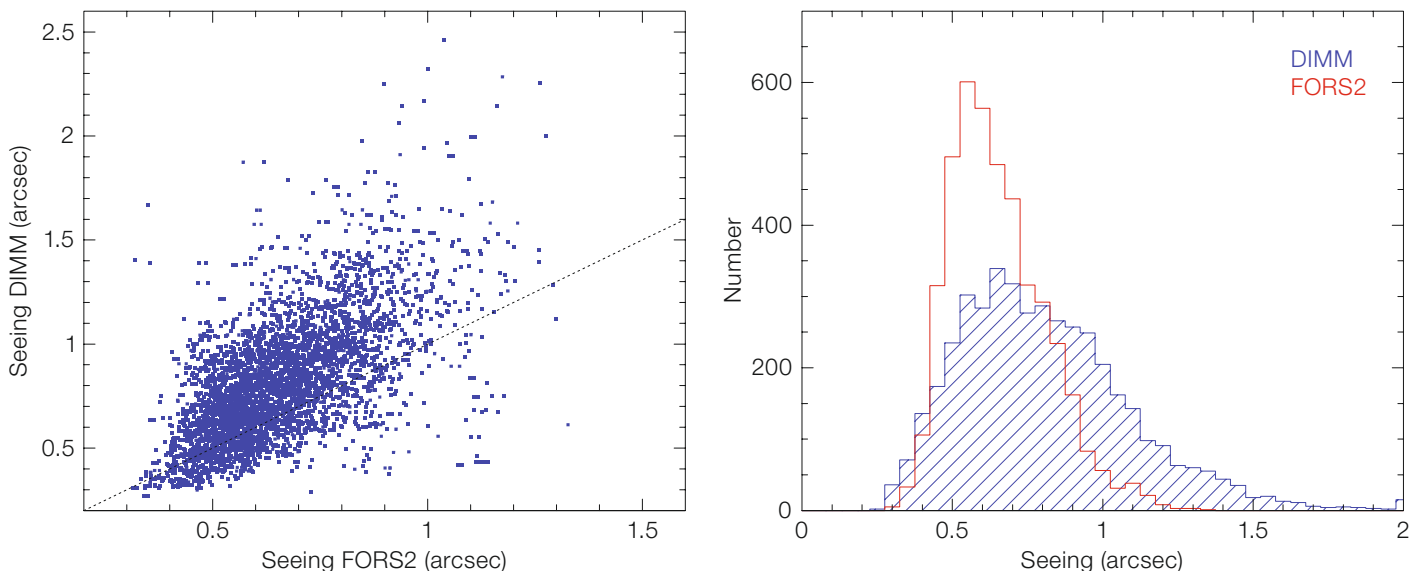
New data

FORS2 imaging data

A wealth of data has accumulated since the commissioning of UT2. For example, the Quality Control process (QC) systematically logs delivered image quality from several instruments together with environmental parameters such as wind speed and direction, air temperature, telescope position, and DIMM seeing. The most complete dataset for image quality is the one for FORS2, which will be used here. Figure 2 shows the relation between DIMM seeing and UT2 image quality measured during regular FORS2 operations. The FORS2 data has been corrected for wavelength and airmass using the standard formulae based on an infinite outer scale assumption. Only images taken at airmasses less than 1.5 and exposure times between 30 s and 300 s were used. The FORS2 measurements are automatically obtained using many objects on each frame, but only

Figure 1. Left: Evolution of DIMM seeing on Paranal since 1989. Right: Evolution of the FORS2 image quality in the R-band and of ISAAC image quality in the K-band since January 2002 (MJD = 52275). The big squares show the averages over 2-month bins.





values for which the image quality dispersion is less than $0.1''$ rms have been retained.

The correlation between DIMM and FORS2 reproduces the trend observed with the test camera during the commissioning of UT2. The mean DIMM seeing is $0.81''$ while the mean FORS2 image quality is $0.65''$, so on average the DIMM overpredicts image quality by about $0.16''$, similar to the value of $\sim 0.2''$ measured with the test camera. It may be tempting to apply a rule-of-thumb correction of $\sim 0.15''$ to go from DIMM seeing to UT image quality (at similar airmass and wavelength), but one should notice that for very good seeing conditions the DIMM seeing may be better than the FORS2 image quality, while under very bad conditions, the DIMM may indicate a seeing more than $1''$ worse than FORS2. So it is important to understand the origin of the discrepancy between DIMM seeing and UT image quality.

Active optics Shack-Hartmann data

Real-time quality control of service-mode data at the observatory requires a reliable way of assessing whether the data complies with the seeing requirements set by the PI's. While this is straightforward for imaging data, it is not so for spectroscopy. Thus, the observatory operations staff typically rely on the FWHM of the stars in the guide probes to estimate the

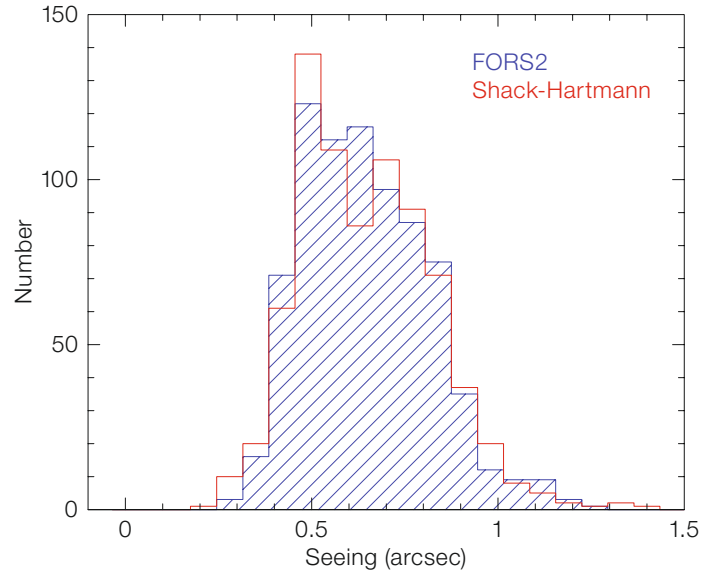
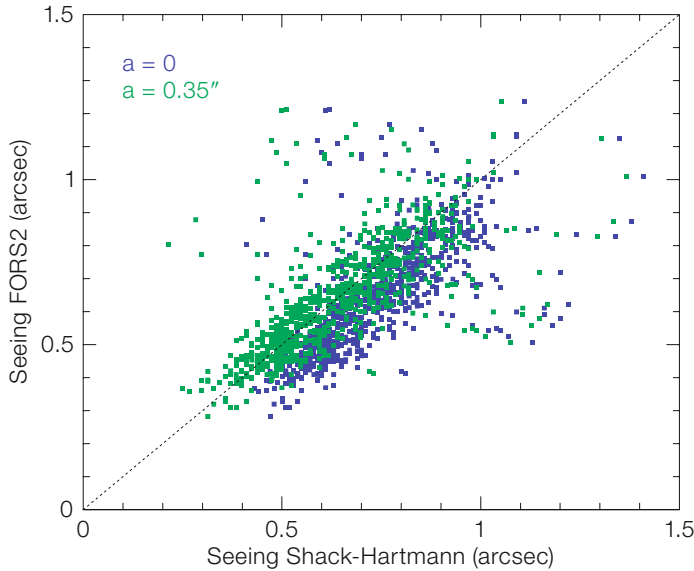
seeing. While this has its shortcomings, it seems to be sufficiently accurate for OB validation purposes. The possibility of systematically using the sizes of the (Cassegrain) Shack-Hartmann (SH) spots of the active optics system of the UT's has been investigated in this context by two of the authors (Julio Navarrete and Marc Sarazin). This has the advantage that the sizes are routinely logged by the telescope control software and therefore could provide a readily available real-time estimate of the image quality. Figure 3 shows, in the left panel, a comparison between the image quality measured by FORS2 and the SH for about 750 simultaneous observations between 2002 and 2007 (blue dots). The Shack-Hartmann data were corrected by the aberrations of the SH lenslet array ($0.35''$) measured on an internal reference source (green dots). The right panel shows the corresponding histograms. The median image quality measured by FORS2 is $0.64''$, and $0.63''$ by the (corrected) SH spots; both histograms are seen to coincide very nicely. The figure shows that indeed the (aberration-corrected) size of the SH spots provides an excellent proxy for image quality. Using the SH information we now have access to a much larger dataset to compare DIMM seeing with UT image quality.

Atmospheric turbulence profiles – $C_n^2(h)$

Modern site characterisation campaigns aim at determining the vertical turbulence

Figure 2. Relation between DIMM seeing and image quality measured by FORS2 between 2004 and 2006. In the left plot is shown a point plot, and the dashed line indicates DIMM = FORS2 seeing. In the right plot, the measurements are shown as histograms of the seeing values for both instruments.

profiles of the atmosphere at each site. The most direct way of doing this is to fly balloons equipped with very sensitive sensors that can measure the temperature and wind speed fluctuations as a function of altitude. Of course these experiments are costly and cannot provide real-time diagnostics of the conditions on a given night. Thus, a number of techniques have been developed to do the job from the ground. The Multi-Aperture Scintillation Sensor (MASS) is a compact single-star instrument that measures scintillation on four concentric zones of the telescope pupil using photomultipliers (Kornilov et al., 2003). A statistical analysis of these signals measures the vertical profile of turbulence $C_n^2(h)$ in six layers at 0.5, 1, 2, 4, 8, and 16 km above the telescope. A MASS unit developed at the Sternberg Institute (Moscow) under joint ESO-CTIO funding observed continuously on Paranal between 2004 and June 2007. In addition to its low-altitude resolution (about half the layer altitude, i.e. ± 250 m at 500 m and ± 8 km at 16 km), a distinct disadvantage of MASS is that it is blind to turbulence close to the ground (the ground layer), which produces little scintillation. We will show below, however, that for the purpose of understanding the discrepancy between



DIMM and UT's, this turns out to be an important advantage.

The ground layer

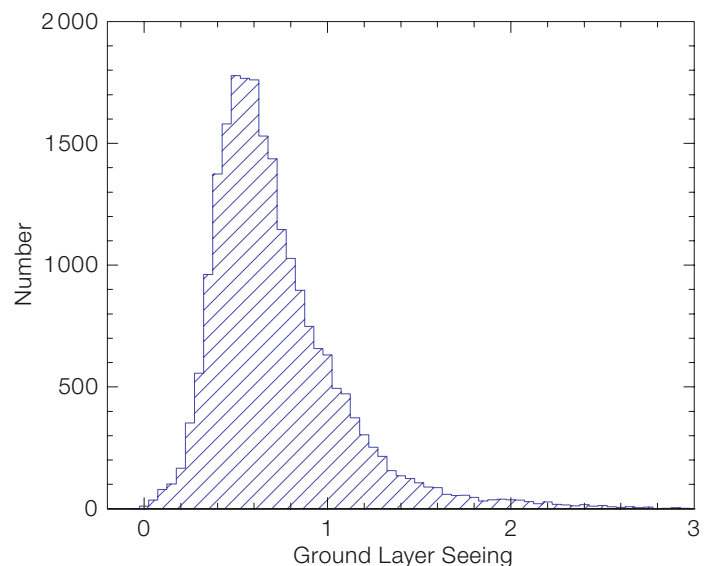
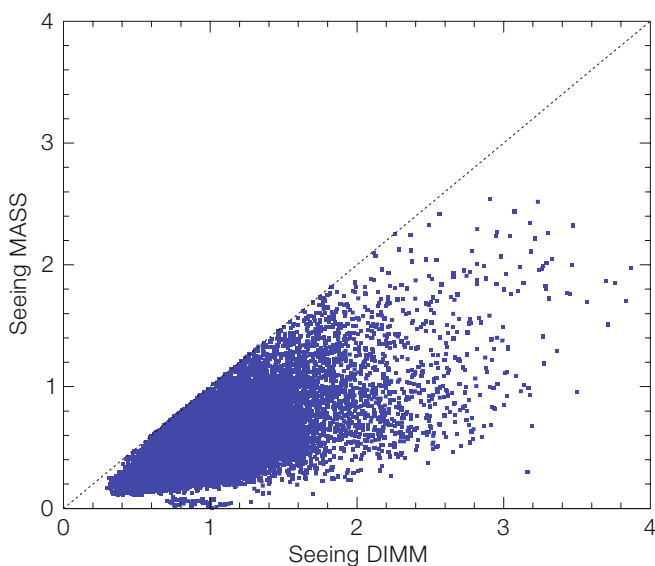
A straightforward application of the MASS data is to integrate the profiles to measure the seeing. This is shown in the left panel of Figure 4 where the seeing measured by the MASS is compared to the seeing observed simultaneously by the DIMM. As expected, the MASS systematically underestimates the 'real' seeing because it does not see the turbulence that is close to the ground. Therefore, Figure 4 tells us that a signifi-

cant fraction of the seeing over Paranal is produced by a turbulent layer located well below 500 m from the ground. This is something that was already known from previous experiments involving microthermal sensors on a mast (Martin et al., 2000). What is new is that we have a substantial body of simultaneous observations which we can use to quantify the contribution of the ground layer with excellent time resolution.

The seeing ϵ is linearly proportional to wavelength and inversely proportional to the Fried parameter r_0 . If we assume that the atmosphere has only two turbulent layers, a ground layer (GL) and a high-alti-

Figure 3. Left: Relation between the image quality delivered by UT1 estimated using the Shack-Hartmann (SH) spots of the active optics sensor, and the value determined on long (30 s–300 s) exposures with FORS2 in the *R*-band. The data have been normalised to airmass 1.0 and 500 nm wavelength. The blue points are the original SH data, and the green points show the values corrected for a lenslet aberration of 0.35". The dotted line corresponds to FORS2 = SH. **Right:** Measurements presented as histograms for FORS2 and the SH.

Figure 4. Left: Comparison between DIMM and MASS seeing (arcsec). The MASS seeing is always smaller indicating a significant contribution from a the ground layer ($h < 500$ m). **Right:** Histogram of the ground layer seeing contribution.



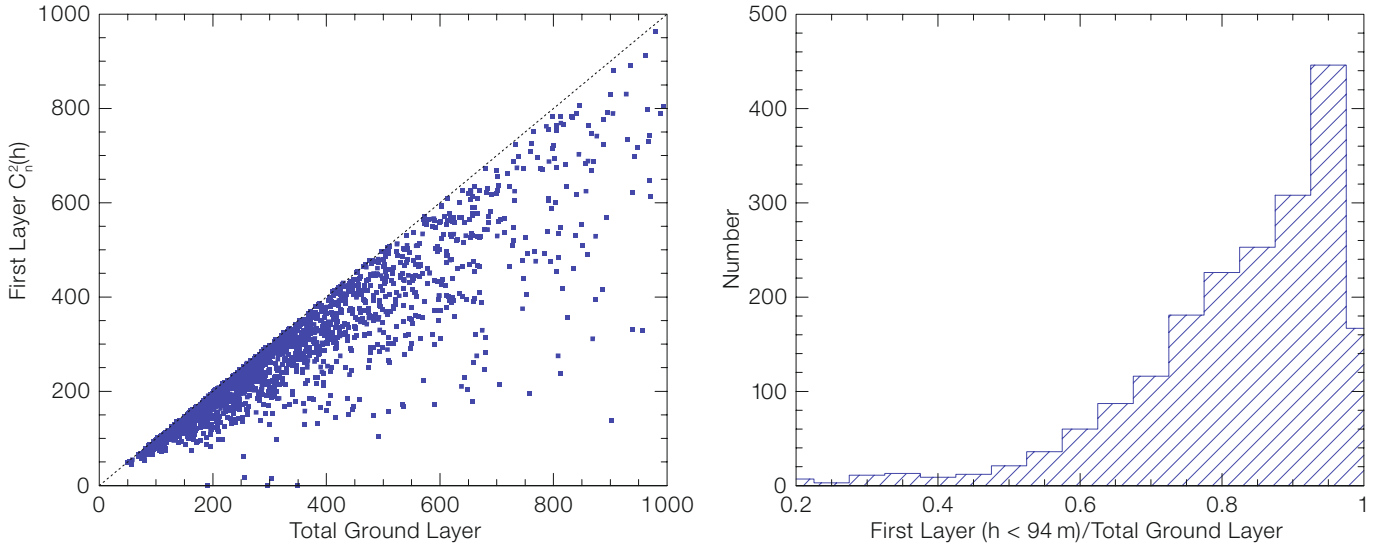


Figure 5. Left: $C_n^2(h)$ ($h < 94$ m) versus total ground layer turbulence measured by SLODAR. Right: Fraction of the total ground layer turbulence that comes from the first SLODAR layer. Most of the time the ground layer contribution is dominated by the $h < 94$ m component.

tude layer (HA), then the total seeing is:

$$\varepsilon_{Tot}^{5/3} = \varepsilon_{GL}^{5/3} + \varepsilon_{HA}^{5/3}$$

Using this equation we can estimate the ground layer component since DIMM measures ε_{Tot} and MASS measures ε_{HA} . The result is presented in the right panel of Figure 4 that shows the histogram of ground layer seeing. The mean ground layer seeing on Paranal is $0.72''$ with a rather large dispersion of $0.36''$ (σ) indicating that the ground layer varies significantly with time. So the comparison between MASS and DIMM tells us that a substantial fraction of the seeing on Paranal originates in turbulent layers below 500 m altitude. The resolution of MASS does now allow us to say more, but there are other instruments that can get us closer to the ground.

SLODAR

The Slope Detection and Ranging instrument (SLODAR) uses an optical triangulation method on double stars to measure the atmospheric turbulence profile (Butterley et al., 2006). SLODAR, that has had observing runs on Paranal since 2005, gives $C_n^2(h)$ for eight layers with a

resolution between 50 m and 100 m, depending on the separation of the double star and the zenith angle. While MASS measures the atmosphere between 0.5 and 16 km, SLODAR measures below 1 km, so both instruments are nicely complementary (although as stressed above MASS has a much lower vertical resolution). Figure 5 shows the distribution of the ratio of the contribution of the first (SLODAR) layer ($h < 94$ m) to the total ground layer turbulence determined by combining together DIMM, MASS, and SLODAR data taken simultaneously (Lombardi et al., 2008). The plot shows that most of the time the ground layer turbulence is concentrated below 94 m. The median value of the distribution is $0.86''$ and the mean $0.82''$, but the distribution is heavily skewed toward large values indicating that conditions where the ground turbulence is not below 94 m are quite rare. The strong turbulence at a mean altitude of ~ 50 m revealed by these observations suggests that the inconvenient discrepancy could be explained if much of this turbulence is in fact below ~ 20 m, so it is seen by the DIMM but not by the UT's. Some evidence in support of this hypothesis comes from the Lunar Scintillometer (LuSci) developed by Tokovinin (2007). LuSci allows the ground turbulence to be measured with a resolution of ~ 10 m from observations of the lunar disc. A very preliminary LuSci test run at Paranal in December 2007 indicates that a substantial fraction of the ground layer turbu-

lence is indeed lower than ~ 15 m above the platform on Paranal. Hereafter we will refer to this (low) layer as the 'surface layer'.

Understanding the inconvenient discrepancy

We can test our hypothesis about the nature of the *inconvenient discrepancy* by correcting the DIMM seeing for the ground component using the MASS data and comparing the results with the UT image quality as measured by the SH spots. For this comparison we need to know the fraction of the total ground layer seeing contributed by the surface layer ($h < 20$ m). The SLODAR data tells us the average value is ~ 0.8 . The best fit shown in Figure 6 is obtained for lenslet aberration $a = 0.35''$ and a mean surface layer fraction of 0.8. For these values the least squares fit (solid line) agrees within 1% with the $X = Y$ solution, but the histograms for the two datasets do not overlap exactly. The best match is obtained for a surface layer fraction of 0.7. This is not surprising since, as we have seen above, the value changes with time, so assuming a constant is just an approximation. The generally good agreement between surface-layer corrected DIMM seeing and UT image quality, however, provides convincing evidence that the surface layer is indeed the most likely explanation for the *inconvenient discrepancy*.

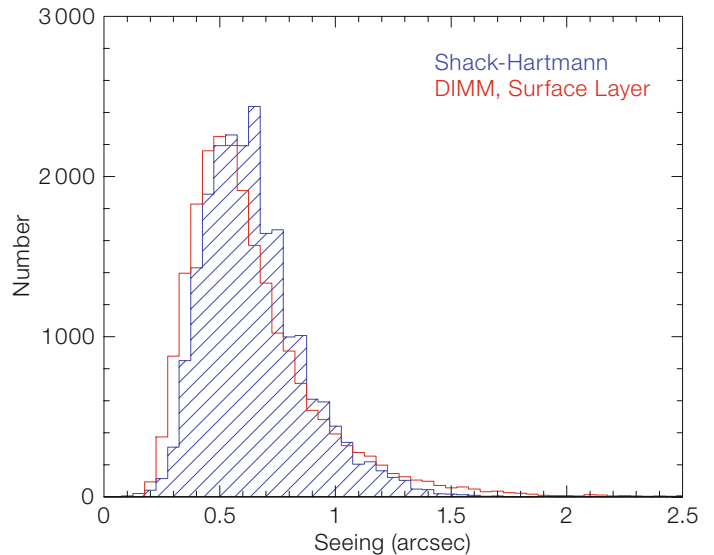
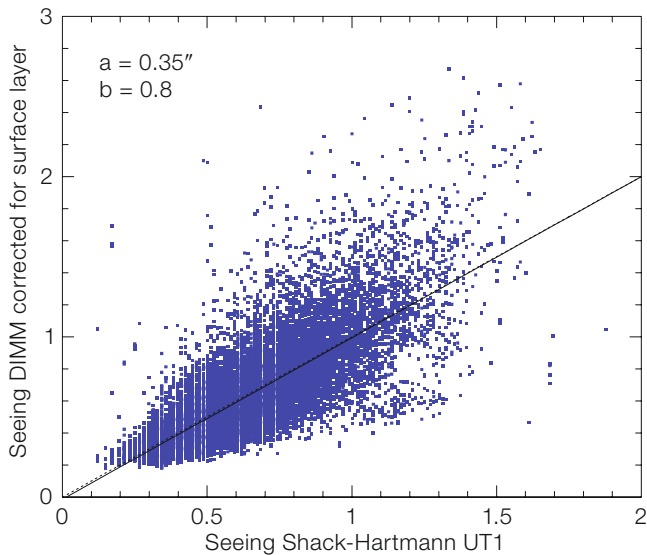


Figure 6. Left: Relation between DIMM seeing above the surface layer determined as described in the text, and the UT1 image quality estimated using the size of Shack-Hartmann (SH) spots of the active optics. The solid line shows a least squares fit to the data of slope 1.0. The best match of the two lines is obtained for an intrinsic SH spot size of $a = 0.35''$, and a surface layer which contributes about 80% of the total ground layer seeing measured comparing DIMM and MASS. **Right:** Histograms of DIMM seeing corrected for surface layer and the SH image quality. While the mean values of the two histograms coincide, the overlap is best for 70% surface layer contribution.

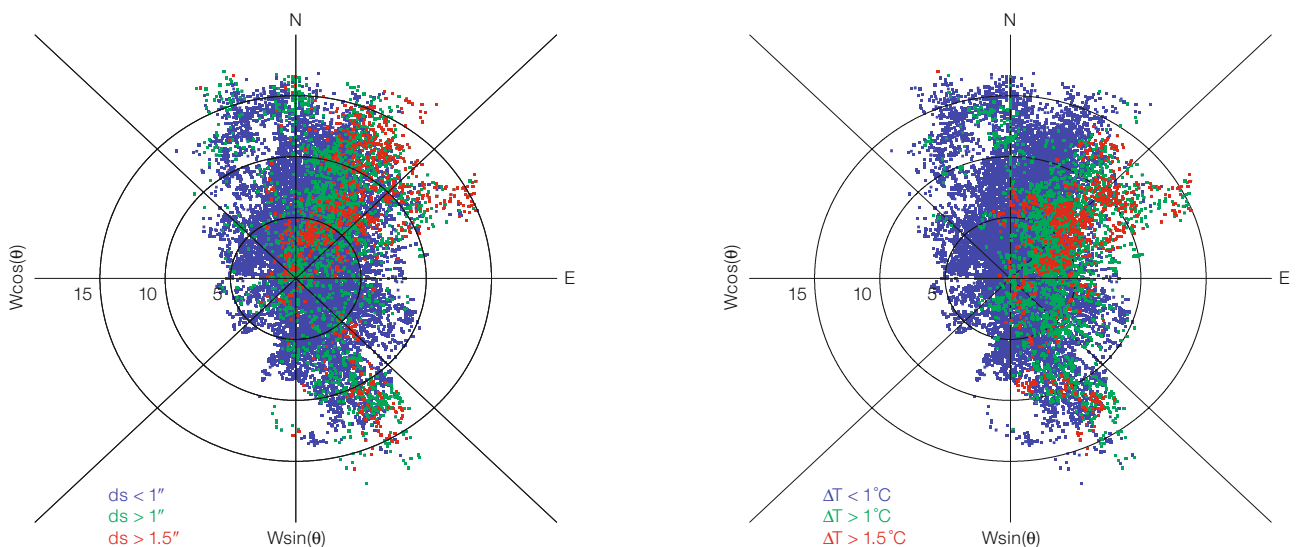
that influence the presence and strength of the surface layer. Assuming that the DIMM/UT discrepancy, ds (see caption of Figure 7), measures the strength of the *surface layer*, we can use the Vaisala data to check whether the surface layer strength correlates with Paranal environmental parameters. Figure 7 shows the wind-rose of Paranal colour coded according to ds on the left panel, and by the difference in temperature between 30 m and 2 m on the right panel. The discrepancy is seen to be strongest when the wind comes from the NNE and from the SSE (with a broad distribution about these directions), while the temperature gradient is largest when the wind comes from the NE and SSE. This suggests that

the bad seeing occurs when the wind blows warm turbulent air from nearby summits along the Atacama fault (which traces most of the road between the Panamerican highway and Paranal) over the top of the mountain. A temperature inversion of 0.5°C is present most of the time on Paranal and there is a weak trend of the DIMM/UT discrepancy increasing with the 2–30 m temperature difference, indicating that local conditions may play a role in determining the properties of the

When the seeing is bad

The automated Vaisala weather tower on Paranal provides continuous data that we can use to investigate the conditions

Figure 7. Left: The wind-rose of Paranal colour coded by the discrepancy between DIMM seeing and UT1 image quality; $ds = (\text{DIMM}^{5/3} - \text{SH}^{5/3})^{3/5}$. **Right:** Wind-rose coded by temperature gradient between 2 m and 30 m above ground.



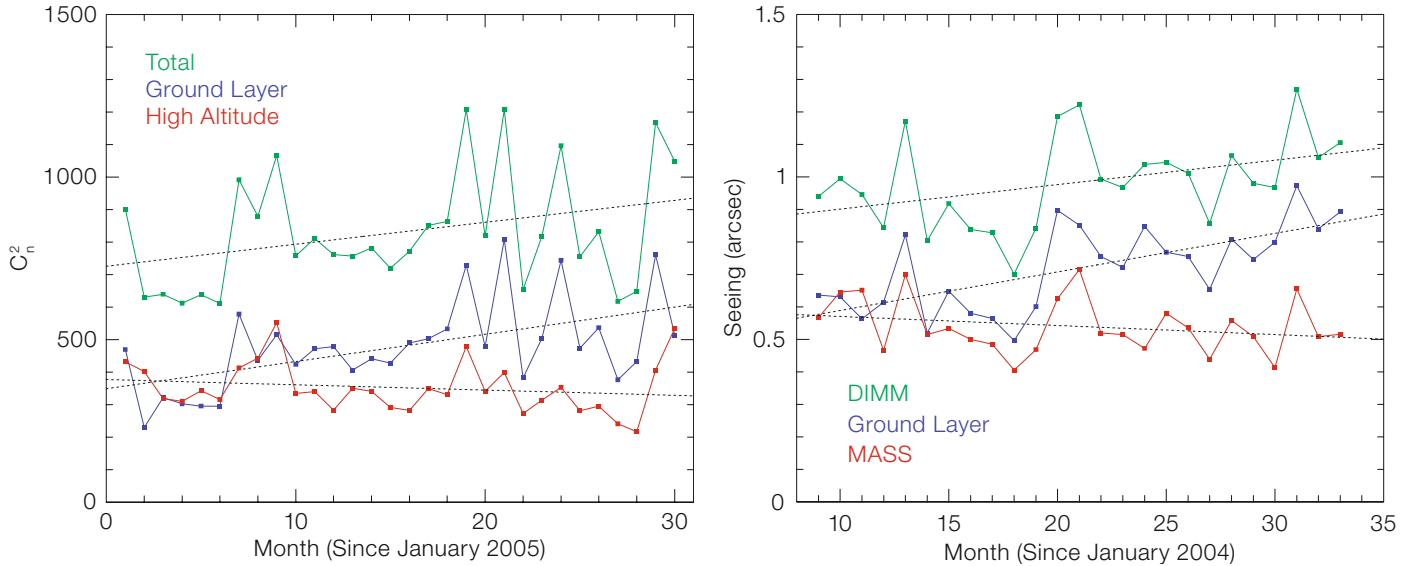


Figure 8. Left: Evolution of the components of atmospheric turbulence over Paranal (C_n^2) between 2005 and 2007 determined by combining DIMM, MASS, and SLODAR data (from Lombardi et al., 2008). Right: Evolution of the seeing components determined combining the DIMM and MASS data as described in the text.

surface layer (e.g. by confining it to very low altitudes). An investigation of this aspect of the problem is underway, but is beyond the scope of this article.

Blown with the wind

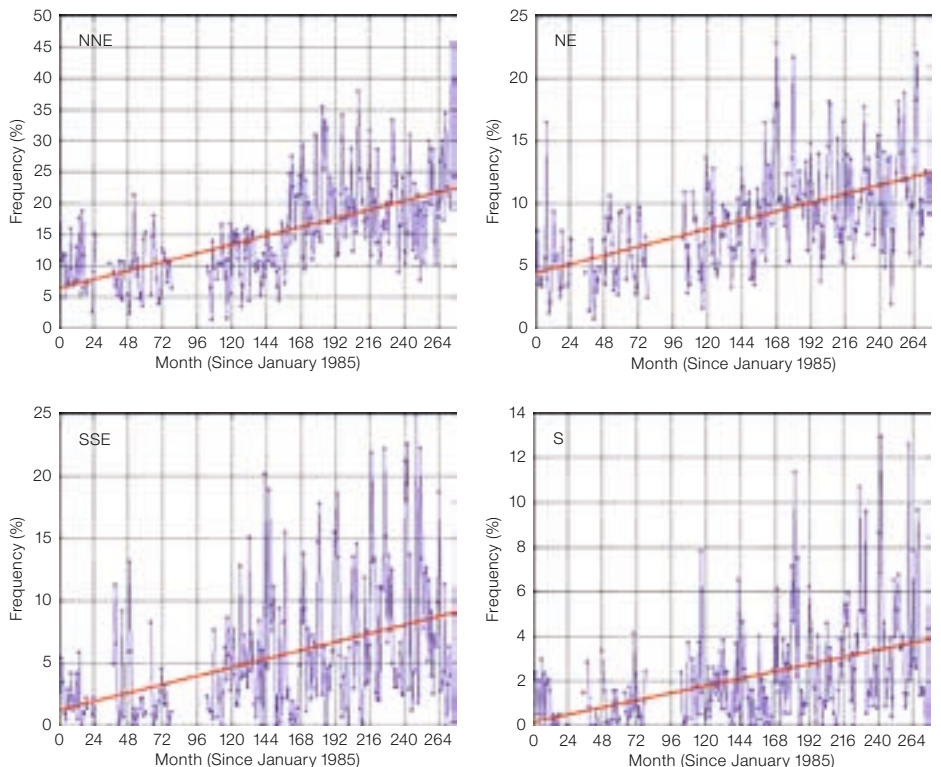
If our interpretation of the *inconvenient discrepancy* is correct, we expect the surface layer to have become increasingly important with time, but the other components of the seeing to have remained constant. Lombardi et al. (2008) have examined this question using the combined DIMM+MASS+SLODAR data taken simultaneously between 2005 and 2007. Their results, reproduced in the right panel of Figure 8, show that this is indeed the situation. The degradation of DIMM seeing on Paranal is seen to be completely due to changes in the ground layer, while, if anything, the high-altitude layer seems to be getting better. A similar result spanning a longer time interval, albeit with lower altitude resolution, is obtained comparing the DIMM and MASS data only (right panel in Figure 8). The surface layer (which as we saw is the main component of the total ground layer) has become significantly stronger over the

past four years, and from the evolution of the DIMM seeing shown in Figure 1 we infer that this has been going on for the past 12–15 years. Notice that, just as indicated by the FORS2 and ISAAC data displayed in Figure 1, the high-altitude layer seems to be getting better with time.

If the surface layer is *blown with the wind* over Paranal, we expect the wind distri-

bution to have changed over the years. The evolution of the wind pattern on Paranal since 1985 is shown in Figure 9.

Figure 9. Evolution of the wind patterns over Paranal since 1985. The frequency of NE and NNE winds has increased dramatically since just about the time VLT commissioning started. The S and SSE wind fluctuations have increased such that during some months the frequency of these winds is also dramatically increased.



The analysis of the astroclimatology data (www.eso.org/astclim/paranal) shows that indeed the frequency of 'bad winds' (NE, NNE, SSE, and S) has increased over the past 15 years. The seeing is local, but the wind is global. The change in seeing over Paranal is due to changes in the wind pattern, which in turn must be caused by climate change on a global scale. Fortunately, at Paranal the turbulence blown by the wind is very close to the ground, so telescopes high above the ground don't see it. Unfortunately, telescopes close to the ground do!

Conclusions

We can safely draw two quite strong conclusions about the evolution of seeing on Paranal:

- The discrepancy between the seeing measured by the DIMM and the image

quality delivered by the VLT Unit Telescopes, and the notable degradation of DIMM seeing observed over the past 15 years have a common origin: the presence of a thin, time variable turbulent layer – the *surface layer* – over the mountain that is seen by the DIMM, but not by the UT's.

- The *surface layer* is strongest when the wind blows from the NNE and from the SSE. These winds have become increasingly frequent over the past 15 years explaining why the surface layer appears more and more often. This change in the prevailing winds over Paranal is due to climate change. In fact, it is climate change.

Site testing campaigns must pay close attention to the surface layer through the use of micro-thermal towers, or sensitive astronomical instruments such as SLODAR and LuSci. Extensive cam-

paigns on existing observatories now underway should be intensified and the results cross-correlated, especially if different techniques are used. Close attention must be paid to the local orography, and the effects of changes in the prevailing winds modelled. Seen through the light of modern site testing techniques and global climate change, it is sobering to realise that our ancestor's conventional wisdom – put thy telescope as high above the ground as possible – is still right!

References

- Butterley, T., Wilson, R. W. & Sarazin, M. 2006, MNRAS, 369, 835
- Kornilov, V., et al. 2003, Proc. SPIE, 4839, 837
- Lombardi, G., Navarrete, J. & Sarazin, M. 2008, E-ELT-TRE-222-0215, ESO Garching
- Martin, F., et al. 2000, A&AS, 114, 39
- Tokovinin, A. 2007, Rev. Mex. Astron. Astrophys. (Conf. Series), 31, 61

Photo: S. Brunier



View of the Galactic Centre above La Silla with the domes of the 3.6-m telescope and the CAT illuminated by the setting Moon.

EFOSC2 Episode IV: A New Hope

Colin Snodgrass, Ivo Saviane,
Lorenzo Monaco, Peter Sinclair
(all ESO)

As part of the long-term plan for the La Silla Observatory, ESO is reducing the number of instruments offered. EMMI and SUSI have been decommissioned at the NTT, and EFOSC2 has been moved to the NTT, replacing EMMI, to leave HARPS as the sole instrument at the 3.6-m. Here we describe EFOSC2 and its many capabilities, highlight the changes that the move to the NTT brings, and look forward to future plans for this instrument.

During the Transition Phase (2007–2009), the La Silla Observatory will see a reduction of the number of offered instruments and modes, with the goal of minimising the level of support from the Science Operations department. Within this framework, starting from Period 81, EFOSC2 is offered at the NTT instead of the 3.6-m telescope, initially together with SOFI. In April 2008 the instrument was transferred to its new home, the Nasmyth B focus of the NTT. Here we recall some of the long history of EFOSC2 and its many capabilities, and describe the changes that the move to its new telescope brings.

EFOSC2, the second ESO Faint Object Spectrograph and Camera, was originally built by ESO staff at La Silla for the NTT, to provide an imager and spectrograph for the first commissioning work and early scientific programmes before EMMI was ready. The design concept was based on the robust and versatile original EFOSC on the 3.6-m, but with various improvements including a larger CCD (see Buzzoni et al., 1984 and Eckert et al., 1989). It saw first light on the NTT on 11 May 1989, and the catalogue of Planetary Nebulae that came from commissioning observations for this telescope remains EFOSC2's most popular paper (Schwarz et al., 1992). Once EMMI arrived at the NTT in 1990, EFOSC2 was moved to the 2.2-m telescope, before moving in October 1997 to the 3.6-m, where it replaced the original EFOSC and served for over 10 years. Scientific highlights from the instrument during this time include work on dark matter in galaxy

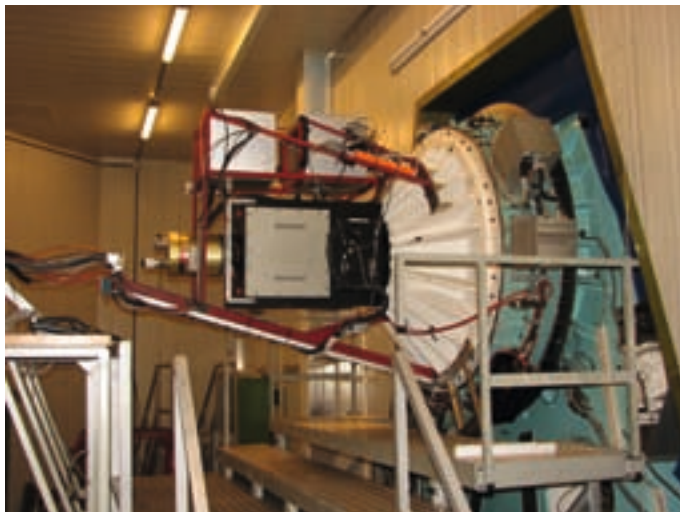


Figure 1. EFOSC2 mounted at the Nasmyth B focus of the NTT.

clusters (Böhringer et al., 2001) and also optical studies of supernovae associated with GRBs (Levan et al., 2005). Now, with the decommissioning of EMMI, EFOSC2 enters its fourth tour of duty, and returns to its original home at the NTT (Figure 1).

One of the main reasons for the longevity and reliability of EFOSC2 is the fact that its design is relatively simple, and yet it offers many observing modes and is highly versatile. It has undergone various improvements over the years, the most recent being the addition of a quarter wave plate for polarimetry (Saviane et al., 2007) and new high-resolution volume-phase holographic grisms (see following article by Saviane & Monaco).

Return to the NTT

With the move back to the NTT, some further changes were implemented, mostly due to the change of focal station from the f/8 Cassegrain focus of the 3.6-m to the f/11 Nasmyth focus of the NTT. The observing modes offered at the NTT are: Broad- and Narrowband Imaging; Coronagraphic Imaging; Polarimetric Imaging; Long-Slit Spectroscopy; Multi-Object Spectroscopy; Slitless Spectroscopy; and Spectropolarimetry. All of these modes were successfully tested during recommissioning on the NTT in April 2008.

The image quality of EFOSC2+NTT is very good: Figure 2 shows an image of

the globular cluster NGC 3201, in which the stellar PSF is measured to have a FWHM of 0.6". Figure 3 shows a re-commissioning image of the galaxy group Arp 321. At the NTT we measured the pixel scale to be 0.12"/pixel, the rotation centre to be near the centre of the CCD at pixel (1016, 990), and the orientation at zero rotator angle to be North up and East right. This information has been used to allow full World Coordinate System (WCS) information to be stored in the FITS headers of data taken with EFOSC2, which was shown in tests to be accurate to within the typical pointing accuracy of the NTT (a few arcseconds).



Figure 2. An image of NGC 3201 taken to demonstrate the image quality. The stellar Full Width at Half Maximum (FWHM) of the star images in the R-band was measured to be 0.6", matching the DIMM seeing.

The field of view of the full 2048×2048 pixel CCD is $4.1' \times 4.1'$, although there is some vignetting at the corners of the CCD, beyond a radius of approximately $2.4'$ from the centre, which corresponds to approximately 8% of the full field of view. There is also some distortion of the image PSF in the radial direction due to the focal reducing optics of the instrument, which was measured to reach 10% beyond approximately $2'$ from the centre. The lower pixel scale means that stellar PSFs are oversampled in all but the best seeing, so higher binning modes than the current standard 2×2 will be offered for imaging (3×3 and 4×4 ; also 1×3 , 1×3 , 2×3 and 2×4 modes for spectroscopy). These modes still remain to be implemented, but are expected to be offered during the first half of P81. The high sensitivity in the blue is maintained following a UV-flooding of the CCD during the move, while the response is better at red wavelengths than it was at the 3.6-m. The zero-points for *UBVRI* are shown in Figure 4. The fluxes for a 15th magnitude star in e-/sec are $U = 5.7 \times 10^3$, $B = 2.9 \times 10^4$, $V = 3.3 \times 10^4$, $R = 3.5 \times 10^4$, $I = 1.5 \times 10^4$.

In the spectroscopic modes the change of plate scale means that the old slits have different effective widths, so new slits with $0.3''$, $0.5''$, $0.7''$, $1.0''$, $1.2''$, $1.5''$, $2''$, $5''$ and $10''$ widths have been prepared, each with a length of $4.1'$ (i.e. covering the full field of view). The default slit alignment is in the East-West direction (horizontally across the chip), so to align the slit along a given Position Angle, an offset of $PA + 90^\circ$ must be applied to the rotator (this is done automatically when presetting to the parallactic angle). During commissioning it was found that, with the instrument now mounted horizontally at the NTT Nasmyth B focus (instead of vertically at the 3.6-m Cassegrain), there is significant flexure. A shift of 3.5 pixels in the spectral (y-axis) direction was measured over the full rotator motion. Further work is planned to stiffen the instrument, but those users wanting to measure radial velocities are advised to take regular arc lamp exposures.

The polarimetry modes of EFOSC2 are the most strongly affected by the move, as the reflection from the NTT M3 introduces linear polarisation dependent on



Figure 3. The interacting galaxy group Arp 321, taken as a test image during the recommissioning.

the telescope pointing. Measurements of both polarised and unpolarised stars at many telescope positions were taken during the commissioning time, and the instrument polarisation as a function of telescope position is now being modelled.

The future of EFOSC2

The demand for all of EFOSC2's observing modes remains high. With 51 proposals submitted for P82, it is the most highly requested La Silla instrument, while in terms of time requested (8% of total time requested on all ESO instruments) it is in

higher demand than all VLT instruments except FORS2 and VIMOS, even with the end of service mode observing at La Silla. With the end of EMMI operations, EFOSC2 now takes on the considerable load of being ESO's only general-purpose imager and spectrograph on a mid-size telescope. With this in mind we are also planning further future improvements to the instrument: We are in the process of looking for a good replacement CCD that would give improved readout noise and readout speed, and would be compatible with a continuous flow cryostat to simplify operations and providing improved long-term stability. Implementation of calibration OB's (CALOB) and a full reduction pipeline will also enhance operations in the near future. We look forward to many more years of exciting science with EFOSC2 in its new home.

Acknowledgements

We thank all the members of the La Silla staff involved in the transfer of the instrument to the NTT, who ensured not only a smooth move, but also took the opportunity to carry out numerous improvements that have been on the Instrument Scientist 'wish list' for some time.

References

- Böhringer, H., et al. 2001, A&A, 369, 826
- Buzzoni, B., et al. 1984, The Messenger, 38, 9
- Eckert, W., Hofstadt, D. & Melnick, J. 1989, The Messenger, 57, 66
- Levan, A., et al. 2005, ApJ, 624, 880
- Saviane, I., et al. 2007, The Messenger, 129, 14
- Schwarz, H. E., Corradi, R. L. M. & Melnick, J. 1992, A&AS, 96, 23

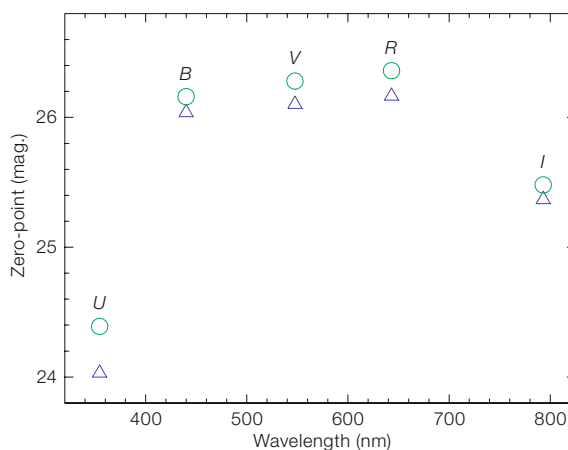


Figure 4. The *UBVRI* zero points of EFOSC2 (with CCD No. 40) on the NTT. The new values (green open circles) compare favourably with the mean values (blue open triangles) for the same instrument on the 3.6-m.

Two Volume-phased Holographic Grisms Now Available for EFOSC2

Ivo Saviane, Lorenzo Monaco (ESO)

Starting from Period 81, two new volume-phased holographic gratings are available to be used with EFOSC2. Testing of the gratings is described. Some results on measurement of the stellar Lithium doublet and galaxy rotation curves demonstrate the performance of the new gratings.

Two volume-phased holographic gratings (VPHG) were procured by the ULTRASPEC project (see Dhillon et al., 2007), and were first used in January–February 2008 for some of the science runs. Afterwards, the VPHGs were tested for scientific performance, and on the basis of the overall positive evaluation, it was decided to offer them to the community. Here we report on some of the tests that were performed on 13 and 14 February 2008. At that time the instrument was installed at the 3.6-m telescope; during the commissioning of EFOSC2 at the NTT (April 2008) the tests were repeated to assess the performance at the new focal station. The basic parameters of the two gratings are summarised in Table 1.

Basic characteristics

To characterise the gratings the usual set of calibration frames were taken: bias frames, one arc frame, and dome flat-field frames. In both cases, it was soon evident that part of the CCD is not illuminated because, after passing through the VPHG, the beam suffers a deviation in the spatial direction. Only ~ 70 % of the field of view is available when using the red VPHG, and ~ 65 % when using the blue grism. In terms of pixels, the useful area is 2021×1411 px for the blue grism, and 2021×1231 px for the red grism. Some reflections are also visible in the arc frame of the red grism, caused by the Helium lamp. It is thus suggested

to have very short exposure times for this lamp, of the order of 0.1 sec. Redder than ~ 7000 Å fringes are visible in the flat-field frames of the red grism.

Arc lamp exposures were used to measure the dispersions and resolutions, which are listed in Table 1. Note that at the extremes of the spectral range the resolutions are degraded by ~ 50 % for the blue grism and ~ 30 % for the red grism. The highest dispersion of the current EFOSC2 gratings is 1 Å/px, so the blue and red VPH gratings offer values three and two times larger than what is currently available, respectively. Plots of the wavelength calibrated arcs are shown in Figure 1.

The two technical nights at the 3.6-m telescope were not photometric, so system efficiencies were obtained later with EFOSC2 at the NTT. They are shown in Figure 2, together with the efficiencies of the other gratings. The efficiency of the blue VPHG goes from 30 % at the red end, down to 20 % at the blue end. The red VPHG has a more constant response, with an efficiency around 30 %. In general, as Figure 2 shows, the system efficiencies are comparable to those obtained with the existing EFOSC2 gratings.

In order to determine whether the gratings are useful to obtain valuable science data, we took spectra to measure stellar abundances and to study the kinematics of spiral galaxies.

Measurement of Lithium line 6707.8 Å

Lithium is a fragile element which is easily destroyed in stellar interiors at relatively low temperatures. As a star approaches the giant phase, the deepening of the convective envelope brings to the star surface material which was depleted in Li in the stellar interior. Such mixing of Li-depleted and unprocessed material causes an overall dilution of the Li abun-

dance at the star surface. Assuming that a star is born with a meteoric Li abundance ($A_{\text{Li}} \sim 3$ dex), standard models predict that in giants the Li abundance should not exceed ~ 1.5 dex. Yet, about 1–2 % of K giants have Li abundances exceeding this value. A few of them even have a Li abundance similar or larger than the meteoric value.

The occurrence of Li-rich stars is usually explained in terms of a Li-production mechanism (Cameron & Fowler, 1971) in the stellar interior associated with a circulation mechanism to bring the produced Li to the star surface. However, a complete theory capable of explaining all the observational facts is still missing and particularly puzzling is the case of low-mass stars (e.g., Charbonnel & Balachandran, 2000; Uttenthaler et al., 2007).

For this reason, in parallel with improving models, data are being collected to construct a more complete observational picture. The Li abundance is routinely measured using the doublet at 6707.8 Å. To test the feasibility of such a measurement, we took spectra of three stars with different equivalent width (EW) of the Li doublet. The extracted and continuum-normalised spectra are shown in Figure 3, with signal-to-noise ratios better than 50. Clearly EWs of the Li line down to 300 mÅ can be easily measured, while the star with a 200 mÅ line is more ambiguous, because of its late spectral type. The doublet is probably detected, but a confirmation with an earlier type star is needed.

Rotation curves of spiral galaxies

Rotation curves of spiral galaxies are used to study their kinematics, in the search for the amount and distribution of dark matter (DM), which are constrained by departures from the expected velocity curve of a rotating disc. The rotation

Grism	Lines/mm	λ_{min}	λ_{cen}	λ_{max}	RS	nm/px	FWHM	Binning	Slit	Table 1. Parameters of VPHGs provided by the ULTRASPEC team. Wavelengths are measured in nm.
#19/475	1557	444	478	511	3200 ¹	0.034	0.15	1	0.5"	
					3200	0.067	0.15	2	0.5"	
					2200	0.067	0.21	2	1.0"	
#20/656	1070	605	660	714	3400	0.055	0.20	1	0.5"	
					3000	0.108	0.22	2	0.5"	
					2000	0.109	0.33	2	1.0"	

¹ A resolution greater than 4000 is found by Vik Dhillon with Ultraspec; investigations are ongoing to see whether EFOSC2 can match this performance.

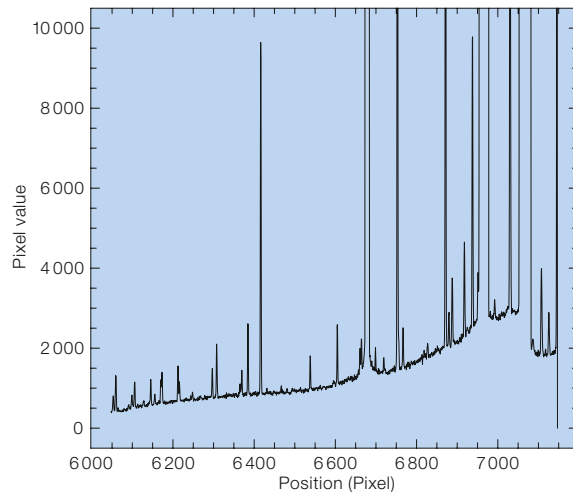
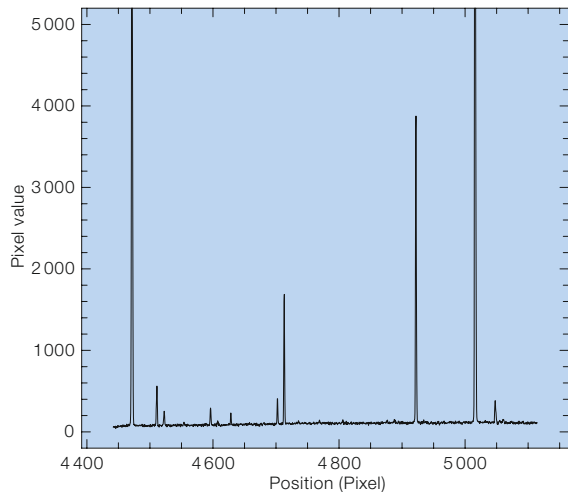


Figure 1. Wavelength-calibrated spectra of the Helium + Argon arc lamps taken with the blue VPH grism (left) and the red VPH grism (right). The high background in the red arc can be reduced by decreasing the exposure time of the He lamp.

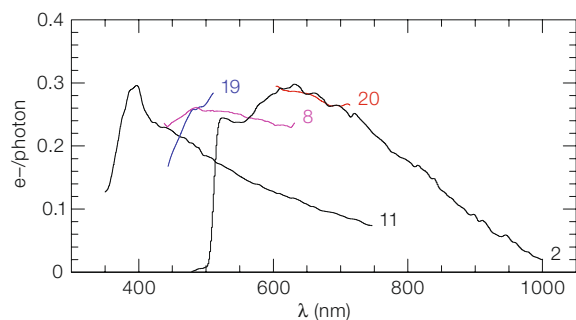


Figure 2. System efficiency given by the blue VPHG #19 (blue curve) and the red VPHG #20 (red curve) compared to that of other EFOC2 grisms.

curves also offer clues on the role of interactions and their impact on evolutionary histories. Galaxy evolution in general can also be explored by comparing rotation curves of distant galaxies with those of nearby objects.

Rotation curves derived from emission lines, and in particular those of $H\alpha$ and $[NII]$ are particularly useful to derive the mass distribution in disc galaxies, because they trace the motion of interstellar gas of the young population (HII regions). This gas has a velocity dispersion (of the order of 5–10 km/s) that is much smaller than its rotational velocity, allowing accurate measurements. Among spiral galaxies, giant spirals seem to be the best laboratories to study the structure and kinematics (see Figure 5). They have extended discs and rotational velocities up to ~ 400 km/s. Through their rotation curves we can study the angular

momentum properties and the DM distribution on the 100 kpc scale.

To measure rotation curves of giant spiral galaxies we took spectra of two objects with the red VPHG. A 1200-sec exposure was made of the giant spiral UGC 5711, with the slit oriented along its major axis (see Figure 4). A portion of the 2D spectrum near $H\alpha$ is also shown in Figure 4. The differential velocity can easily be seen on the frame, and the rotation curve is plotted in Figure 5 out to ~ 30 kpc. The figure shows that the systemic velocity is compatible with that of the RC3 catalogue, and that the precision we obtain is comparable to that of standard studies of this kind.

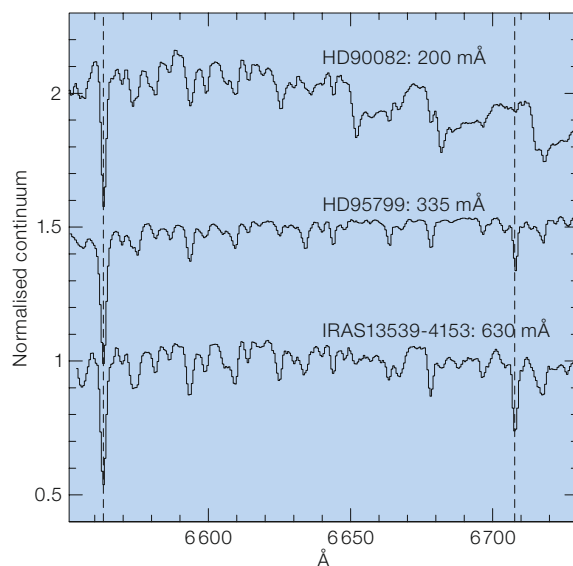


Figure 3. A portion of the spectrum of three stars with different EWs of the lithium doublet at 6707.8 Å (see the labels above each spectrum). The spectra have been obtained with the red VPHG, and the dashed vertical segments mark the position of $H\alpha$ (left) and the Lithium doublet (right).

The same exercise was done with PGC 048532, whose rotation curve is also displayed in Figure 5. As for UGC 5711, the quality of the data is very good out to 10 kpc. For this galaxy, Yegorova et al. (2008, in preparation) obtained an independent rotation curve with a 2×2000 sec spectrum collected with grating 6 of the EMMI/REMD arm. The resolution was 4900 with a slit width of $1''$. The resulting rotation curve is shown with open circles in Figure 5. It is clear that the two curves are consistent with each

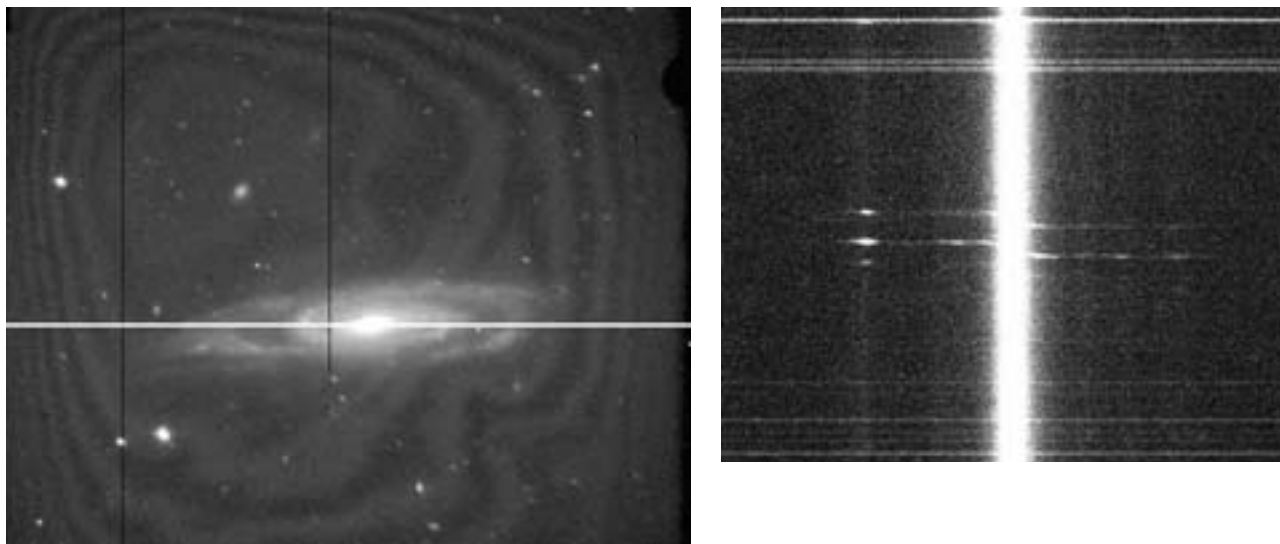


Figure 4. The left panel contains the acquisition image of UGC 5711 in white light, showing the location of the slit across the galaxy. The right panel shows the wavelength-calibrated and distortion-free spectrum in the region of $H\alpha$. The wavelength increases upward.

other, demonstrating the suitability of the red VPHG for this kind of study. Moreover, the EFOSC2 result was obtained in a 70% shorter exposure time.

Caveats

To make the best use of these grisms, users must be aware of the following issues. The flat-fields of both grisms show gradients in the cross-dispersion direction. These gradients are also wavelength-dependent, which means that the response functions depend on the position along the slit. For point sources, an accurate flux calibration then requires the spectrum of spectrophotometric stand-

ards to be obtained in the same position as the targets. For extended sources the spectrophotometric standards should be placed in different positions across the CCD, or corrections to some fiducial response function should be obtained based on flat-fields. Second order contamination is apparent in the red grism for $\lambda > 6800 \text{ \AA}$, so it is advisable to use order-sorting filters to cut out the blue flux, if flux calibration is an issue for the science case. Note also that the spectral range of the blue grism does not reach the Mg triplet at 5200 \AA or the G-band at 4300 \AA . However, using the movable slit we verified that the two features can be reached with a slit offset of 15 mm in either direction (the dispersion is 14.5 \AA/mm). Therefore two additional sets of slits were made, with 15 mm offsets to the blue and to the red, with respect to a central slit. They can be used to cover a more interesting blue spectral range, by merging two spectra.

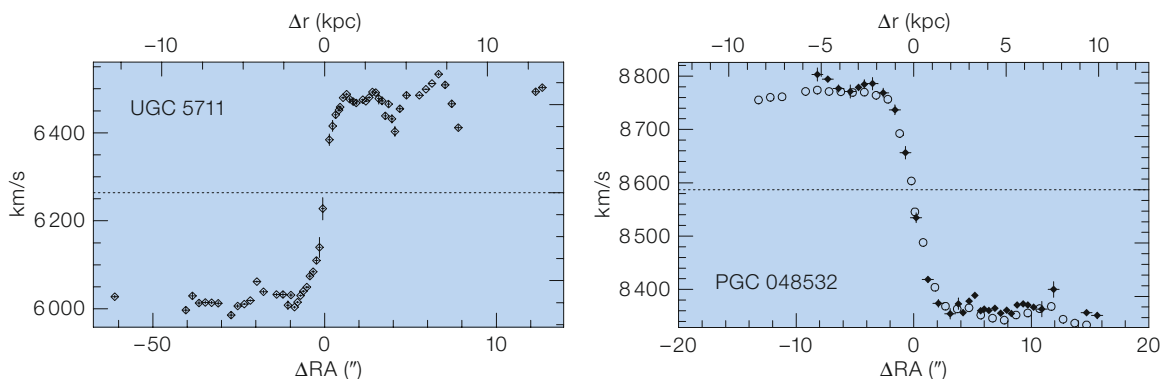
Acknowledgements

We thank Irina Yegorova and Alessandro Pizzella for computing the kinematic data of the spiral galaxies.

References

- Cameron, A. G. W. & Fowler, W. A. 1971, *ApJ*, 164, 111
 Charbonnel, C. & Balachandran, S. C. 2000, *A&A*, 359, 563
 Dhillon, V., et al. 2007, *The Messenger*, 127, 41
 Uttenthaler, S., Lebzelter, T., Palmerini, S., et al. 2007, *A&A*, 471, L41

Figure 5. Left: The rotation curve of UGC 5711 measured with the red VPHG. The dotted line shows the recession velocity of 6264 km/s from RC3. Right: The rotation curve of PGC 048532 measured with the red VPHG (filled diamonds + error bars) compared to the result (open circles) obtained with EMMI by Yegorova et al. (2008, in preparation). The dotted line shows the recession velocity of 8587 km/s from RC3. The physical radii have been computed assuming $H_0 = 72 \text{ km sec}^{-1} \text{ Mpc}^{-1}$.



The ALMA Antenna Transporter

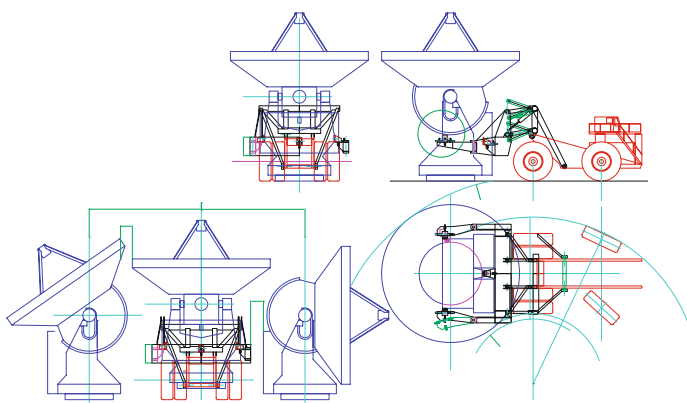
Max Kraus, Stefano Stanghellini, Pascal Martinez, Franz Koch, Martin Dimmler, Jean Michel Moresmau, Hans Rykaczewski (all ESO)

The ALMA observatory will consist of an array of 54 12-m diameter and 12 7-m diameter antennas. In order to configure the different array modes, it is necessary to move the antennas to different configurations. In the compact array configuration, the antennas are packed as closely as possible within a circle of 200 m diameter; in the extended configuration the antennas are spread over an area of about 15 km in diameter. The frequent relocations of antennas will be accomplished by two special vehicles, the ALMA Antenna Transporters. The challenges encountered during their development and their main characteristics are described.

Definition of requirements and interfaces

Already in the early design phase of ALMA, the basic requirements for the ALMA Antenna Transporters were defined. They should, for example, have rubber tyres and be capable of negotiating slopes up to 15%. Later more detailed requirements were added, such as the capability to move four antennas a day for array reconfiguration, or transport one antenna from the basecamp

Figure 1. Antenna transport CAD layout based on a mining dump truck. **Upper:** Front and side views of an antenna transporter. **Lower:** Close passage in central cluster is shown in side (left) and top (right) views.



to the observation site within one work shift of six hours. These requirements defined the transport capacity and led to the need for two transporters.

During the site selection phase, the geographical conditions related to transport were studied, since the roads are also a primary component of antenna transport. The cost of the roads easily exceeds the cost of the transport vehicle. It was decided early in the planning phase to build a dedicated road from the selected basecamp location (the Operations Support Facility, OSF) at 3000 m altitude up to the observation site (the Array Operations Site, AOS). The decision to build this road then allowed the definition of the road parameters to be fed into the specification for the transporter. Together with the site engineers the main road parameters were defined, with feedback from the basic parameters of the transporters (such as dimensions and weight). The second important and obvious component of the antenna transporters is their attachment to the antennas. After a first survey of possible industrial solutions for heavy transport vehicles and, in discussion with the teams developing the prototype antennas, the necessary details of attachment flanges on the antennas were defined.

A third important design consideration for an antenna transporter is the interface between the antenna and the foundation. After a transporter lifts off an antenna and sets it down on a foundation, the antenna is required to perform without realignment. The lifting and lowering mechanism of the transporter has to be designed such that reliable and precise loading/un-

loading to the antenna-foundation coupling can be achieved quickly and safely. The coupling interfaces were defined such that the various antenna types can use one standard interface.

Close cooperation was necessary with the scientists defining the antenna array configuration of the central cluster, where the antennas are placed as close together as possible. For efficient reconfiguration, and in case an antenna needs repair, it is necessary to carry antennas out of any location. After several iterations, transport passageways were designed into the antenna patterns to allow any antenna to be reached efficiently. The tolerance on the passageways limited the maximum dimensions of the transporter. The early definition of the interfaces and main parameters was a necessary process in order to allow the Call for Tender for industrial contracts for the transporters to be drafted.

Early concepts

In parallel with the discussion and definition of requirements, the available industrial solutions for heavy transport in the class of 50 to 100 tons were studied. Already proven industrial concepts were preferred in order to reduce development risk and cost and achieve a more reliable transport concept. First ideas were based on mining dump trucks or a mobile crane (see Figures 1 and 2).

Figure 2. Transporter concept using a large mobile crane (to be used in combination with rented transport vehicles).

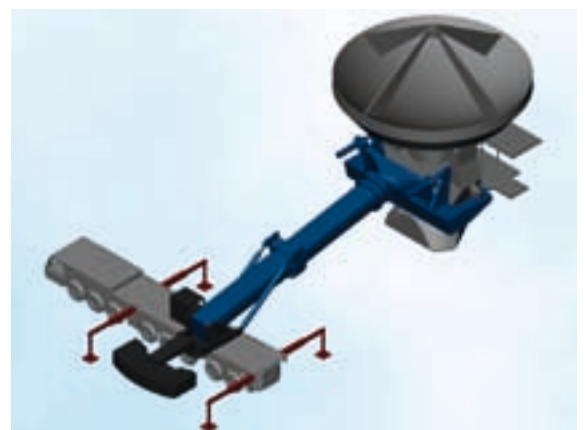




Figure 3. Advanced transporter concept based on an industrial dump truck, which is shown on the right.

Further studies showed that a transport concept requiring a minimum road width and low wheel loads is the most economic, since the majority of the investment costs for antenna transport would go into road construction, not into vehicle production. This resulted in a concept derived from a so-called ‘slag pot carrier’ used in the metallurgy industry and consisting of a prime mover and a load trailer (see Figure 3). This concept was further developed and later investigated by two industrial feasibility studies. These studies confirmed the feasibility of this early ESO concept, but



Photo: Scheuerle Fahrzeug GmbH

one of the studies showed that a hydrostatic drive for all wheels, instead of just the prime mover, has advantages: the total vehicle weight is reduced and the traction on critical road conditions is improved. A vehicle with a U-shaped frame and a large number of hydrostatically driven wheels was selected as a baseline concept (Figure 4) for the tendering process carried out by ESO.

Specification, tendering and contract

From the internal studies and the two industrial studies, sufficient material was collected to write a detailed technical specification for the ESO tendering process. Before the production antenna con-



Figure 4. Transporter design with hydrostatically driven wheels.

tracts were signed, a common antenna transport interface was designed at ESO and agreed with all teams involved in the antenna design. With the specifications all agreed, the tendering process could be started and resulted in a contract with the German company Scheuerle Fahrzeugfabrik GmbH (www.scheuerle.com). Scheuerle is a world market leader in hydrostatically propelled module and shipyard transporters and regularly builds transporters with capacities of 1000 tons or more. Loads up to 16000 tons have been successfully moved with their equipment. Scheuerle has all the required de-

Photo: A. Schilling, Scheuerle Fahrzeug GmbH



Figure 5. Transport with dummy load during loading sequence test.



Figure 6. Both transporters parked at the OSF at the end of acceptance.

sign capacity in-house and collaborates closely with an established network of suppliers of major components, such as Deutz AG for the engines, Mannesmann Rexroth AG for the hydraulic drive system or Kessler & Co GmbH for the axles with brakes. At the Scheuerle premises in Pfedelbach near Heilbronn (Germany), the required manufacturing, assembly and testing facilities were all available.

Design challenges

In the early design phase a promising vehicle concept was quickly developed based on the results of the bidding process. But it soon became clear that the selected concept could not easily be realised, because the layout relied on large wheels with tyres from the earth-moving industry. These very large tyres were sold out at that time and no supplier could be found who could provide the tyres reliably within the required delivery time of about 15 months. As a consequence, a new vehicle layout had to be developed, calculated and investigated based on a larger number of smaller wheels which were available in the required production schedule.

Another challenge addressed during the design and production phase was the operation of the vehicle at the very high altitude of 5 000 m. Little experience exists in the relevant industries with machines operated under these conditions and most major components are rated for altitudes not exceeding 3 000 m. Special sub-contracting conditions were necessary to ensure operation under the required environmental conditions. The high altitude with the reduced oxygen content also affects humans with the consequence of reduced physical and men-

tal capacities. Handling and transporting heavy loads is always dangerous and special care and experience is required. To allow safe operations under the high altitude conditions, various safety interlocks and supervision systems have been developed and built into the control system of the transporters to prevent dangerous operations when commanded by the operator.

Transporter design features

For the final design, an open U-frame layout was selected. On top of the vehicle is the loading system with two ramps which slide the antenna, after pick-up, to the centre of the vehicle. This design allows a relatively low weight of the vehicle and distributes the antenna weight evenly on the axles during driving. The loading system has two x-y-tables on each side which take the antenna on two dedicated brackets mounted permanently on the antenna transport flanges. These x-y-tables can position the antenna precisely on top of the station before setting down. Strong pins and automatic clamps block the x-y-tables during transport to secure the antenna.

On top of the frame are two identical engine units to power the transporter and a generator unit to supply the antenna with electric power during transport. This latter is necessary to maintain the cryogenic cooling of the antenna which remains operational during transportation and avoids warming up of the cooled



Figure 7. Fast downhill test drive on the road between the OSF and AOS.

detector systems. Both engine units are redundant and allow operation at reduced speed with one engine only (see Figure 9). All critical components are concentrated in the engine unit, which can be replaced within a few hours in case of fault or for maintenance.

Below the frame is the driver cabin for two persons. This position was selected for safety reasons because all the wheels, and the edge of the road, are in the direct field of view of the driver. It is equipped with all controls and monitors for the cameras mounted on all corners and other critical areas of the vehicle. During the loading process and in other critical situations, the vehicle can also be operated from a remote control panel with fail-safe radiolink. Except for the safety functions of the service brake and the emergency stop system, all functions of the transporter are controlled via computers and specially developed software.

The wheels are mounted in pairs on bogies with swing axle and hydraulic support. All bogies are identical to facilitate maintenance. In case of a failure of one bogie the faulty bogie can be lifted and operation can be continued with reduced speed. The transporters are also equipped with a vehicle positioning system and an anti-collision system. The positioning system consists of a rotating laser installed on the antenna foundations and laser sensors on the vehicle. The sensors guide the driver to the final unloading position with a precision of a few centimetres. The anti-collision system consists of four laser scanners and a numbers of ultrasonic sensors. The laser scanners detect the structures of nearby antennas before the driver comes too close to them and would stop the transporter, after a warning, to avoid collisions. Both systems will ensure safe operation also under the difficult high altitude conditions.

Technical data

Weight (empty): 132.5 tons
 Max. payload: 115 tons
 Engine power main engines: 2 × 500 kW
 (2 × 320 kW @ 5 000 m)
 Electric power generator: 100 kW
 (ca 50 kW @ 5 000 m)

Fuel capacity: 2 × 1500 l, diesel
 Wheels: 28 × 6.00 R20 (1.35-m diameter) on 14 axles
 Three brake systems:
 – Emergency and park brake: spring operated (hydraulically opened) on all wheels
 – Service brake: oil immersed multiple disc brakes on all wheels with oil circulation
 – Continuous brake: engine brake with exhaust flap on all engines
 Drive system:
 – 2 pumps with variable flow rate on each engine
 – 1 hydrostatic oil motor in each axle
 – Differential lock and overdrive protection in each axle
 – Max speed unloaded: 20 km/h (software limited)
 – Max speed loaded: 12 km/h
 – Speed limit with overspeed protection depending on road slope
 – Max slope: 15 %
 Steering system:
 – Steering angle +/- 70 deg hydraulically actuated on each axle
 – Electronically controlled by a safety certified system
 – 4 selectable steering programmes

Support system:
 – Hydraulic support with 600 mm vertical stroke on each axle
 – Interconnected to 3 groups for isostatic support
 – 2 additional outriggers for loading
 Loading system:
 – Loading time: < 20 min
 – Unloading time: < 20 min
 – Antenna adjustment on foundation: > 150 mm in all directions

Damping system

During the specification of the interface between antenna and transporter, the maximum possible oscillation of the antenna during transport was carefully studied. The antenna is a piece of precision mechanics requiring delicate alignment of the reflector surface. Investigations concluded that preparatory studies could not be performed because the outcome depended primarily on the performance of the tyres, and no reliable tyre data could be obtained from the manufacturers. Therefore the problem could only be solved at that stage by adopting conservative estimates and specifying large



Figure 8. Uphill test drive with dummy load on road between OSF and AOS.

Photo: A. Schilling, Scheuerle Fahrzeug GmbH

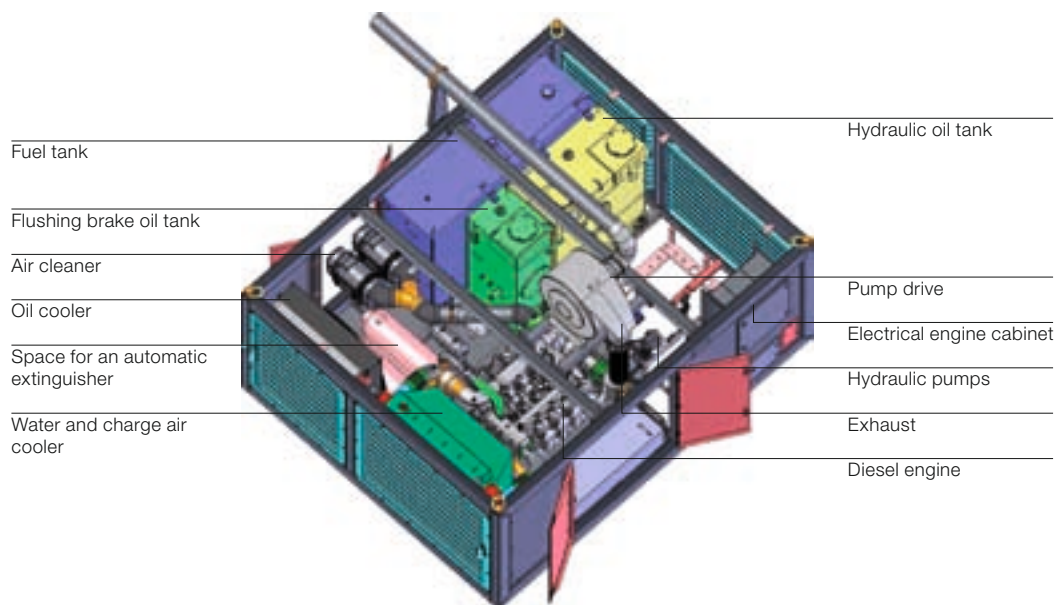


Figure 9. One of two installed engine units. Each unit is self-sufficient and can be quickly changed in case of problems. One unit is capable of moving the transporter in cases of emergency. (Figure: Scheuerle Fahrzeug GmbH)

margins in the interface control document. The experience at ESO in calculating and specifying earthquake loads from the VLT were very helpful in this study.

Provisions for adding a damping system in the transporter specification were defined, but the damping system was excluded from the contract since the specialist know-how for simulation was not available in the relevant industries. Later in the project, when the design was finished and the entire vehicle performance data were available, further studies could be conducted by ESO on this subject. It became evident that under certain road conditions with a washboard profile, dangerous excitations of the vehicle and the antenna could occur. Consequently a damping system was necessary. Using the ESO capabilities for dynamic simulations, usually employed for simulating the performance of telescope systems, the damping behaviour of the transporter was simulated and the components for a damping system were identified. With the help of the Scheuerle engineers, the

final system was designed and implemented just before the vehicle left the factory.

Into operation

Although only an auxiliary logistic system for the ALMA observatory, with technologies coming from completely different areas compared to the other components of ALMA, the transporters are fundamental for the achievement of the scientific objectives of the observatory. High reliability and availability of the transporters are essential for minimal observatory down time. With the early collaboration between ESO, the international ALMA partners and industry, good technical solutions could already be developed and realised in the project definition phase. The anticipation of potential problems and the configuration control of interfaces and specifications has allowed parallel and undisturbed development of antennas, transporters and the site infrastructure.

The first ALMA Antenna Transporter was completed in July 2007 (see ESO PR 32/07) and given the name “Otto” at a naming ceremony at the Scheuerle factory (see ESO PR 45/07). The second transporter was completed shortly after and was named “Lore”. Both transporters were then shipped to Chile and arrived at the OSF on 14 February 2008. They were successfully commissioned at the OSF in the following months and will enter service moving the first antennas, which are currently being commissioned at the OSF, to the Chajnantor plateau.

References

Haupt, C. & Rykacewski, H. 2007, *The Messenger*, 128, 25

Cute-SCIDAR at Paranal for E-ELT Site Characterisation

Héctor Vázquez Ramío¹
 Marcos Reyes¹
 José Miguel Delgado¹
 Elvio Hernández¹
 Miguel Núñez Cagigal¹
 Jesús J. Fuensalida¹
 Gianluca Lombardi^{2,3,4}
 Frédéric Derie²
 Julio Navarrete²
 Marc Sarazin²

¹ Instituto de Astrofísica de Canarias,
 Spain

² ESO

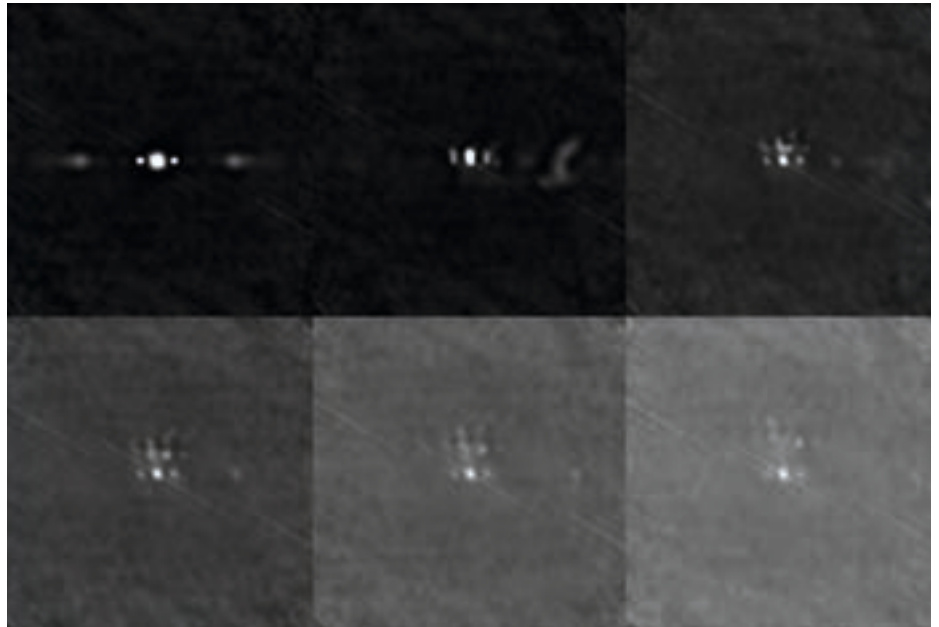
³ National Institute for Astrophysics,
 Bologna Astronomical Observatory, Italy

⁴ University of Bologna, Department
 of Astronomy, Italy

A new version of the cute-SCIDAR instrument, which employs the generalised SCIntillation Detection And Ranging technique to obtain detailed atmospheric turbulence profiles with height, has been designed, developed and tested by the Instituto de Astrofísica de Canarias. The instrument was developed to match the requirements of the ESO VLT Auxiliary Telescopes, within the framework of the European Extremely Large Telescope site characterisation project. Commissioning at Paranal was successfully carried out in November 2007. This upgraded version of the original instrument, presently working at the Roque de los Muchachos Observatory, allows g-SCIDAR turbulence profiles to be obtained in real time, a novel achievement in site testing and also a crucial tool for the optimum design and operation of Adaptive Optics and Multi-Conjugate Adaptive Optics systems.

The SCIDAR technique

SCIDAR, SCIntillation Detection And Ranging, has proved to be the most efficient and reliable technique to accurately measure the optical vertical structure of the atmospheric turbulence strength from ground level. The concept (Vernin & Roddier, 1973) and technique come from the original one developed since the 80's by Jean Vernin, Max Azouit and collaborators at Nice University (Vernin &



Azouit, 1983; Vernin & Muñoz-Tuñón, 1992). The method consists of the acquisition of a large number of images with very short exposure time (typically from 1 to 3 ms, depending on the object and the desired signal-to-noise ratio) of scintillation patterns produced by a double star. The average autocorrelation function computed from these images shows a linear sequence of peaks corresponding to the different turbulent layers. The distance between each peak and the centre gives information on the height of the turbulent layer (see example in Figure 1).

Initially, the *classical* SCIDAR was unable to sample the layers closest to the ground. However a smart modification of the technique (Fuchs, Tallon & Vernin, 1998) consisted in placing the analysis plane not in the pupil plane but in a conjugated plane located a few km below the former. This development thus allowed the measurement of the turbulence intensity from ground to about 25 km height. This version of SCIDAR is known as generalised-SCIDAR (g-SCIDAR).

In practice, the implementation of such a technique requires a minimum telescope diameter of approximately 1 m. So, performing routine measurements using g-SCIDAR at a particular observatory requires the use of significant resources. However, g-SCIDAR provides extremely valuable information regarding the optical

Figure 1. Top left: Normalised autocorrelation of a series of scintillation pattern images of a binary star; two turbulent layers can be distinguished clearly. From the 2D autocorrelation, the structure constant of the refractive index with height, $C_n^2(h)$, can be derived. The second to the sixth frames (left to right, top to bottom) show the cross-correlations between two scintillation pattern images: cross-correlations between an image and the ensuing correlation image (upper centre), the second consecutive image (upper right), and so on (bottom row). From these 2D cross-correlations, wind velocity, $V(h)$, can be inferred.

atmospheric turbulence, in particular the knowledge of $C_n^2(h)$ (the structure constant of the atmospheric refractive index with height) and the wind profile (horizontal velocity of the layers) with a vertical resolution better than 500 m. Many essential parameters such as seeing (ϵ), Fried's parameter (r_0), coherence lengths and time of the wave fronts, isoplanatic angles (θ_0), etc. can be computed from g-SCIDAR data. The wind speed and direction with height $V(h)$ can be retrieved by analysing the 2D cross-correlation functions from consecutive mean normalised images (see Figure 1).

Cute-SCIDAR since 2002 at the Canary Islands

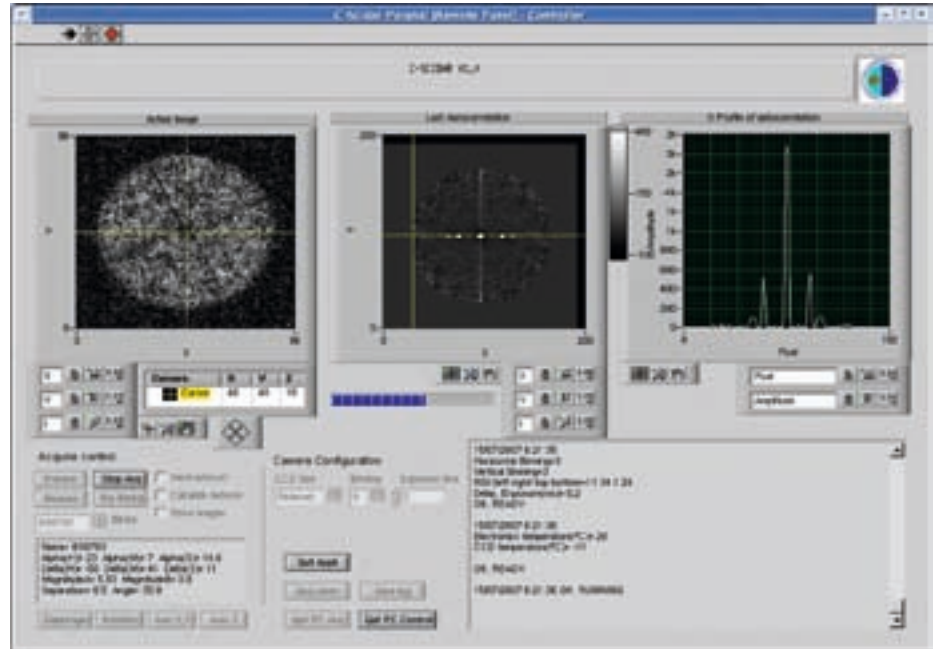
Since 2002 campaigns have been carried out by the IAC staff (Fuensalida et al., 2004a; Fuensalida et al., 2004b, Fuensalida et al., 2007) at their observa-

ories: the Observatorio del Teide (OT) on Tenerife island and the Observatorio del Roque de los Muchachos (ORM) on La Palma island, both in the Canary Islands. In order to perform routine observations, two g-SCIDAR instruments were designed and manufactured to fit the particular specifications of the telescopes which had to house them. They were Telescopio Carlos Sánchez (TCS) at the OT with 1.5 m diameter, and the Jacobus Kapteyn Telescope (JKT) belonging to the Isaac Newton Group of Telescopes at the ORM with 1 m aperture. Both systems implement the g-SCIDAR technique and include remote operation with facilities for conjugated plane positioning, spatial (X, Y) positioning (centring), a rotating system to adjust the direction of the pixel grid to the observed binary axis, etc. The remotely operated instrument is called cute-SCIDAR (c-SCIDAR).

The high resource cost entailed by the monitoring of the turbulence with quite high resolution justifies the development of an instrument with few constraints. The plans for a long campaign of measurements of the vertical structure of the turbulence in the ORM and OT observatories has encouraged us to build an instrument with high performance and minimal operational overheads. With this experience, we have been able to develop a new version for the Paranal Observatory, within the European Extremely Large Telescope Design Study (Contract 011863 with the European Commission) which was supported by the European Community (Framework Programme 6, E-ELT Design Study).

C-SCIDAR at the Paranal Observatory

The c-SCIDAR/Paranal is a fully automatic instrument. This means a complete automation of both displacement of optical elements and rotation of the instrument itself. These movements are controlled by a user-friendly interface (Figure 2). Moreover, a custom-made software package performs fast data acquisition and processing, which can provide the turbulence profiles in real time, with and without the turbulence contribution of the dome. As a consequence, alignment and observation procedures are facili-



tated with minimal effort in the dome. The instrument, based in the original g-SCIDAR concept of the Nice University, was conceived to work in the coudé focus of one of the 1.8-m Auxilliary Telescopes (ATs) of the VLT. The coudé focus is available in the focal station through the Upper Relay Optics Structure (UROS), which becomes the interface between the AT and c-SCIDAR (see Figure 3).

The main features of c-SCIDAR/Paranal can be summarised as follows:

- Mechanical and electronic matching to the UROS/AT interface.

Figure 2. Snapshot of the c-SCIDAR/Paranal GUI. The image on the left shows the scintillation pattern of a binary star. The normalised autocorrelation function can be seen in the middle frame, while the right panel shows a cut of the autocorrelation along the binary axis.

- The instrument has its own cooling system.
- Power supplies of the different systems are remotely controlled.
- Operation and data acquisition is fully remote by means of a user-friendly Graphical User Interface (GUI).
- Reduction of raw data is performed at a rate that is higher than that of the



Figure 3. Left: The cute-SCIDAR/Paranal attached to the AT4 crane, during the November 2007 commissioning. Upper: The original mechanical design of the instrument.

observations, so allowing the profiling of the optical vertical turbulence in real time (see Figure 4).

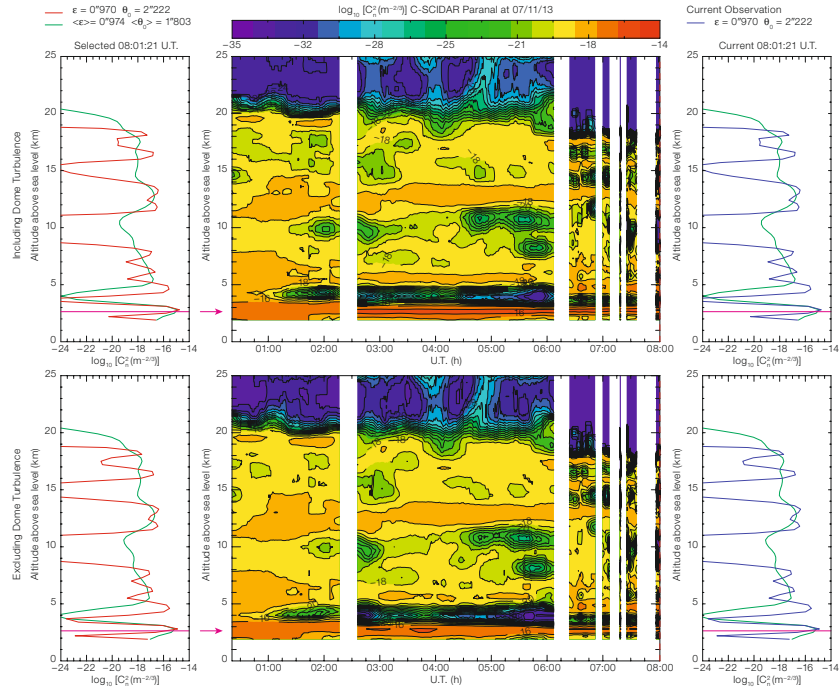
These design features lead to a high temporal efficiency during the observing campaign as well as providing an essential tool in order to optimise the efficiency of Adaptive Optics (AO) and Multi-Conjugate Adaptive Optics (MCAO) systems.

Regarding the c-SCIDAR mechanisms, the camera is attached to three movable stages which allow its movement along X, Y and Z directions. The Z axis is employed both to determine the position of the pupil plane and the focus (a single star allows the state of collimation of the beam to be easily verified), but is mainly used to fix the conjugated plane where the observations will take place. The X and Y direction stages are devoted to the centring of the camera in the XY plane, correcting small displacements in the observation plane produced by flexure. The maximum range in the X and Y directions is 25 mm, whilst in Z it is 100 mm. An iris mechanism – an adjustable aperture diaphragm placed in the focal plane – facilitates the centring of the pupil image of the double star onto the camera field of view; the M6 mirror of the AT also plays an important role in this particular procedure. Finally, a rotator mechanism allows the rotation of the instrument as a whole in a range from 0° to 270°, thus permitting the orientation of the binary star axis with the array of the CCD camera.

All the observations and data analysis procedures applied to this upgraded version are the result of the development work carried out during the last few years by the IAC with the previous instruments at the Canaries Observatories. ESO will now operate the Paranal instrument and take care of the measurements while the IAC SCIDAR team will continue collaborating with ESO, within the FP6 Site Characterisation WP, on the data validation and analysis.

Present status

Cute-SCIDAR/Paranal was successfully commissioned during November 2007 by the IAC team with the collaboration of the Paranal staff. In principle, regular long



runs were planned to be performed for the duration of the FP6 contract. Actually they took place just after the commissioning period during a week in November and later, during 10 nights in December. No new campaigns have been carried out since then due to the lack of a free UROS (since the one initially devoted to SCIDAR was re-assigned to PRIMA).

References

Fuchs, A., Tallon, M. & Vernin, J. 1998, PASP, 110, 86
 Fuensalida, J. J., Delgado, J. M., García-Lorenzo, B., et al. 2004a, in *Second Backaskog Workshop on Extremely Large Telescopes*, eds. A. L. Ardeberg and T. Andersen, Proc. SPIE, 5382, 643

Figure 4. Output in real time of the profiles during an actual observing night. The central part is a representation of $C_2^2(h)$. The contour plots are updated in real time during the observation. The upper contours represent turbulence intensity with dome seeing included, while the lower panel shows the same but excluding dome turbulence (the white vertical gaps are associated with a change of object). The left and right columns of the panel show individual vertical profiles: green is the average profile, navy corresponds to the last profile, and red to the particular profile chosen with the cursor.

Fuensalida, J. J., Chueca, S., Delgado, J. M., et al. 2004b, in *Advancements in Adaptive Optics*, eds. D. Bonaccini Calia, B. L. Ellerbroek and R. Ragazzoni, Proc. SPIE, 5490, 749
 Fuensalida, J. J., García-Lorenzo, B., Delgado, J. M., et al. 2007, *Rev. Mex. Astron. Astrof.*, 31, 86
 Vernin, J. & Roddier, F. 1973, *J. Opt. Soc. Am.*, 64, 270
 Vernin, J. & Azouit, M. 1983, *J. Opt. (Paris)*, 14, 131
 Vernin, J. & Muñoz-Tuñón, C. 1992, *A&A*, 257, 811



Figure 5. Picture taken at the moment when cute-SCIDAR/Paranal was providing real-time profiles for the first time during the scientific commissioning in November 2007.

An early VLT UT1 colour image made from VLT Test Camera exposures in *B*, *V* and *R* filters of the polar disc galaxy NGC 4650A (see ESO Press Photo 19/98).



The Antares Emission Nebula and Mass Loss of α Sco A

Dieter Reimers, Hans-Jürgen Hagen,
Robert Baade, Kilian Braun
(all Hamburger Sternwarte, Universität
Hamburg, Germany)

The Antares nebula has been known as a peculiar [Fe II] emission nebula, apparently without normal H II region lines. Long-slit VLT/UVES mapping shows that it is an H II region 3" in size around the B type star α Sco B, with a Balmer line recombination spectrum and [N II] lines, but no [O II] and [O III]. The reason for the non-visibility of [O II] is the low electron temperature of 4 900 K, while [N II] is seen because the nitrogen abundance is enhanced by a factor of three due to the CNO cycle. We derive a mass-loss rate of $1.05 \pm 0.3 \times 10^{-6} M_{\odot}/\text{yr}$ for the M supergiant α Sco A. The [Fe II] lines seem to come mainly from the edges of the H II region.

An iron rich nebula?

The story of the Antares nebula began in 1937 with the finding of O. C. Wilson and R. F. Sanford at the Mount Wilson Observatory that the spectrum of the B-type companion of Antares, itself an M supergiant, showed forbidden emission lines of Fe II. Later Otto Struve showed that the [Fe II] lines extend $\sim 2''$ beyond the seeing disc of the B star. Struve & Zeberg (1962) describe extensively the Antares nebula and conclude: "It is strange that the nebulosity around the B type component shows only emission lines of iron and silicon, but not those of hydrogen. The enormous abundance of hydrogen in all known gaseous nebulae and the conditions of excitation and ionization resulting from the radiation of a B type star would render it almost inexplicable for a gas of normal composition to show only the iron and silicon lines in emission. This gave rise to the hypothesis that the material in the vicinity of Antares is metal rich, in turn leading to the supposition that the envelope may be composed of solid substances such as meteors that have become vaporized and are excited by the radiation of the hot B star. This hypothesis is admittedly improbable and may have to be abandoned in the light of future work." We may add here that the mystery has lasted 45 years until, with

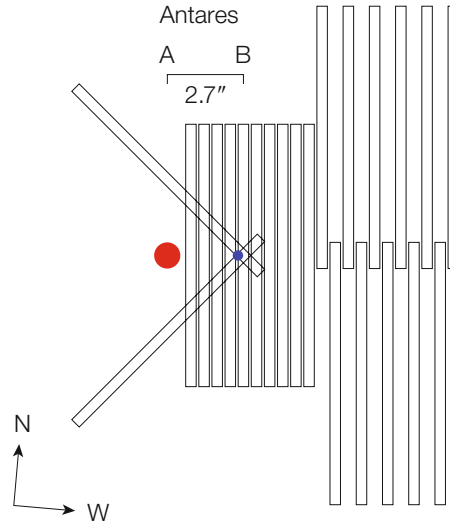


Figure 1. Geometry of the Antares system together with the UVES spectrograph slit sizes and positions shown to scale.

UVES/VLT spectra, the Antares nebula puzzle could be solved.

The most extensive previous study was that by Swings & Preston (1978) based on high-resolution long-slit photographic spectra taken with the Mt. Wilson 100" and Palomar 200" telescopes. They found that the '[Fe II] rich nebula' is strong roughly 3.5" around the B star and is surrounded by a zone of weaker lines which may extend in a NW-SE direction up to 15". However, they neither observed Balmer recombination lines nor any classical H II region lines from ions like O II, O III, S II, and N II. Therefore the nature of the Antares nebula could not be understood. In a first quantitative study of the Antares system it could be shown that the B star creates an H II region within the wind of α Sco A and that the [Fe II] lines must be formed in this H II region (Kudritzki & Reimers, 1978). Later the H II region was detected as an optically thin radio emitter with a diameter of $\sim 3''$ (Hjellming & Newell, 1983).

UVES 2-D spectroscopy

With the construction and operation of UVES at the VLT it was obvious that progress in our understanding of the kinematics of the Antares nebula should be possible with its high spectral resolution and high pointing accuracy, making pos-

sible a 2-D mapping of the nebula with long-slit spectroscopy. We used UVES with a 0.4" slit and a resolution of 80 000 and covered the nebula with 23 long-slit positions (Figure 1). Exposure times were between 50 and 100 s (the Antares nebula is bright!); the typical seeing was 0.6" which means that the angular resolution corresponds roughly to the slit steps as shown in Figure 1.

Quite unexpected was that all spectra – even 10" from the M supergiant – are completely corrupted by scattered light from the M supergiant. This was a surprise, also to the UVES team at ESO. ESO finally made a test placing the UVES slit 10" from a bright star – with the same result as in our spectra. Apparently, light from the bright star is scattered by the slit jaws back to the slit viewing camera and from there again into the spectrograph slit. This should be a warning for anybody using UVES on faint targets close to bright sources, e.g. a disc, around a bright star.

Did this mean that our spectra were useless? It meant that, due to the ubiquitous scattered light, no general background reduction was possible and no absolute line fluxes could be deduced. Data reduction required an enormous load of extra work. In brief, the scaled M star spectrum was used as a background template. The template was fitted to the spectrum – allowing for an offset and a scaling – outside a region of ± 30 km/s of each detected emission line and was finally subtracted from the data.

The final results after this elaborate data reduction – each of the roughly 90 detected emission lines had to be treated individually in each of the spectra – are 2-D brightness distributions (location on the slit versus velocity) as a function of the location relative to the M supergiant, as shown for the H α line in Figure 2 and for [Fe II] 4 814.55 Å in Figure 3.

A peculiar H II region?

The main puzzle of the Antares Nebula has been resolved by our UVES data. The Balmer recombination lines expected for an H II region: H α , H β ... up to H10 are present, and their geometrical extent on the sky is virtually identical to that of

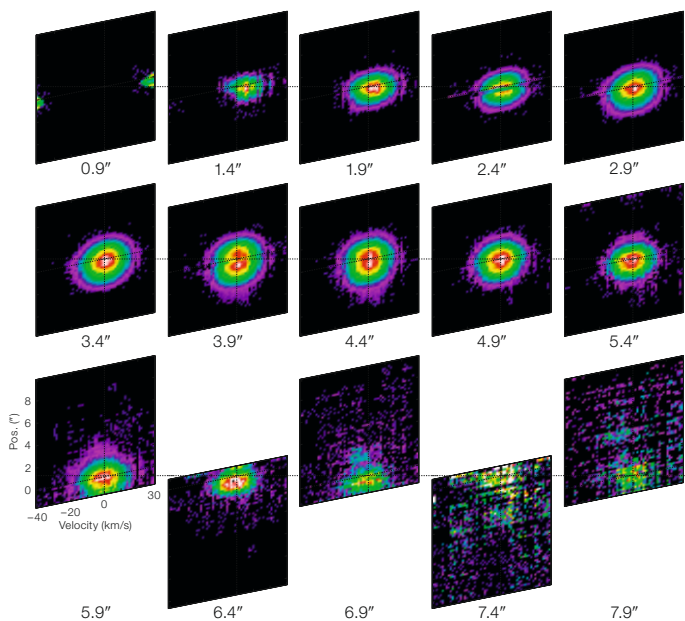


Figure 2. $H\alpha$ 2-D brightness distributions (location on the slit versus velocity) as a function of spectrograph slit position relative to α Sco A. Offsets from the position of α Sco A are shown in arcsec. Notice that due to the M star wind expansion, the velocity coordinate corresponds to the spatial depth (perpendicular to the plane of the sky). The density in the plots has been rescaled in order to provide maximum visibility. The true line fluxes vary by a factor of 150 between 1.9" and 7.9".

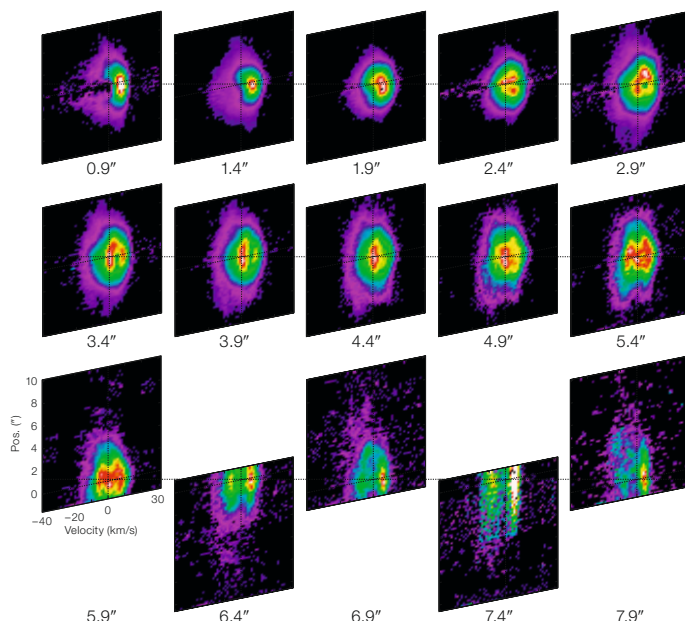


Figure 3. $[Fe II]$ 4814.55 Å 2-D brightness distributions as a function of spectrograph slit position (see caption of Figure 2). Notice the double structure is probably formed by the front (blueshifted) and rear (redshifted) edges of the $H II$ region carried by the wind to large distances from the system.

the radio emission seen with the VLA (Figure 4). So why have previous observations not shown the hydrogen lines? The reason is probably that the strongest lines $H\alpha$ and $H\beta$ suffered, in the Mt. Wilson and Mt. Palomar photographic spectra, from seeing-dominated contamination by the M supergiant and the signal-to-noise of the photographic spectra was never sufficient to enable an efficient background subtraction.

The strongest lines are of $[Fe II]$ such as 4287.4 Å, 4359.34 Å and 4814.55 Å. Altogether we have identified some 90 emission lines, besides $[Fe II]$ a few $[Ni II]$ and several strong allowed $Fe II$ lines like 3177.53 Å and 4923.9/5018.4/5169.0 Å (see below). Besides the $Si II$ lines 3856 and 3862 Å we have detected further $S III$ lines around 5050 Å and at 6347/6371 Å (for details and a line list cf. Reimers et al., 2008).

In all previous investigations of the Antares nebula the question remained open why the 'classical' emission lines

normally prominent in $H II$ region spectra like $[O III]$ 4959/5007 Å, $[O II]$ 3726/3729 Å, $[N II]$ 6583/6548 Å and $[S II]$ 6716/6731 Å had not been detected. Our UVES spectra allow a more critical assessment than earlier photographic spectra. The answer is that we do see faint $[N II]$ 6583 Å and 6548 Å lines, and that none of the other lines is present. $[N II]$ 6583 Å follows closely the $H\alpha$ distribution on the sky shown in Figure 2. Since it is close to $H\alpha$, we can measure the $H\alpha/[N II]$ 6583.4 Å ratio as a function of the location in the nebula. Close to the B star – in the middle of the $H II$ region – $H\alpha/[N II] \approx 3.5$ while 3" west of B, at the outer edge of the $H II$ region, it is ~ 10 .

For $[O II]$ we can give an upper limit: we have detected the Balmer line series up to H_{10} , but H_{11} (close to $[O II]$ 3726/3729) was not visible. Thus, the H_{10} intensity as predicted by recombination theory, can be regarded as an upper limit to $[O II]$ which yields $[O II]/H\alpha < 0.017$ for 3726 Å. So why is $[N II]$ present, while the lines of $[O II]$ and $[O III]$, usually stronger in $H II$

regions, are not? There are two reasons: a low electron temperature T_e and an enhanced N/O ratio. At first, the electron temperature T_e must be so low that the $[O II]$ lines are not excited and below the detection limit. We have modelled the $H II$ region created by α Sco B in the wind of the M supergiant using the Cloudy code (version 07.02.00, last described by Ferland et al., 1998). Since the B star, with an effective temperature of 18200 K, is relatively cool, the resulting electron temperature is below 5000 K which does not allow $[O III]$ to exist and predicts $[O II]/H\alpha$ below our detection limit. But the same model would also predict $[N II]$ below our detection limit! The solution to this problem is that Antares must have CNO-processed material in its atmosphere and wind. Indeed, it has been shown by Harris & Lambert (1984) that in the atmosphere of Antares ^{13}C and ^{17}O are enhanced, a clear indication of CNO cycle material. Unfortunately there is no direct measurement of the N abundance (or N/O). Typical values for the N enhancement in M supergiants of comparable luminos-

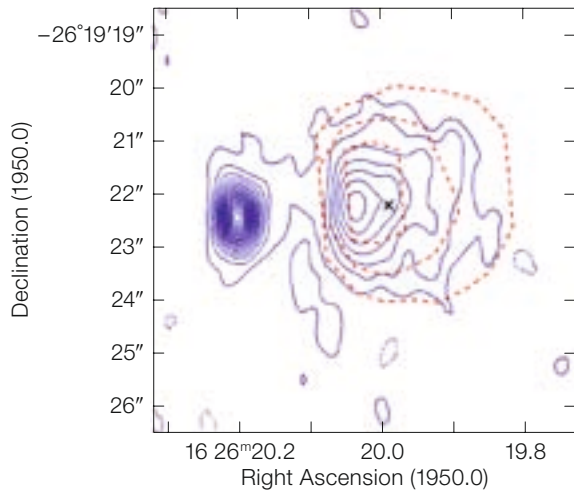


Figure 4. Comparison of the distribution of $H\alpha$ emission with radio free-free emission (Hjellming & Newell, 1983) (blue). Dashed red lines represent half, fourth, and tenth of the central $H\alpha$ emission flux.

ity are $[N/H] = 0.6$ (logarithmic abundance ratio relative to solar), while oxygen is slightly reduced, $[O/H] = -0.1$. Our best value for the nitrogen abundance determined independently from a fit of the Cloudy models to observed $[N_{II}]/H\alpha$ values is $[N/H] = 0.52 \pm 0.1$ with $[O/H] \leq -0.05$ which is fully consistent with the expectations.

Last but not least: the same Cloudy models with the above mentioned abundances show that metal line cooling of the H_{II} region is dominated by $[N_{II}]$ and collisionally excited $[Fe_{II}]$. This is at least part of the explanation for the strong $[Fe_{II}]$ spectrum of the Antares nebula.

[FeII] emission

The comparison of the distribution of the $[Fe_{II}]$ emission in position and velocity space with $H\alpha$ (Figures 2 and 3) shows distinct differences:

- The $[Fe_{II}]$ emission is not smoothly distributed like $H\alpha$ and $[N_{II}]$ but is apparently concentrated on the edges – the ionisation shock fronts – of the H_{II} region. The $[Fe_{II}]$ emission thus gives rise to a ring-like structure (extending up to $\sim 6''$ from Antares outside the H_{II} region itself), which ends roughly at $6''$, thus making a double structure. This ring-like and double-peak shape are apparent from the front and rear side of the H_{II} region respectively, where the red component (rear side) is always stronger. We notice in passing that the occurrence of $[Fe_{II}]$ in the Orion Nebula

has also been observed close to the ionisation front (Bautista et al., 1994).

- In addition to emission from the ionisation fronts there is apparently a further component (cf. Figure 3, 4'' to 6'' offset) in the centre of the H_{II} region. This is again consistent with our Cloudy simulations which show such a further maximum. We notice, however, that the 'central' $[Fe_{II}]$ emission varies strongly with slit position which may have its origin in a time-variable (episodic) supergiant wind. There is independent evidence, from both IR interferometric imaging of the immediate surrounding of Antares and from the multiple component structure of CS absorption lines seen in HST spectra of α Sco B (Baade & Reimers, 2007), for a time-variable wind.

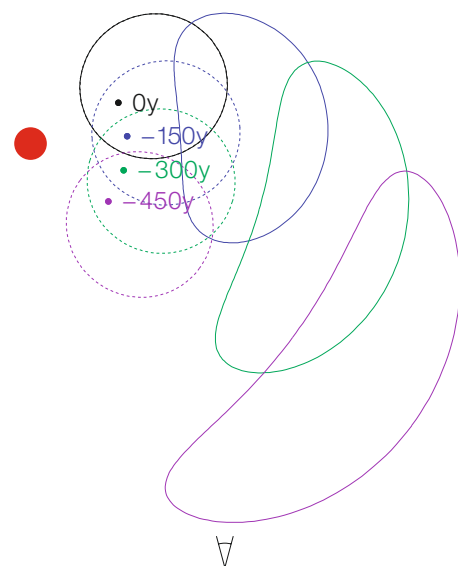
- Emission is clearly seen outside of the H_{II} region: beyond $5.9''$ west of A, the $[Fe_{II}]$ emission becomes more extended and more structured. In velocity space the $[Fe_{II}]$ emission moves in the mean from 4 km s^{-1} $1.9''$ west of A through 3 km s^{-1} at B to 0 km s^{-1} $5.9''$ west of A and $\sim -5.5 \text{ km s}^{-1}$ at $9.9''$ west of A.

Apparently we start to see here time-dependent effects: the M supergiant wind carries the structure imprinted by the H_{II} region ('shock fronts') to large distances from the system outside the H_{II} region, where hydrogen is again neutral. In addition, the systematic shift in velocity can be explained by a combination of B star orbital motion with wind expansion. An analysis of the orbit

shows that at present the B star moves nearly perpendicularly into the plane of the sky (Reimers et al., 2008) which, combined with wind expansion, produces a cometary structure (cf. Figure 5).

- The UVES observations with 45° slit position (Figure 1) confirm what Swings & Preston (1978) had seen, namely that faint $[Fe_{II}]$ emission is seen all along the slit, i.e. in the neutral M star wind. The explanation comes from the observation that one of the allowed lines, Fe_{II} 5169 \AA , appears both in the neutral wind (position $0.9''$ from the M star) and in the H_{II} region. Apparently one channel for the excitation of the forbidden $[Fe_{II}]$ lines is line scattering of B star photons in the strong UV resonance lines, which was first seen with IUE (Hagen et al., 1987). One of the strong UV resonance (scattering) lines in the UV spectrum of α Sco B is the Fe_{II} UV mult. 3 line at 2344 \AA , which shows a P Cyg type profile. In the case of the 2344 \AA line, a second downward channel exists via the Fe_{II} lines 4923 , 5018 , and 5169 \AA so that part of the

Figure 5. 'Look back' contours (solid lines) of H_{II} region borders in a plane perpendicular to the plane of the sky caused by the combination of wind expansion with orbital motion of α Sco B relative to α Sco A. Contours are shown for present and previous phases (-150 yrs to -450 yrs; 150 years being the wind travel time for the projected distance between A and B). This is a qualitative model for the cometary-like structure of the $[Fe_{II}]$ emission regions.



downward cascade is via these lines and this is what we observe – FeII 5169 Å in emission. This channel populates the upper level of the strongest [FeII] lines 4287 Å and 4359 Å. In conclusion, we have identified in detail from IUE and UVES observations the [FeII] excitation mechanism in the cold, neutral M star wind far outside the HII region.

Mass loss of α Sco A

The number of Lyman continuum photons and the wind density (mass-loss rate) determine the shape (size) of the HII region. At this time we have performed only static HII region model calculations assuming that the density structure is not grossly disturbed by the

HII region shock fronts – which is certainly an oversimplification. The geometry, i.e. the location of the B star and its HII region relative to the plane of the sky at the M supergiant, has been determined using the H α and [FeII] velocities as 23° behind the plane of the sky.

The best match of the Cloudy models with the observed H α intensity distribution (Figures 2 and 4) yields a mass-loss rate of $1.05 \times 10^{-6} M_{\odot}/\text{yr}$ with an uncertainty of $\pm 30\%$. This is a mean value over the crossing time of the wind through the HII region of roughly 150 yrs. We believe that the new value for the mass-loss rate is more reliable than (our own) previous measurements, mainly because the use of circumstellar absorption lines in the B star spectrum, formed in the vast circumstellar envelope of the M supergiant, suf-

fers from the episodic nature of mass loss (multicomponent absorption) and from the observation that dust depletion onto grains is important (Baade & Reimers, 2007).

References

- Baade, R. & Reimers, D. 2007, *A&A*, 474, 229
 Bautista, M. A., Pradhan, A. K. & Osterbrock, D. E. 1994, *ApJ*, 432, L135
 Ferland, G. J., Korista, K. T., Verner, D. A., et al. 1998, *PASP*, 110, 761
 Hagen, H.-J., Hempe, K. & Reimers, D. 1987, *A&A*, 184, 256
 Harris, M. J. & Lambert, D. L. 1984, *ApJ*, 281, 739
 Hjellming, R. M. & Newell, R. T. 1983, *ApJ*, 275, 704
 Kudritzki, R. & Reimers, D. 1978, *A&A*, 70, 227
 Reimers, D., Hagen, H.-J., Baade, R., et al. 2008, *A&A*, submitted
 Struve, O. & Zeberg, V. 1962, *Astronomy of the 20th Century*, (New York: MacMillan Comp.), 303
 Swings, J. P. & Preston, G. W. 1978, *ApJ*, 220, 883



Another early VLT image showing the high ionisation bipolar planetary nebula NGC 6302. This colour picture is a composite of three VLT UT1 Test Camera exposures through *B*, *V* and *R* filters, taken in June 1998. The extremely hot ($\sim 200\,000$ K) central star is hidden within the slender wisp of dust at the core of the nebula.

SINFONI Observations of Comet-shaped Knots in the Planetary Nebula NGC 7293 (the Helix Nebula)

Mikako Matsuura^{1,2}
 Angela Speck³
 Michael Smith⁴
 Albert Zijlstra⁵
 Krispian Lowe⁶
 Serena Viti²
 Matt Redman⁷
 Christopher Wareing⁸
 Eric Lagadec⁵

¹ National Astronomical Observatory of Japan, Tokyo, Japan

² Department of Physics and Astronomy, University College London, United Kingdom

³ Physics and Astronomy, University of Missouri, Columbia, USA

⁴ Centre for Astrophysics and Planetary Science, School of Physical Sciences, The University of Kent, Canterbury, United Kingdom

⁵ School of Physics and Astronomy, University of Manchester, United Kingdom

⁶ Science and Technology Research Centre, University of Hertfordshire, Hatfield, United Kingdom

⁷ Department of Physics, National University of Ireland Galway, Republic of Ireland

⁸ School of Mathematics, University of Leeds, United Kingdom

Cometary knots in the planetary nebula NGC 7293

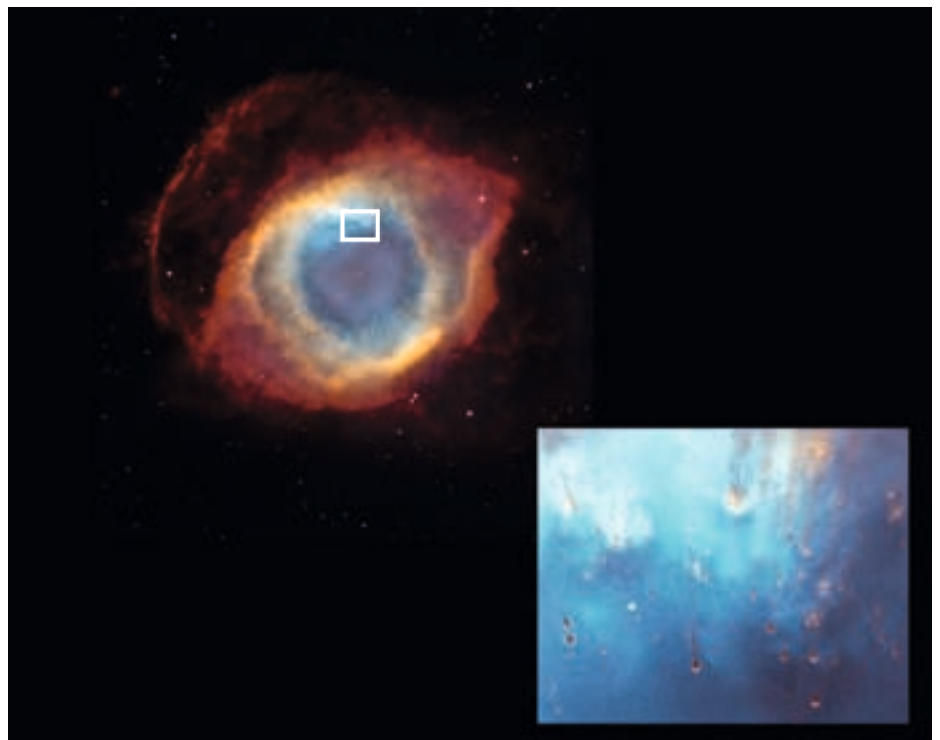
The Helix Nebula (NGC 7293; Figure 1), located at 219 pc (Harris et al., 2007), is one of the closest planetary nebulae (PNe). The diameter of the entire nebula is approximately a quarter of the size of the full moon. This proximity enables a study of the detailed structure inside the nebula. The most interesting feature in the Helix Nebula is its knots, which have a typical size of 0.5–3 arcsec at their heads and are accompanied by tails up to 15 arcsec long (O'Dell and Handron 1996; Figure 1). All of the knots have bright tips facing the central star and the tails extend in the opposite direction away from the central star. The knots were first discovered by Walter Baade in about 1940, according to Vorontsov-Velyaminov (1968). The formation mechanism of these tails is not well understood: the two most likely explanations are mass injection from cores followed by hydrodynamic processes creating a tail, or photo-ionisation of an optically thick globule creating a shadow. Furthermore, ionised lines, hydrogen recombination lines, and molecular emission (H_2 and CO) have been detected from these knots. However, the excitation mechanisms of the

molecular lines are not yet known. In particular, the H_2 line excitation mechanism of PNe in general is still a subject of dispute and UV excitation and shock excitation have both been proposed.

Planetary nebulae are the late stages of the stellar evolution for low- and intermediate-mass stars (1–8 M_{\odot} on the main sequence). The Sun is expected to reach this stage in about 5 billion years. The circumstellar shell was produced by mass-loss processes during the previous evolutionary stage, the asymptotic giant branch (AGB). As the central star evolves from the AGB towards the PN phase, the effective temperature increases, and the circumstellar material in the nebula is photo-ionised. PNe are regarded as a typical case of a photon-dominant region. Moreover, a fast but low mass-loss rate stellar wind from the PN central star catches up with the slow but dense AGB wind, and so the circumstellar envelopes

Figure 1. The optical image of the Helix Nebula (top) formed from images in a 502 nm filter ([O III]) and 658 nm filter ($H\alpha$ and [N II]) is shown. The square region is enlarged in the lower panel to show the knots in the inner region of the Helix Nebula. Adopted from images taken with HST and NOAO. (Credit: NASA, NOAO, ESA, M. Meixner and T. A. Rector)

One of the most interesting characteristics of the planetary nebula NGC 7293 (the Helix Nebula) is its comet-shaped knots. We have observed one of the knots using the SINFONI imaging spectrometer on the VLT with adaptive optics. The spectra are analysed to obtain the spatial variation of molecular hydrogen line intensities within the knot. The images clearly show the detailed structure, which resembles a tadpole in shape, suggesting that hydrodynamic flows around the knot core create a pressure gradient behind the core. The three-dimensional spectra reveal that the excitation temperature is uniform at approximately 1800 K within the knot. The SINFONI observations help to determine the H_2 excitation mechanism in planetary nebulae, as well as the importance of hydrodynamics in shaping the knots.



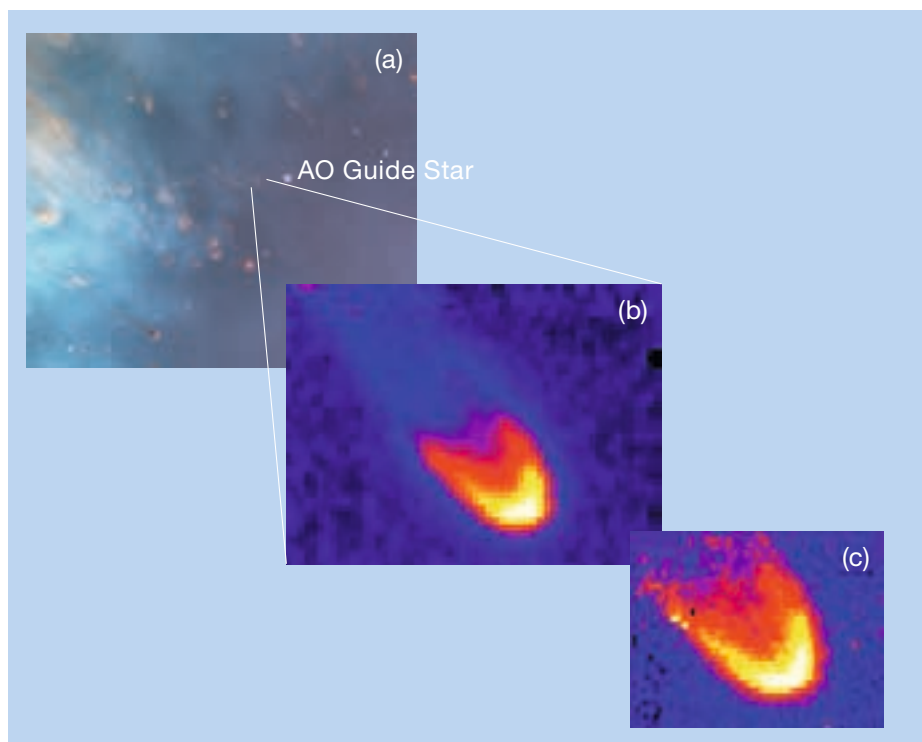
of PNe are a good test case for hydrodynamic simulations.

The power of SINFONI

Integral field spectrometers allow the simultaneous measurements of an image and many spectra on an individual pixel basis, and so these instruments are ideal for investigating spatial variation of line intensities, and thus line excitation mechanisms within nebulae (e.g. Tsamis et al., 2008). SINFONI is a near-infrared integral field spectrometer, covering the wavelength range which contains molecular hydrogen rotational-vibrational lines around 2 microns. SINFONI can be supported by an adaptive optics (AO) system, which allows observations to be taken with high spatial resolution. Thus it is an ideal instrument to investigate the structure of small-scale (a few arcsec) objects, such as knots in planetary nebulae.

We used SINFONI to obtain 2 micron integral field spectra of a knot within the Helix Nebula (Matsuura et al., 2007). There are many field stars inside this nebula, and we chose a knot close to one of the field stars, which was used as a guide star for the AO system. The images obtained with AO assistance achieve the highest angular resolution of any images of the Helix Nebula, up to about 70 milliarcsec. Figure 2 shows the SINFONI image of the knot in the Helix Nebula. The knot was clearly resolved into an elongated head and two narrow tails. The overall shape resembles that of a tadpole. The brightest emission is found in a crescent within the head. The diameter of the head is approximately 2.5 arcsec, while that of the tails is about 2.9 arcsec. We found that the tails are brighter in H₂ than in optical H-alpha+[N II] emission (Figure 3). In the optical, almost only the crescent at the head is found and the tail is barely seen.

As an integral field spectrometer, SINFONI can provide a spectrum at every single spatial pixel over the field. Figure 4 shows representative spectra within the knot obtained by the SINFONI instrument. Integral field spectroscopy enables the spatial variation of the intensities of H₂ lines to be studied. This is the first time



that spatially resolved H₂ spectra have been obtained within a knot. The SINFONI data also provide line ratio maps, which gives a measure of the H₂ excitation temperature. The line ratio maps ap-

Figure 2. (a) Optical image showing the location of the target and a nearby field star which was used for adaptive optics. (b) The SINFONI image of the knot at 2.12 micron covering the H₂ v = 1-0 S(1) line; (c) close-up of the crescent taken with SINFONI at a scale of 100 milliarcsec per pixel but resampled to 50 milliarcsec pixels. The image size is 4.2 arcsec by 3.9 arcsec.

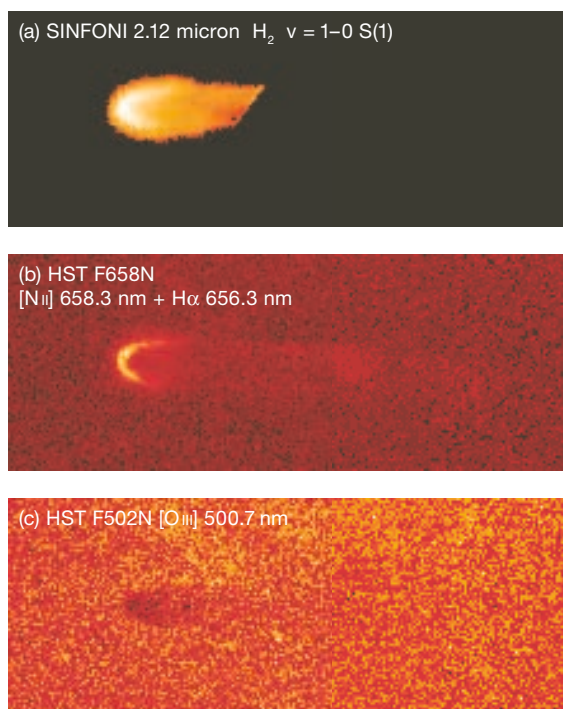


Figure 3. A comparison of SINFONI H₂ and optical images. The tails are much more obvious in the H₂ line (a) than in the 658 nm image (b). The knot is found to be negative in 500.7 nm [O III] line (c), because the dust in the knot absorbs the background emission, while the surrounding area has diffuse [O III] emission unaffected by dust.

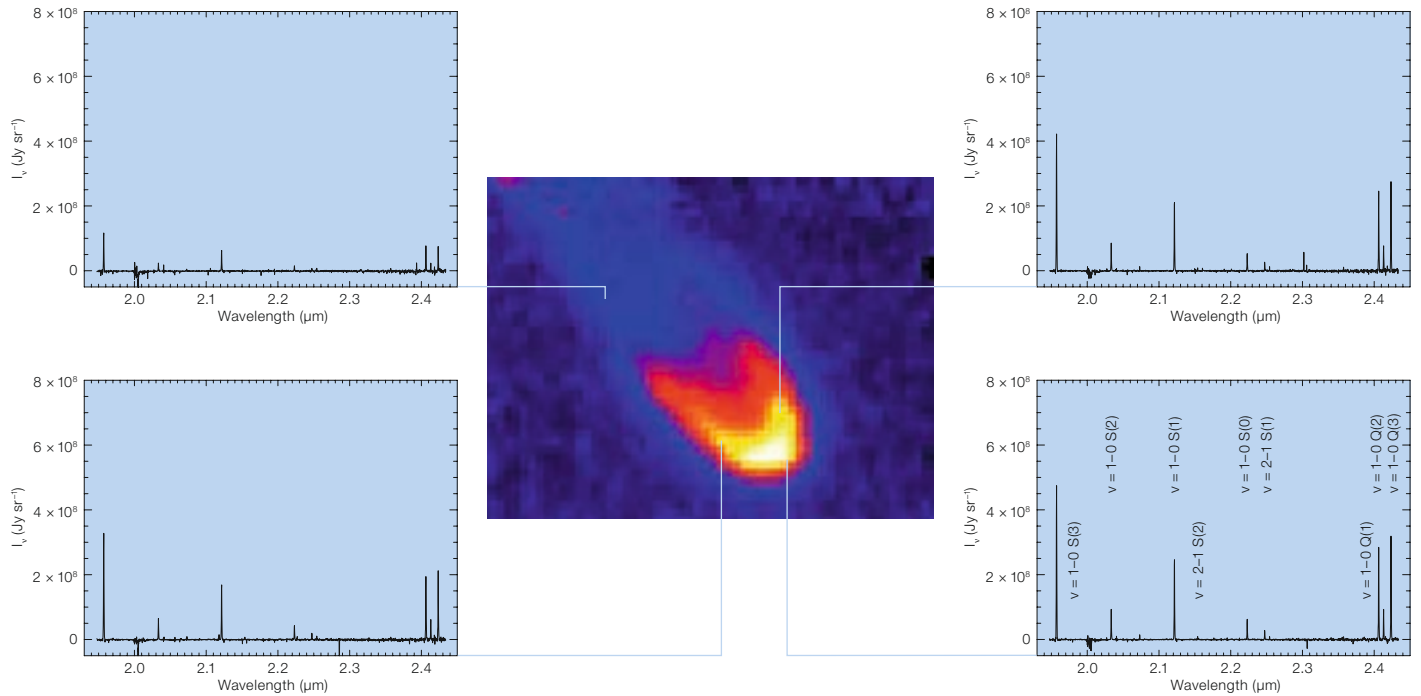
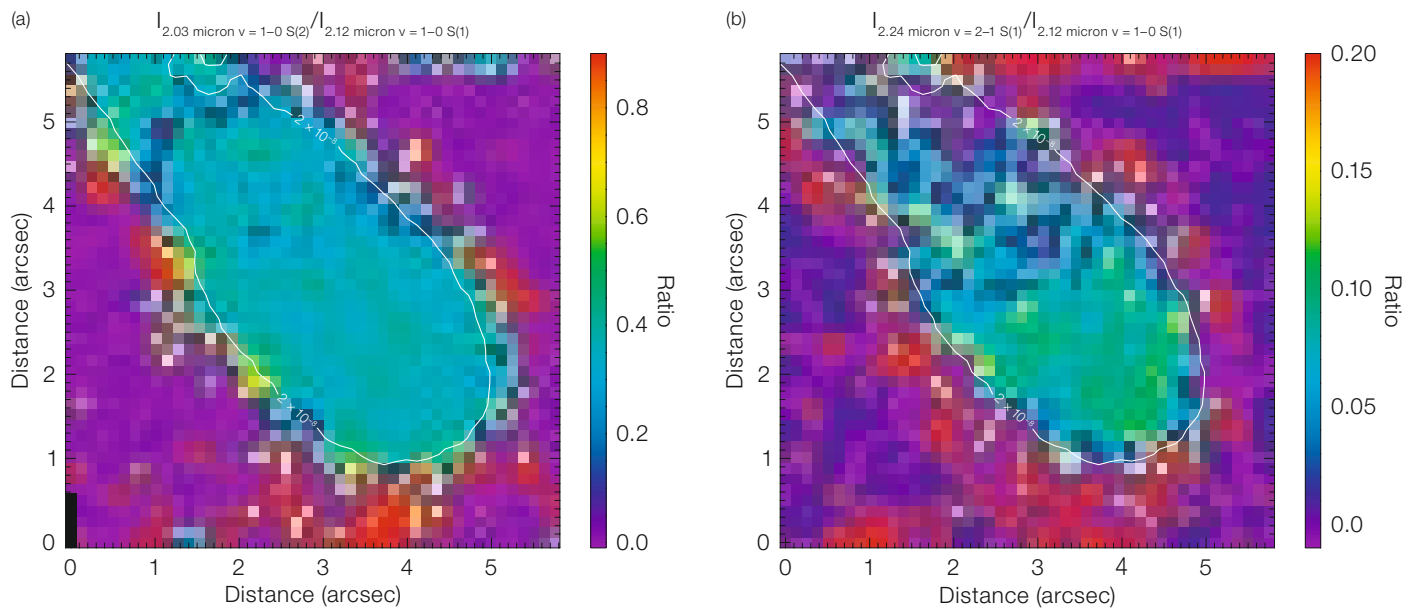


Figure 4 (above). SINFONI spectra of H₂ lines, with identification of transitions in the right bottom panel, at different locations around the knot shown in the central image.

Figure 5 (below). Line ratio maps, showing (a) the rotational temperature and (b) the vibrational temperature of H₂ molecules. The excitation temperatures appear to be uniform within the knot, outlined by a white line.



appear to be uniform within the knot (Figure 5). Using all of the H₂ lines detected at 2 microns (up to 12 lines), we derived an excitation temperature of 1800 K, and all of the intensities follow local thermodynamic equilibrium (LTE).

Shaping of the knots

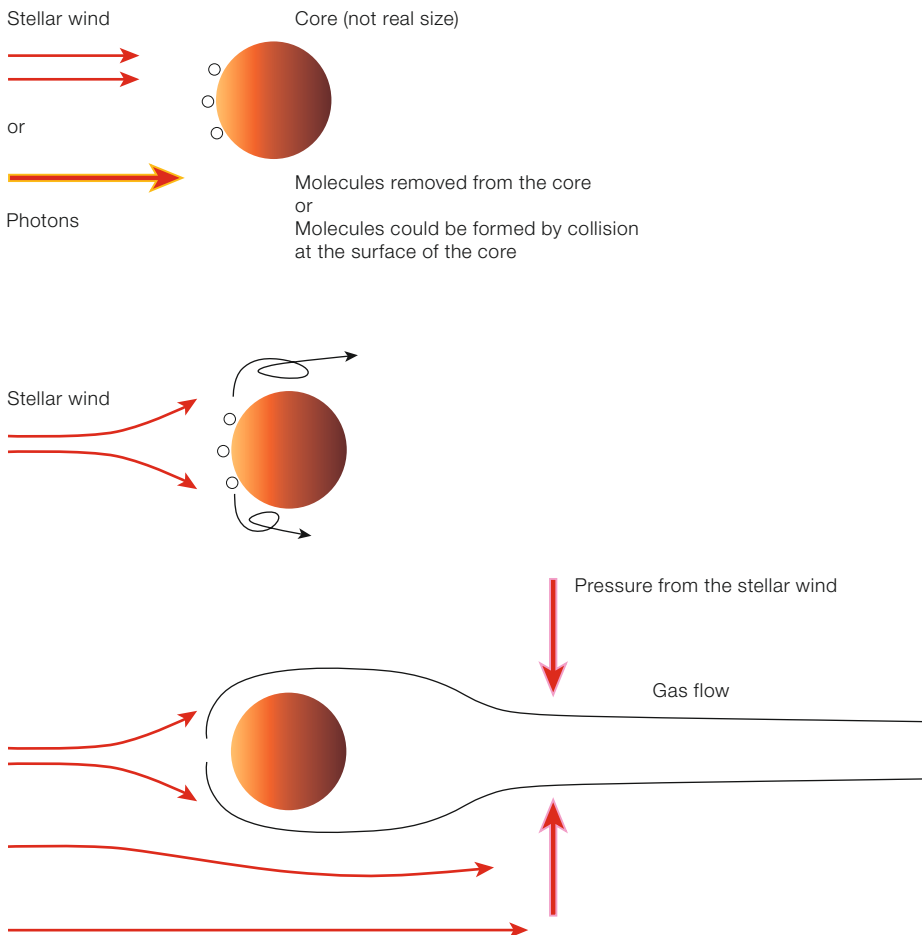
The mechanism responsible for the formation and shaping of the knots has been the subject of a long-term debate. The long tails of the tadpole-like knots

indicate the involvement of hydrodynamics. The bright crescent is a bow shock and the stellar wind from the central star blows the material off, or alternatively radiation from the central star heats the core evaporating the gas which forms

a pony-tail pointing away from the central star. The tail is narrower than the head, probably because of the pressure difference behind the head caused by the stellar wind (Figure 6). One of the best models to reproduce the tadpole shape has been developed by Pittard, Dyson, and their colleagues (e.g. Dyson et al., 2006). According to their model, the tadpole shape can be produced if material is constantly removed from the core of a knot by the stellar wind, and if the velocity of the wind is about supersonic. Their models show that the velocity of the ambient gas is between 26 and 38 km/s in the case of the Helix knots. Such a high expansion velocity component has been detected in the outer part of the Nebula (Walsh and Meaburn, 1987), but not yet in the inner part; in the inner part, only slower (10 km/s) winds have been detected so far. The detection of high velocity components from the knotty region would be of further interest.

The excitation mechanism of molecular hydrogen

The excitation mechanism of molecular hydrogen in PNe has been a long-term controversy. From the knots, CO molecular emission has been detected but their upper level energy is only 6 K, much lower than that for H₂ (typically from 6 000 to 8 000 K for the rotational-vibration lines at 2 microns). In order to reach the energy of such an upper level and to acquire an excitation temperature of thousands of K, a line excitation mechanism should be present. There are two major mechanisms proposed to excite rotational-vibration lines of molecular hydrogen at 2 microns: collisional and fluorescent excitation. For shock excitation, kinetic energy is absorbed in increasing the internal energy of the molecules, and the H₂ line intensities follow a thermal population distribution. However UV radiation in photon-dominant regions increases the population of rotation-vibrationally excited states, and vibrationally excited molecules then decay by emitting photons in the near-infrared. The population of UV excited states are often detected in non-LTE in rotational-vibration lines, but in an intense UV field, and depending on the gas density, fluorescence can create a thermal population distribution.



Within the choice of existing models and their parameter ranges, C-type (continuous) shock models with an ambient gas velocity of 27 km/s (Burton et al., 1992) can reproduce the measured H₂ intensities in the Helix Nebula. In contrast, UV radiation models can fit the observations, only if the UV flux is increased by a factor of 250 above that expected from the central star. Within the current choice, our observations favour shock excitation of H₂ lines.

The non-detection of a shocked region in the SINFONI image still remains a mystery: if the H₂ lines are excited by shocks, the excitation temperature should be highest at the tip of the tadpole, i.e., on the crescent. However, our SINFONI observations did not detect such a shocked region (Figure 5). This could be because the scale of the shocked region is still too small to be resolved even with SINFONI.

Figure 6. A schematic view of the formation of a knot in a planetary nebula by the effects of the stellar wind.

References

- Burton, M. G., Hollenbach, D. J. & Tielens, A. G. G. M. 1992, *ApJ*, 399, 563
 Dyson, J. E., Pittard, J. M., Meaburn, J., et al. 2006, *A&A*, 457, 561
 Harris, H. C., Dahn, C. C., Canzian, B., et al. 2007, *AJ*, 133, 631
 Matsuura, M., Speck, A. K., Smith, M. D., et al. 2007, *MNRAS*, 382, 1447
 Meixner, M., McCullough, P., Hartman, J., et al. 2005, *AJ*, 130, 1784
 O'Dell, C. R. & Handron, K. D. 1996, *AJ*, 111, 1630
 Speck, A. K., Meixner, M., Fong, D., et al. 2002, *AJ*, 123, 346
 Tsamis, Y. G., Walsh, J. R., Pequignot, D., et al. 2008, *MNRAS*, 355, in press
 Vorontsov-Velyaminov, B. A. 1968, *IAU Symp.*, 34, 256
 Walsh, J. R. & Meaburn, J. 1987, *MNRAS*, 224, 885

Hunting for the Building Blocks of Galaxies like our own Milky Way with FORS

Martin G. Haehnelt¹
 Michael Rauch²
 Andrew Bunker³
 George Becker²
 Francine Marleau⁴
 James Graham⁵
 Stefano Cristiani⁶
 Matt J. Jarvis⁷
 Cedric Lacey⁸
 Simon Morris⁹
 Celine Peroux¹⁰
 Huub Röttgering¹¹
 Tom Theuns⁹

- ¹ Institute of Astronomy, Cambridge, United Kingdom
- ² Observatories of the Carnegie Institution of Washington, Pasadena, USA
- ³ Anglo-Australian Observatory, Epping, Australia
- ⁴ Spitzer Science Center, Caltech, Pasadena, USA
- ⁵ University of California, Berkeley, USA
- ⁶ Osservatorio Astronomico di Trieste, INAF, Italy
- ⁷ Centre for Astrophysics, Science & Technology Research Institute, University of Hertfordshire, Hatfield, United Kingdom
- ⁸ Institute for Computational Cosmology, Department of Physics, University of Durham, United Kingdom
- ⁹ Department of Physics, University of Durham, United Kingdom
- ¹⁰ Observatoire Astronomique de Marseille-Provence, France
- ¹¹ Leiden Observatory, the Netherlands

We report results from our ultra-deep spectroscopic survey for low surface brightness Ly α emitters at redshift $z \sim 3$. A 92-hour-long exposure with the ESO VLT FORS2 instrument has yielded a sample of 27 faint line emitters with fluxes of a few times 10^{-18} erg s $^{-1}$ cm $^{-2}$ which we argue are likely to be dominated by Ly α . The large comoving number density, the large covering factor, $dN/dz \sim 0.2-1$, and the spatially extended surface brightness of the emission suggest that the emitters can be identified with the elusive host population of damped Ly α systems (DLAS) and high column density Lyman limit systems. The finding suggests that most Lyman limit systems and DLAS are part of the same low-mass galaxies.

Searches for young galaxies

The search for and discovery of young galaxies at high redshift has involved a number of unexpected twists and turns. Early predictions of young galaxies shining brightly in Ly α line radiation (Partridge & Peebles, 1967) have not been borne out by reality. The first detections of an entire population of ordinary (i.e., non-AGN) high-redshift galaxies came from the observations of damped Ly α systems seen in absorption against background QSOs (e.g. Wolfe et al., 1986). Detections of substantial numbers of high-redshift galaxies in emission had to wait for another decade and larger telescopes, and came to rely not on emission lines but on broadband continuum ('Lyman break') features (e.g. Steidel & Hamilton, 1995). These searches yielded massively star forming galaxies where, ironically, the expected Ly α emission was often highly suppressed because of dust absorption. With the advent of 10-m-class telescopes, narrowband surveys for Ly α line emission finally reached sufficient depth, discovering considerable numbers of galaxies with large Ly α equivalent widths (e.g. Cowie & Hu, 1998). The relation between the galaxy populations selected by these three different methods has so far remained obscure. Galaxies selected by Ly α line emission (down to typical narrowband limiting fluxes of a few $\times 10^{-18}$ erg s $^{-1}$ cm $^{-2}$), though similar in numbers to Lyman break selected galaxies, appear different from these because of their much larger line-to-continuum ratios. Both emitter populations appear more metal-rich and have star-formation rates larger than compatible with the low metallicity and low dust contents of damped Ly α systems (DLAS).

DLAS and the general population of star-forming galaxies

The key to a full understanding of the general population of galaxies at high redshift, likely to be less actively star-forming and, at least according to the CDM paradigm, far more numerous than either of the two bright classes of objects, must lie with the DLAS. Unfortunately, DLA host galaxies have remained largely elusive at high redshift. The attempt to identify individual DLA with galaxy coun-

terparts has usually been frustrated by the difficulty of detecting an extremely faint object (the DLA host) next to an extremely bright object (the QSO). Searches (e.g. Warren et al., 2001, Christensen et al., 2006) have so far produced only a handful of confirmed detections of the underlying galaxies. Such efforts indicated that DLA hosts at high redshift are generally drawn from the very faint end of the general galaxy population at high redshift (Møller et al., 2002), giving support to the idea that DLAS host galaxies have rather low masses (Haehnelt, Steinmetz & Rauch, 2000), albeit with a considerable gas cross-section.

A search for faint Ly α emitters and a surprising discovery

We report here on the results of an ultra-deep, spectroscopic blind survey for low-level Ly α emission using FORS2 on the VLT (Large Programme 173.A-0440). The original motivation was to search for fluorescent Ly α emission from the optically thick part of the gaseous cosmic web (Lyman Limit systems and DLAS), induced by the general UV background (Hogan & Weymann, 1987; Gould & Weinberg, 1996). Line emission in response to recombinations caused by the impinging UV photons would cause any patches of optically thick gas to exhibit a universal 'glow' of Ly α photons. For this purpose we obtained a FORS2 spectrum of a basically blank piece of sky with the $7' \times 2''$ slit exposed for 92 hours (120 hours including overheads).

The field contained a moderately bright QSO and was observed during 2004–2006 with the volume-phased holographic grism 1400 V on FORS2. The resulting 2-dimensional spectrum is shown in Figure 1 with the spatial direction shown vertically and the spectral direction shown horizontally. The spectrum ranges from 4 457 to 5 776 Å. Despite the long exposure time we were able to reach the sky noise limit and the surface brightness detection limit for line photons of our spectrum is an unprecedented 8×10^{-20} erg cm $^{-2}$ s $^{-1}$ arcsec $^{-2}$.

We had expected to detect about 30 optically thick patches fluorescing at very low light levels in Ly α with a median

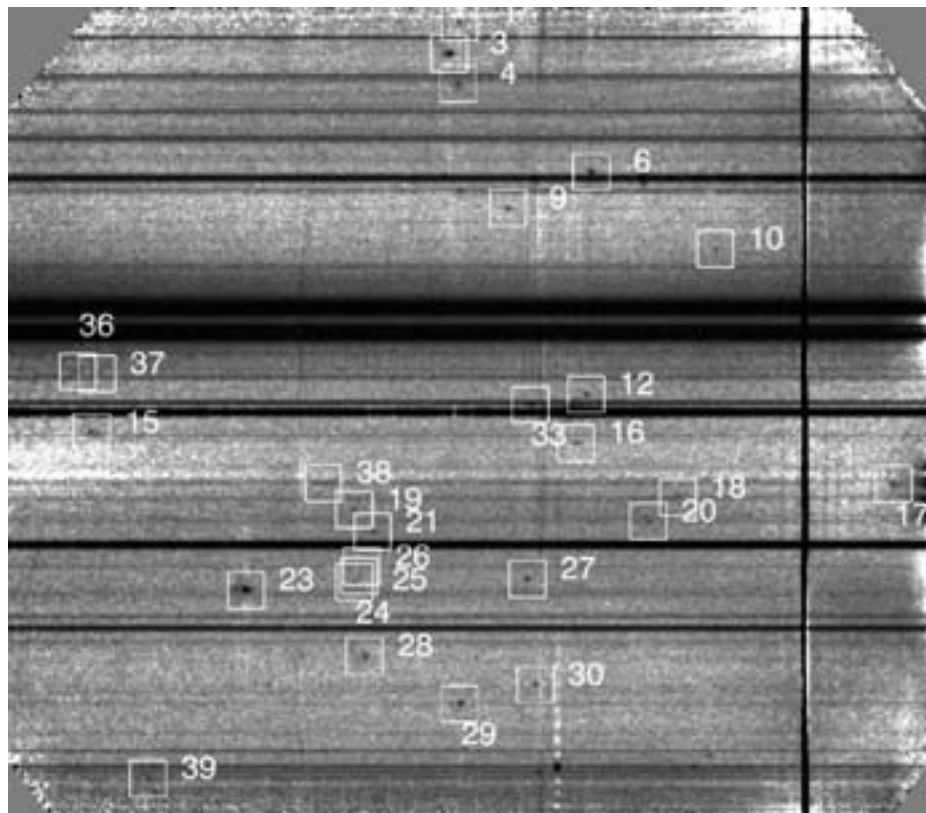


Figure 1. Two-dimensional spectrum obtained in 92 hours of exposure time with FORS2 at the VLT. The line emitter candidates for H I Ly α are enclosed by the numbered boxes. The dispersion direction is horizontal, with blue to the left and red to the right; the spatial direction along the slit is vertical. The figure is adapted from Rauch et al. (2008).

diameter of 5 arcsec. The expected large spatial extent meant that we could accept observing time in periods of moderate seeing for which there is substantially less demand.

However, as we will describe below, theoretical estimates of the UV background intensity had gone down during the project, and so we were probably somewhat short of the signal-to-noise ratio required to detect the fluorescent (re-) emission of the meta-galactic UV background from optically thick regions in a blank field. We nevertheless found 27 single-line emitters on the slit, however with total fluxes typically a factor five to ten higher than our revised expectations for the signal from fluorescence alone. We also detected a number of low-redshift line-emitting interlopers by their [O II], [O III], and H I Balmer series emission.

Figure 2 shows a mosaic of the 27 single-line emitters. Many emitters are considerably extended in wavelength and real space, suggesting the importance of radiative transfer in shaping the appearance of the objects and thus an identification as Ly α line. The detectable emission often extends to ‘radii’ as large as 4 arcsec.

What are the faint spatially extended line emitters?

For the 27 single-line emitters – at least in principle – [O II], [O III] and Ly α are all possible identifications. Obviously the different interpretations differ drastically in the inferred range of redshift, luminosity and star formation and most crucially in the inferred space density (see Table 1).

In a publication to appear in the ApJ (Rauch et al., 2008), we argue in considerable detail that most of the emitters are likely to be Ly α at redshift $z \sim 3.2$. Our main argument concerns the inferred space densities. With an identification as Ly α , the inferred space density is ap-

proaching the total space density of local dwarf galaxies as faint as $M_R = -13$. If the emission were instead due to [O II] or [O III], the corresponding space density would be larger than the space density of local dwarf galaxies by factors 6 and 100, respectively. From a statistical point of view, most of the 27 single-line emitters should thus indeed be Ly α . This interpretation is supported by the typical asymmetric shape of many of the emitters and the fact that we have also detected the expected number of [O II] emission line doublets.

A steeply rising faint end of the luminosity function of Ly α emitters

Even though the inferred space densities are smallest if the line emission is identified as Ly α , the resulting space density still implies a significant steepening of the luminosity function of Ly α emitters below flux levels reached by previous surveys. In Figure 3 we compare the cumulative luminosity function inferred from our 27 line emitters (neglecting slit losses) with the luminosity function from published surveys. Due to the spectroscopic nature of our survey and the long exposure time, we reach more than a factor 10 lower flux levels. There is good agreement in the overlap region at the bright end. Towards fainter magnitudes the luminosity function appears to steepen significantly.

Physical origin of the line emission

An identification of the emission as Ly α raises the question of the potential emission mechanisms. We will briefly consider three possibilities here: fluorescent (re-) emission of the meta-galactic UV background; gas cooling; and emission due to the formation of (massive) stars. As already discussed, the original aim of our project was to detect fluorescent emission from optically thick regions. For this purpose we further increased our sensitivity by stacking the individual spectra of our emitters. In Figure 4 we compare the result of this stacking analysis to our expectation for the fluorescent emission (see Rauch et al. (2008) for more details). The points with error bars and open squares show our measurements of the mean and median surface brightness

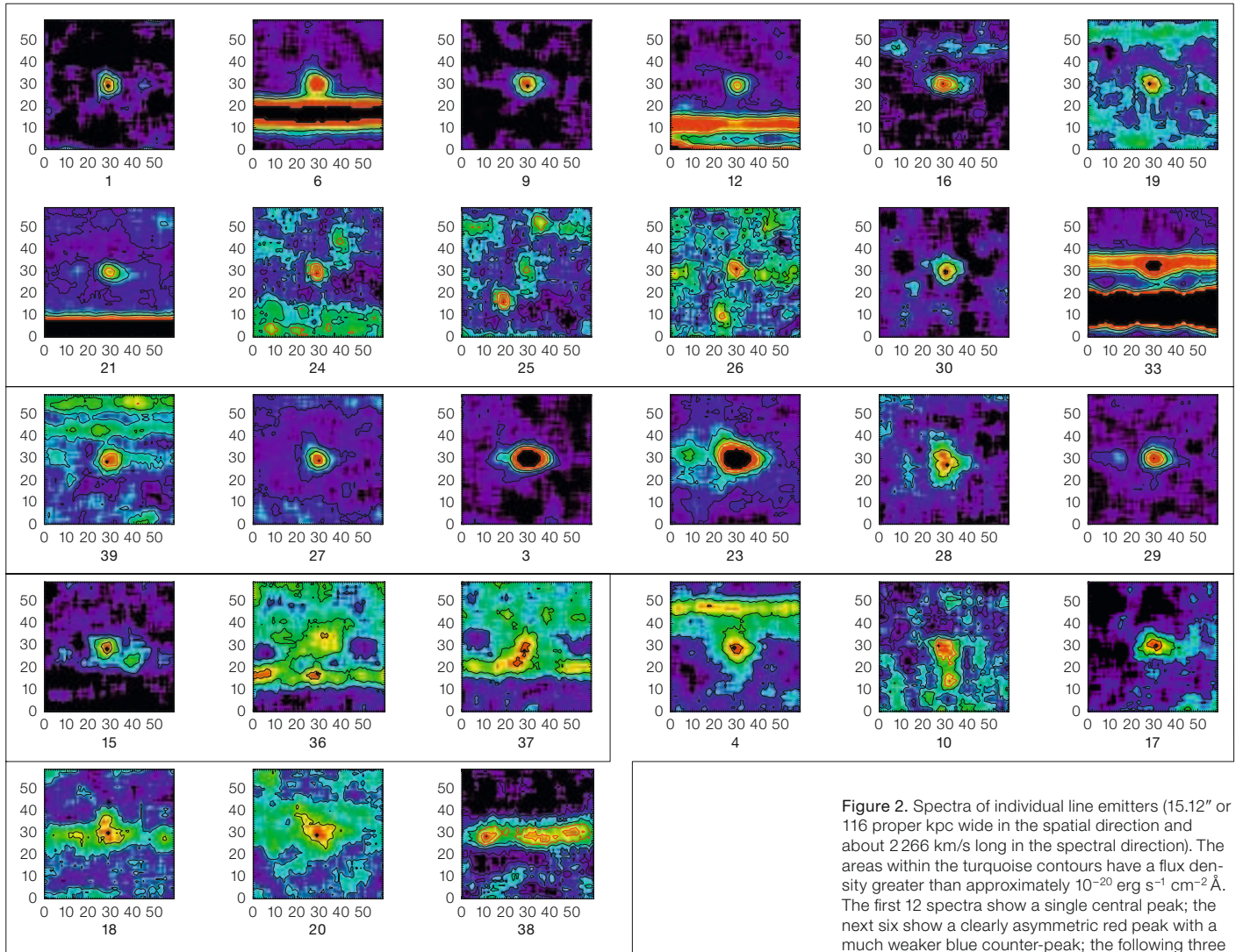


Figure 2. Spectra of individual line emitters (15.12" or 116 proper kpc wide in the spatial direction and about 2266 km/s long in the spectral direction). The areas within the turquoise contours have a flux density greater than approximately 10^{-20} erg s $^{-1}$ cm $^{-2}$ Å. The first 12 spectra show a single central peak; the next six show a clearly asymmetric red peak with a much weaker blue counter-peak; the following three either have a stronger blue than red peak (ID 15) or emission features blueward of an absorption line (36, 37); the remaining six spectra are unclassifiable. The figure is adapted from Rauch et al. (2008).

as a function of angular distance from the centre of emission along the slit, respectively. The dotted curves give the range of the expected surface brightness for the fluorescent (re-) emission of the metagalactic UV background based on recent measurements of photo-ionisation rate of the Intergalactic Medium at $z \sim 3$. The predictions for the Ly α fluorescence are a factor two to four lower than the measured surface brightness of our line emitters in the stacking analysis.

The spectral line shapes and sizes of our emitters suggest that the Ly α photons have been processed by radiative transfer through an optically thick medium. In

principle, the Ly α radiation could be produced by the cooling of gas in galactic haloes. However, as we argue in detail in Rauch et al. (2008), this may be true for a few of our objects but not for the majority. The reason is that the observed Ly α luminosity is too high to be consistent

with the observed high space density and the implied low masses of the underlying haloes. This leaves Ly α radiation from centrally concentrated formation of (massive) stars, resonantly scattered in an optically thick galactic halo, as the most

	[O III]	[O II]	Ly α
Redshift [z]	0–0.15	0.2–0.55	2.67–3.75
Luminosity [h $_{70}^{-2}$ erg s $^{-1}$]	2×10^{36} -3×10^{38}	3.7×10^{38} -2×10^{40}	7.9×10^{40} -1.6×10^{42}
Star-formation rate [h $_{70}^{-2}$ M $_{\odot}$ yr $^{-1}$]		5×10^{-3} –0.3	7×10^{-2} –1.5
Space density [h $_{70}^3$ Mpc $^{-3}$]	9	0.5	3×10^{-2}

Table 1. Properties of line emitters for different possible identifications.

promising remaining emission mechanism.

Have we discovered the host galaxies of DLAS?

As discussed above the difficulties in finding the host galaxies of DLAS, as well as theoretical models within the Λ CDM paradigm for structure formation, suggest that DLA host galaxies are fainter and more numerous than typical Lyman break galaxies. Unfortunately, absorption line studies only constrain the total incidence rate, which depends on the product of space density and cross section for absorption. With our spectroscopic survey we have measured the space density and the size of the objects. We can thus predict the expected rate of incidence for absorption by the emission regions of our putative population of faint spatially extended Ly α emitters. In Figure 5 we show this incidence rate as a function of the measured 'radius' of our emitters. The cumulative rate of incidence is very similar to that of DLAS, suggesting that we may indeed have discovered a substantial part of the elusive population of DLA host galaxies.

The elusive continuum

The essential, but missing piece of evidence in this puzzle is clearly the rest-frame UV continuum radiation of the objects. A knowledge of the continuum would allow us to unambiguously identify each individual case as a high redshift galaxy. Knowledge of the continuum will also give us a more reliable measure of the star-formation rate and provide constraints on the morphology of these galaxies – it will tell us what these objects really are. Unfortunately, the expected continuum emission is very faint. In Figure 6 we compare the cumulative UV continuum luminosity function of Lyman break galaxies in the Hubble Ultra-Deep Field (HUDF) with those predicted for our line emitters assuming a rest-frame EW of 70 Å. The space density of our line emitters is similar to those of the faintest Lyman break galaxies in the HUDF (Bouwens et al., 2007).

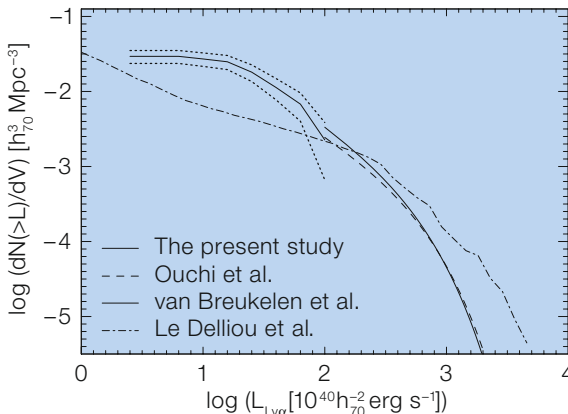


Figure 3. Observed cumulative luminosity function at $z = 3.1$ from Ouchi et al. (2007; dashed curve), $z = 2.9$ from van Breukelen et al. (2005; dash-triple dotted curve) and our sample (solid curve, dotted curves represent 1σ error contours). The dot-dashed curves are theoretical predictions. From Rauch et al. (2008).

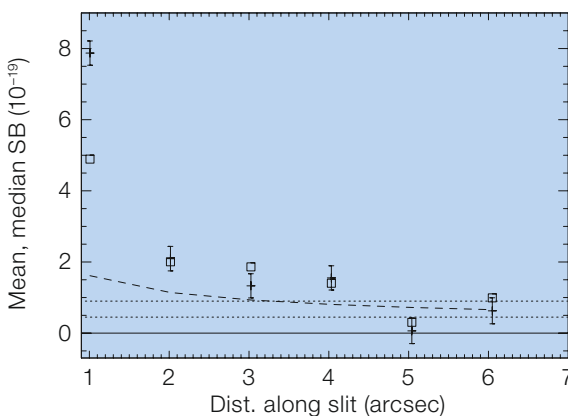


Figure 4. Mean (points with error bars) and median (open squares) surface brightness measurements in units of $10^{-19} \text{erg cm}^{-2} \text{s}^{-1} \text{arcsec}^{-2}$ for the combined surface brightness profiles, as a function of angular distance in arcsecs from the centre of emission along the slit. The dotted curves give the range of the expected surface brightness based on the photo-ionisation rate of the $z \sim 3$ Intergalactic Medium. The upper dotted curve is for a QSO type UV spectrum, the bottom curve for a spectrum where 50% of the flux is contributed by galaxies. The dashed curve is the 4σ surface brightness detection threshold for individual objects. From Rauch et al. (2008).

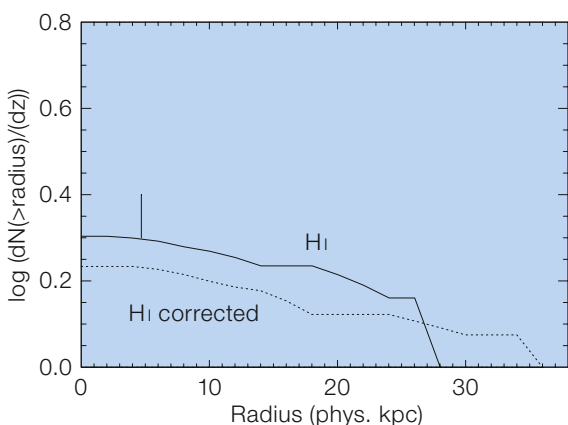


Figure 5. Contribution of objects of different sizes to the predicted rate of incidence per unit redshift, dN/dz for H I with (dotted line) and without (solid line) correction for the extended sizes and our underestimating the radius. The short vertical line on top of the uncorrected curve indicates the spatial resolution limit along the slit. From Rauch et al. (2008).

The next step

The similarity of the space density of our emitters to that of the Lyman break galaxy population at the faint end of the UV continuum luminosity function in the HUDF is tantalising, but circumstantial, evidence that these may be the same objects, once seen by their centrally concentrated continuum and once by their spatially extended Ly α emission. The

most efficient way for testing this hypothesis, and for constraining further the fractions of true Ly α emitters and interlopers, would be to repeat our ultra-deep spectroscopic survey in the HUDF. This should be considered a modest investment of (moderate seeing!) observing time in return for substantial progress in understanding the formation of typical present-day galaxies like our Milky Way.

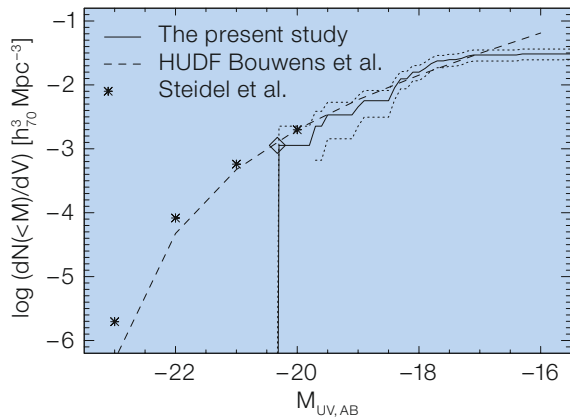


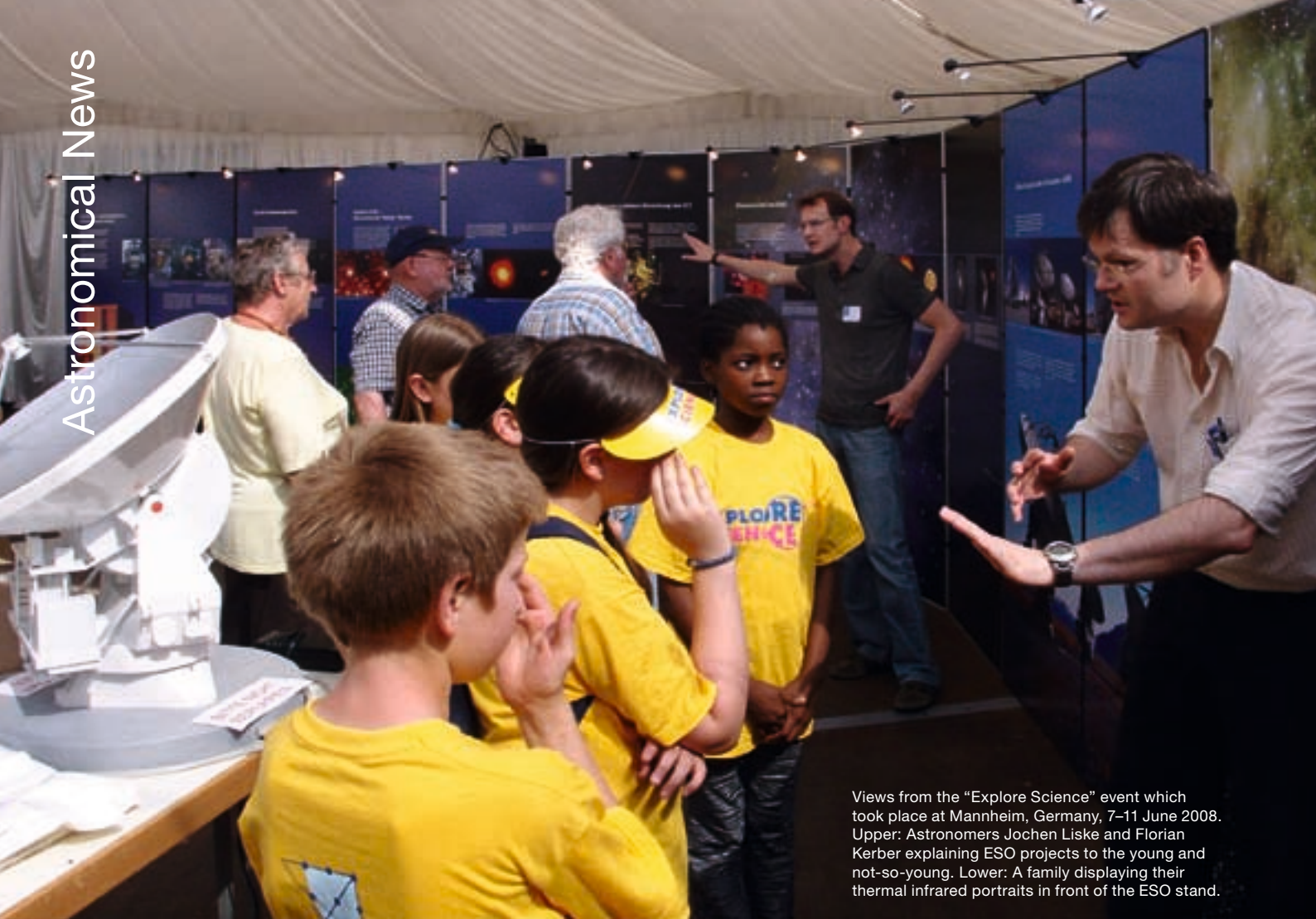
Figure 6. Cumulative UV continuum luminosity functions of Lyman break galaxies and the cumulative distribution of our survey (solid line; dotted lines are $\pm 1\sigma$ errors). The emitters are assumed to have a continuum magnitude predicted by their Ly α line flux assuming a rest-frame equivalent width of 70 Å. From Rauch et al. (2008).

References

- Bouwens, R. J., Illingworth, G. D., Franx, M., et al. 2007, *ApJ*, 670, 929
 Christensen, L., Wisotzki, L., Roth, M. M., et al. 2006, *A&A*, 468, 587
 Cowie, L. L. & Hu, E. M. 1998, *AJ*, 115, 1319
 Gould, A. & Weinberg, D. H. 1996, *ApJ*, 468, 462
 Haehnelt, M. G., Steinmetz, M. & Rauch, M. 2000, *ApJ*, 534, 594
 Hogan, C. J. & Weymann, R. J. 1987, *MNRAS*, 225, 1
 Møller, P., Warren, S. J., Fall, S. M., et al. 2002, *ApJ*, 574, 51
 Ouchi, M., Shimasaku, K., Akiyama, M., et al. 2008, *ApJS*, 176, 301
 Partridge, R. B. & Peebles, P. J. E. 1967, *ApJ*, 147, 868
 Rauch, M., Haehnelt, M. G., Bunker, A., et al. 2008, *ApJ*, 681, 856
 Steidel, C. C. & Hamilton, D. 1995, *ApJ*, 105, 2017
 van Breukelen, C., Jarvis, M. J. & Venemans, B. P. 2005, *ApJ*, 359, 895
 Warren, S. J., Møller, P., Fall, S. M., et al. 2001, *MNRAS*, 326, 759
 Wolfe, A. M., Turnshek, D. A. & Smith, H. E. 1986, *ApJS*, 61, 249



Colour-composite image of a triplet of galaxies which make up part of the Hickson Compact Group HCG 90. The galaxies in the image are NGC 7173 (north), 7174 (south-east) and 7176 (south-west); the image orientation is north up, east to the left and the size is about 5.3 arcminutes. The image is based on data obtained with VLT FORS1 with *B*, *V*, and *R* filters. NGC 7173 and 7176 are elliptical galaxies, while NGC 7174 is a spiral galaxy with a disturbed dust lane. See ESO PR Photo 02/08 for more details. Image processing by Henri Boffin (ESO).



Views from the “Explore Science” event which took place at Mannheim, Germany, 7–11 June 2008. Upper: Astronomers Jochen Liske and Florian Kerber explaining ESO projects to the young and not-so-young. Lower: A family displaying their thermal infrared portraits in front of the ESO stand.



News from the ESO Science Archive Facility

Nausicaa Delmotte (ESO)

Latest developments of the ESO archive including timely access to proprietary data, a new science-oriented query form and new data releases are presented.

PI access to own proprietary data

As of 1 April 2008, Principal Investigators (PIs) can access their own raw proprietary data at any time through the ESO archive. This new feature is an upgrade of the current User Portal system released last year (see Tacconi-Garman 2007). To this end, the archive system was modified and the archive web interfaces were adapted to reflect this change. The results of archive web searches are now colour coded. Datasets for which the proprietary period is over are highlighted in green and are publicly available. Datasets that are still proprietary are highlighted in red and can only be downloaded by the corresponding PI. The data request itself requires authentication through the User Portal. Note that anybody can request proprietary data, e.g. the datasets highlighted in red can also be requested by non PIs, but that only PIs will be able to actually download them. This mode was made necessary to allow all users, irrespective whether they are PIs of ESO data or not, to freely browse the ESO archive without any prior authentication.

PIs with proprietary data should note two important items with regard to accessing their data via the ESO archive:

First, an archive query may return a result for data which are not yet in the archive (thus currently unavailable for download). This is caused by the fact that: (a) the information returned for queries is derived from FITS header information which is available very soon after the data file has been created; and (b) the ingest of the data into the archive can only be done after they are physically transferred to Garching. This latter process typically takes 10–14 days from the time the data were obtained. If a data request is made for data that appear in a query result, but are not yet in the archive, those files requested will not be available and the

requester will be informed that they have N status ("Not available"). The request will be closed and the user should simply try again after waiting for an appropriate time.

Second, the one-year proprietary period for the data requested begins when the corresponding archive request is successfully completed (i.e. data files are made available to the requester). This is consistent with the policy that whenever data are made available to the PI (e.g. through a DVD shipment), then the proprietary clock starts.

Science-oriented query form

A new archive query form was released in May 2008 as a common entry point to search among all the collections of both imaging and spectral ESO advanced data products. See http://archive.eso.org/eso/eso_archive_adp.html.

For the first time at ESO, it is now possible to search the archive by high-level astrophysical parameters: redshift, object class, radial velocity, and wavelength. In addition, dynamic consistency cross-checks of user input are performed on the search screen to restrict the input to what is actually correct for the search. This new interface provides users with a unified access to all advanced data product releases and sets the path towards a scientific search engine. This new service supersedes the query form for only spectral advanced data products released in October 2007.

New data releases

Several major scientific data releases have taken place through the ESO archive over the past few months and are summarised here.

Science Demonstration (SD) data from the Multi-Conjugate Adaptive Optics Demonstrator (MAD, see Marchetti et al., 2007) were released through the ESO archive in February 2008. MAD SD runs took place in November 2007 and January 2008 and largely follow the philosophy applied to the Science Verification of the VLT instruments.

The GOODS/VIMOS spectroscopy data (version 1.0) was released in February 2008. It contains the results of the first half of the GOODS/VIMOS spectroscopic campaign of the ESO/GOODS large programme 171.A-3045 (PI C. Cesarsky) using two different grisms (Low resolution Blue, 3500–6900 Å, and Medium resolution Orange, 4000–10000 Å) between 2004 and 2006. 3312 fully reduced and calibrated spectra of 3121 unique sources down to i_{775} (AB) magnitude of 25, along with a catalogue of 2000 redshifts, of which 985 are classified 'high quality' (grade A), are being released. The 1-sigma redshift accuracies are ~ 300 km/s and ~ 200 km/s for the low- and the medium-resolution observations, respectively. A full description of the survey can be found in Popesso et al., 2008.

Version 1.1 of the GaBoDS WFI data release (Hildebrandt et al., 2006) took place in March 2008. As part of the ESO Deep Public Survey (DPS), imaging observations were carried out in *U, B, V, R, I* bands, using the Wide Field Imager (WFI) mounted at the 2.2-m telescope at La Silla. This survey consisted of three square degrees in three well-separated regions (Deep1, Deep2 and Deep3) split into four adjacent WFI pointings (named a, b, c, d). GaBoDS combines the data from this survey with data from most other ESO programmes that coincide with the original DPS regions, up until December 2006. Compared to the original release from April 2006, there are five more images plus associated weight maps. The new images include a U/38 image of the field Deep2c and U/50 and B/123 images in the Deep1c field. Additionally, V/89 and I/203 images of the Deep1c field now include more data resulting in increased depth.

For the latest information about the ESO archive, or to subscribe to the archive RSS feed, please see <http://archive.eso.org/>. For any questions or comments contact us at archive@eso.org.

References

- Hildebrandt, H., et al. 2006, *A&A*, 452, 1121
 Marchetti, E., et al. 2007, *The Messenger*, 129, 8
 Popesso, P., et al. 2008, *A&A*, submitted
 Tacconi-Garman, L. E. 2007, *The Messenger*, 130, 54

FP7 E-ELT Preparation – Grant Agreement Funded by the European Commission is Underway

Roberto Gilmozzi, Guy Monnet, Mark Robinson (all ESO)

The aim of the FP7 E-ELT Preparation Programme is to complement the 2007–2009 Phase B (detailed design) of the European Extremely Large Telescope (E-ELT), which is presently conducted by ESO as mandated by the ESO Council representing the 13 member states. The FP7 E-ELT Preparation Programme has a total budget of 6.013 M€, including a 5 M€ contribution from the European Commission under the 7th Framework Programme and will run for two years, from 1 January 2008 to 31 December 2009. The ESO executive has been directed by Council to act as a mono-partner in this endeavour, acting on behalf of all member states. The E-ELT Preparation Programme activities will thus be conducted by ESO, in collaboration with 25 third-party institutes in eight member states. Figure 1 shows ESO's Director General, Tim de Zeeuw, and the EC Scientific Officer, Elena Righi-Steele, exchanging the grant agreement to mark the start of the project.

The aim of the E-ELT Preparation Programme Work Packages (WP) is to help ESO to be fully prepared for the anticipated early 2010 decision by the funding agencies in the member states to give a go-ahead for building the facility. Some of the Work Packages deal with organisational matters such as: setting-up of the internal structure of the project office (WP8); management of the full financial package (WP7) to build the 800 M€ plus facility; close links with critical industries (WP3); and establishment of efficient coordination with other similar projects world-wide (WP2). Optimising the science output of the E-ELT is paramount, and further development of the Design Reference Mission (WP4) and a detailed blueprint for Science Access (WP5) will occur. Finally, the basic R&D knowledge for crucial upgrades of the E-ELT observing capabilities, e.g. for exo-planet detection, study of the first light in the Universe, etc., will be developed (WP9) and the ESO community will organise itself in networks (WP6) to be fully prepared for its future crucial role in building powerful and innovative focal instruments for the E-ELT facility.

Photo: H. H. Meyer, ESO



Figure 1. The formal exchange of the grant agreement for the FP7 E-ELT Preparation Programme between Tim de Zeeuw, ESO Director General, and the EC Scientific Officer, Elena Righi-Steele.

Key to the E-ELT endeavour is the high level of involvement and commitment of the ESO member states throughout the life cycle of the E-ELT, making it a facility “for the community and by the community”. This is invaluable for the establishment of a comprehensive science case and the development of crucial enabling technologies. It is also the vehicle by which the complex post-focal instruments will start their respective development phases.

Overall strategy and general description

The FP7 E-ELT Preparation Programme comprises a number of *transnational activities* for which EC support will be integral in establishing the appropriate framework to conduct them. Apart from “E-ELT Preparation Management” (WP1), these are:

International Cooperation (WP2) will explore the possibilities of involving external partners for the E-ELT development and link it with the other planned ELT projects to optimise their combined scientific output.

Industrial Links (WP3) will maximise the links with industrial partners and establish policies on connected issues, e.g. public relations and knowledge transfer.

Design Reference Mission (WP4) will develop a comprehensive set of observing proposals and simulated science data, in particular to maintain the alignment of the E-ELT Project with its community's scientific aspirations.

Science Access (WP5) will define scientific requirements on key areas of the interaction between science users and the E-ELT facility.

Networks of Nodes of Expertise (WP6) will help the European institutes with prime expertise in the technologies crucial to the Upgrade Paths Work Package (WP9) to coordinate their work and co-opt newly formed groups inside and outside ESO member states.

Financial Mechanisms (WP7) will explore external public and private funding possibilities.

Project Structure and Planning (WP8) is focused on the preparation of the organisation of the E-ELT project structure.

Upgrade Paths (WP9) will pursue, by design and prototyping, the development of the advanced Instrumentation and Adaptive Optics subsystems required to further enhance the E-ELT scientific capabilities five to ten years after the start of operations.

The strategic goal of the FP7 E-ELT Preparation Programme is to ensure that by 2010 the level of legal, financial, managerial and technical maturity required to launch the E-ELT construction is met. The project PI is Roberto Gilmozzi, the project manager is Mark Robinson and his deputy is Guy Monnet. The project web site is <http://www.eso.org/sci/facilities/eelt/fp7-elt/>.

The username and password can be provided on request by e-mailing mrobinso@eso.org or gmonnet@eso.org.

Report on the International Workshop on

Star Formation Across the Milky Way Galaxy

held at ESO, Vitacura, Chile, 3–6 March 2008

Michael Sterzik, Jorge Melnick,
Claudio Melo (all ESO)

The workshop “Star Formation Across the Milky Way Galaxy” brought four days of intensive scientific discussions and excellent presentations to our Vitacura premises in Chile. The idea of the workshop was to trace star-formation activity spatially spanning outward from the Solar Neighborhood, nearby star-forming regions and OB associations, to spiral arms, the Galactic disc, around the central bar and bulge, and towards the Galactic Centre. We aimed to link different communities that usually work on specific scales and environments, and thus had asked some of the most prestigious and acknowledged scientists in the field to help to develop a synoptic view of our current understanding of Galactic star formation. Almost all speakers in our ‘wish-list’ immediately agreed to come the long way down to Chile. This event confirmed once again that ESO/Chile and its faculty have become a prime address for international conferences of the finest scientific quality (see also the report on last year’s conference on “Observing Planetary Systems”, reported in *The Messenger*, 128, 72, 2007).

We present a short summary of some, subjectively selected, scientific highlights that were discussed during the workshop. All 45 oral presentations and 19 posters contributions can be accessed and downloaded through a dedicated page: <http://www.eso.org/sci/meetings/MilkyWayStarFormation/>

Intended as a ‘prelude’ to the entire workshop, global star formation was introduced by Bruce Elmegreen, who outlined the main physical processes responsible for large-scale structuring in galaxies: gravitational instabilities; turbulent compression; and sequential triggering. The predictions of fundamental theoretical considerations appear to agree well with the observed global structure of star-formation regions in galaxies.

Starting with the immediate Solar Neighborhood, the closest star-forming regions allow the most detailed, and highest spatial resolution studies, as reviewed by João Alves. He highlighted the power of the near-infrared cloud extinction mapping (NICER) technique, and discussed the relation of cloud core stability to the stellar initial mass function, and multiplicity. John Bally gave an impressive view on star formation in the Orion complex, the nearest site of ongoing high- and low-mass star formation. Orion allows to address some of the most fundamental questions in star formation, such as: How do massive stars form? Do most stars form in clusters? Are dynamical processes dominant during star formation? In addition, Thierry Montmerle pointed out the relevance of the high X-ray activity of young stars to star and planet formation through the effects of feedback. UKIDSS and the GLIMPS survey enable deep views into star-formation activity in the Galactic Plane and were highlighted by Phil Lucas.

The classical picture of the relation of star formation and spiral density waves in

galactic discs was reviewed by Preben Grosbøl, and the models of spiral shocks including clumps, magnetic fields and bars remain an active field of research, given the difficulties and uncertainties to precisely map the spiral structure of our Galaxy on the far side (Leo Blitz). In this context, more global agents like the interaction with satellite galaxies, and in particular the LMC, may act as an external trigger for star-forming activity in the outer parts of the Milky Way (Giovanni Carraro).

Is there a dominant mode of star formation? According to Tom Megeath, and his impressive collection of images showing the spatial distribution of young stars based on Spitzer, Chandra and ground-based surveys, there is a continuum of scales and environments in which star formation happens, ranging from relative isolation to the densest regions in Giant Molecular Clouds (GMCs). This view is backed up by the analysis of hierarchical structures and substructures, and favours a scale-free fragmentation and formation process.

Is the stellar Initial Mass Function the same in clusters and in the field? According to Jorge Melnick, there is no evidence to assume the contrary (e.g., a top-heavy IMF), based on careful analysis of the stellar masses in several young massive clusters. Another, often controversial,

The participants at the ESO/Vitacura conference on “Star Formation across the Milky Way Galaxy” assembled on the lawn.



aspect of star formation in clusters is early mass segregation as expected from N-body models, and Joana Ascenso cautioned against an interpretation without careful consideration of the low-number statistics at the high-mass end. Mark Gieles examined the short, but dramatic, phase when expulsion of natal gas from clusters results in “infant mortality”. Hans Zinnecker reminded us that probably up to half of all stars in the Milky Way form in open clusters.

Stellar populations towards the inner bulge and bar were reviewed by Fred Schuller (as seen through ISO, Spitzer, and APEX), and Livia Origlia (through characterisation by their kinematical, chemical and evolutionary properties, mainly from near-infrared spectroscopy). Towards the Galactic Centre a some-

what surprisingly high star-forming efficiency and rate are found, as evidenced either by the strong X-ray emission (Sergei Nayakshin), or by the apparent over-abundance of many young O stars in the immediate surroundings of the massive black hole at the centre of our Galaxy (Andrea Stolte), which seems to bias the IMF in this environment.

Francesco Palla concluded and summarised the workshop with an excellent ‘postlude’. With our current understanding, the ‘problem’ of star formation is probably not solved. There is a bewildering diversity of star-forming regions, and a continuum of star formation from isolation to dense clustering, on many scales, and no single theory may be able to catch and explain all relevant processes. It remains also to be seen if global scal-

ing relations, such as the relation of gas densities with star-formation rates known from other galaxies, hold in the Milky Way.

Coffee breaks including ample snacks, well-organised poster exhibitions, and delicious cocktails in the garden of our Vitacura office contributed to the friendly and stimulating atmosphere of this workshop. The conference dinner in the vineyard *Casa del Bosque* will remain a memorable event for many participants. Many thanks to Maria-Eugenia Gomez and her team who, once again, managed flawless and efficient local organisation for more than 100 guests. We are all looking forward to next year’s ESO workshop hosted in our ESO-Chile ‘science headquarters’!

Announcement of the

ESO Workshop on Large Programmes

13–15 October 2008, Garching, Germany

Over the first ten years of science operations of the VLT, 15 % of the science time has been devoted to the execution of Large Programmes. In May 2003, ESO organised a Large Programmes workshop to obtain a first assessment of the scientific return of Large Programmes. In agreement with its Observing Programmes Committee (OPC), ESO is planning a further overview of the scientific results achieved through Large Programmes conducted at the La Silla Paranal Observatory. To this effect, ESO is organising a three-day workshop in Garching.

The workshop will feature scientific presentations of all Large Programmes that have been completed since the May 2003 workshop. The teams of investigators in charge of these Large Programmes will be invited to present their scientific results, and the impact that their project has had on its particular field.

The presentations will be followed by a discussion session on the general scientific impact of ESO facilities.

One of the outcomes of the May 2003 Large Programme workshop was a suggestion that ESO store the legacy data products of Large Programmes in its science archive. This suggestion was implemented with the requirement that Large Programmes that started after 1 April 2005 deliver Advanced Data Products (ADP) to the ESO archive at the time of publication of their results in a refereed journal. The workshop will also feature a presentation of the ADP submission process and a discussion of its value to the ESO scientific community.

For further details of the workshop, please refer to <http://www.eso.org/sci/meetings/LP2008/>, where the registration form can also be found. The registration deadline is 15 July 2008.

Photo: H. H. Heyer, ESO



“Science with the E-ELT” at JENAM 2008

8–12 September 2008, Vienna, Austria

The next Joint European Astronomy Meeting and National Astronomy Meeting (JENAM) will be held on 8–12 September 2008 in Vienna (Austria). Its unifying theme is to explore the “New Challenges to European Astronomy”. In that framework, ESO and Opticon are jointly organising one of the nine JENAM 2008 topical Symposia, viz. Symposium #1 on “Science with the E-ELT”.

This Symposium is a timely opportunity to discuss and assess the main science goals of a major potential ground-based

observing facility for European Astronomy, the European Extremely Large Telescope (E-ELT) project, which is now in the midst of its three-year (2007–2009) detailed design study and due for decision to build by early 2010. Prime motivations are to inform the community on the scientific perspectives opened up by such a facility and, especially, to gather feedback on the science goals and requirements needed to help make the E-ELT the best possible scientific tool for European astronomy in the next decades.

Input from the community is eagerly sought on every aspect of such a facility: scientific impact, including in synergy with other major observatories on ground and in space; technical and operational requirements to get maximum science value. To participate to the Symposium, you just need to register for the main JENAM event at <http://www.univie.ac.at/jenam2008/>. Your contribution to the debate will be invaluable to help steer the project to the future needs of European astronomers.

Fellows at ESO



Michelle Doherty

My interest in Astronomy began in the final years of high school and continued throughout my undergraduate studies in physics at the University of Sydney. I wrote my final Honours thesis in astronomy and subsequently moved to England to pursue a PhD at the Institute of Astronomy, Cambridge. There I worked with the instrument CIRPASS (Cambridge Infra-Red Panoramic Survey Spectrograph), developing an interest in near-infrared spectroscopy and, in particular, fibre-fed spectroscopy.

During my doctorate I worked on projects related to the star-formation rates of distant galaxies (at redshift $z \sim 1$) and the nature of extremely red galaxies at high redshift. After receiving my PhD in 2005 I moved to ESO Garching to take up a fellowship. For my duties I chose to be involved in science operations at Paranal, travelling out to Chile once every three

months. I very much like the practical side of the job, i.e. being involved in the operations of the observatory, and eventually transferred to complete my fellowship in Chile. My scientific research interests have expanded, primarily through new collaborations at ESO, and now include studying massive galaxies at high redshift, clusters of galaxies at high redshift and using planetary nebulae as dynamical tracers in nearby clusters of galaxies.



Rachel Gilmour

Unlike many astronomers, as a teenager I was not at all interested in astronomy, particularly the practical sort that involved standing in the cold drizzle waiting for a gap in the clouds! However, whilst studying physics at university I found myself in the astronomy building at midnight on a Friday, and realised that I was hooked. After completing my Masters project at Oxford looking for gravitational lenses,

and taking a year out, I started a PhD at the Royal Observatory in Edinburgh investigating X-ray detected AGN in galaxy clusters.

Although I mainly worked with X-ray data for my research, the highlights of my PhD were the occasional trips to ‘real’ observatories in Chile and La Palma. After surviving, and enjoying, the exhausting experience of a five-night run on the INT in January, I was keen to work at an observatory. This fitted well with my scientific aims of obtaining optical data for my X-ray sources, as well as my desire to work in a different culture, so I accepted an ESO fellowship in 2005.

I have found the experience of working at Paranal both challenging and enjoyable. Being part of a large team, with problems to be solved in real time, is quite different from my research life back in Santiago. It has been interesting to learn about so many different observing techniques, and the buzz of the observatory means that there is always something new going on. I particularly enjoy the opportunities to meet scientists with many different specialities, and to observe the whole spectrum of (optical) astronomical objects, from planets to gamma-ray bursts. I plan to expand on these interests in the forth year of my fellowship, when I hope to go to a UK institute to continue my research and to learn more about communicating astronomy with the public.



ESO

European Organisation
for Astronomical
Research in the
Southern Hemisphere



ESO Fellowship Programme 2008/2009

The European Organisation for Astronomical Research in the Southern Hemisphere awards several postdoctoral fellowships each year. The goal of these fellowships is to offer outstanding young scientists the opportunities and facilities to enhance their research programmes by promoting close contact between young astronomers and the activities and staff at one of the world's foremost observatories.

With ALMA becoming operational in a few years, ESO offers ALMA fellowships to complement its regular fellowship programme. Applications by young astronomers with expertise in mm/sub-mm astronomy are encouraged.

In *Garching*, the fellowships start with an initial contract of one year followed by a two-year extension (three years total). The fellows spend up to 25% of their time on support or development activities in the area of instrumentation, operations support, archive/virtual observatory, VLT, ALMA, ELT, public affairs or science operations at the Observatory in Chile.

In *Chile*, the fellowships are granted for one year initially with an extension of three additional years (four years total). During the first three years, the fellows are assigned to one of the operation groups on Paranal, La Silla or APEX/ALMA. Fellows contribute to the operations at a level of 80 nights per year at the Observatory and 35 days per year at the Santiago Office. During the fourth year there is no functional work and several options are provided. The fellow may be hosted by a Chilean institution (and will thus have access to all telescopes in Chile via the Chilean observing time). Alternatively, she/he may choose to spend the fourth year either at ESO's Astronomy Centre in Santiago, or at the ESO Headquarters in Garching, or at any institute of astronomy/astrophysics in an ESO member state.

In addition to pursuing independent research, all fellows have ample opportunities for scientific collaboration within ESO, both in Garching and Santiago. For more information about ESO's astronomical research activities and available projects open for collaborations to fellows please consult <http://www.eso.org/sci/activities/ESOfellowship.html>. A list of current ESO staff and fellows and their research interests can be found at <http://www.eso.org/sci/activities/personnel.html>. Additionally, the ESO Headquarters in Munich, Germany, is situated in the immediate neighbourhood of the Max-

Planck Institutes for Astrophysics and for Extraterrestrial Physics and only a few kilometres away from the Observatory of the Ludwig-Maximilian University. ESO is participating in the newly formed Excellence Cluster on astrophysics on the Garching Campus. In Chile, fellows have the opportunity to collaborate with the rapidly expanding Chilean astronomical community in a growing partnership.

We offer an attractive remuneration package including a competitive salary (tax-free), comprehensive social benefits, and provide financial support for relocating families. Furthermore, an expatriation allowance as well as some other allowances may be added. The outline of the terms of service for fellows (<http://www.eso.org/public/employment/fellows.html>) provides some more details on employment conditions/benefits.

Candidates will be notified of the results of the selection process between December 2008 and February 2009. Fellowships begin between April and October of the year in which they are awarded. Selected fellows can join ESO only after having completed their doctorate.

The closing date for applications is 15 October 2008.

Please apply by filling the web form available at the recruitment page <http://jobs.eso.org> attaching to your application (preferred format is PDF):

- your Curriculum Vitae including a list of (refereed) publications
- your proposed research plan (maximum two pages)
- a brief outline of your technical/observational experience (maximum one page)

In addition three letters of reference from persons familiar with your scientific work should be sent directly to ESO to vacancy@eso.org by the application deadline.

Please also read our list of FAQs at <http://www.eso.org/sci/activities/ESOfellowship-faq.html> regarding fellowship applications.

Questions not answered by the above FAQ page can be sent to: Marina Rejkuba, Tel +49 89 320 06-4 53, Fax +49 89 320 06-4 80, e-mail: mrejkuba@eso.org



New Staff at ESO



Gerard Van Belle

I joined ESO in September 2007 as the PRIMA Instrument Scientist for the VLTI. Over the years I have had the distinct pleasure to work with a variety of excellent teams on a number of optical interferometry projects, and it seemed a natural step forward to accept an offer to join the PRIMA group in Garching. Previously I had worked on the Keck Interferometer as an instrument architect, and observed extensively with the Palomar Testbed Interferometer, the CHARA Array and the IOTA Array, so joining ESO in this capacity is a welcome new challenge.

PRIMA to me represents the final, full flowering of the first generation of VLTI instruments, and has a real opportunity to showcase the truly unique capabilities – and discoveries – possible only with interferometry. The PRIMA team members, both inside and outside ESO, have been working hard on the project for many years, and I feel a little spoiled join-

ing this talented, friendly group so close to the beginning of commissioning observations, which will take place towards the end of the year. Taming the many and subtle aspects of this facility will be a demanding task, but I expect it to be rewarding in equal measure as we use its unprecedented angular resolution to catch unmatched glimpses of nearby worlds.

The additional challenge of leaving the US West Coast and moving my whole family to lovely Bavaria has presented some unique hurdles, but we are thrilled to have the opportunity to enjoy life in Munich and the surrounding areas in a way that is much more intimate than a tourist sees. Such a big move is always bound to have its painful moments, but we have found no shortage of new friends at ESO and in our new neighbourhood that have helped smooth the transition. My family and I thank all those in Garching and Neufahrn who have been so hospitable to us.

Bodo Ziegler

Since last December I have been enjoying the scientific environment, the instrumental expertise and the cooperative spirit of colleagues at ESO as a new member of the User Support Department. I support programmes conducting observations with the FORS1 and FORS2 spectrographs in all modes (IMG, HIT, LSS, MOS, PMOS, MXU) and with the recently commissioned HAWK-I near-infrared camera. Being the link between users from the general astronomical community and ESO Paranal staff, I try to maximise the scientific return of observing runs for the given instrumental and technical feasibility. Other tasks are related to the ESO survey team that is responsible for an efficient implementation and execution of the public large-scale surveys to be conducted at the new survey telescopes VST and VISTA.

Before joining ESO I was the head of a Junior Research Group supported by the Volkswagen Foundation at the University of Göttingen for almost seven years and temporary professor at the University of Bonn for half a year. Having spent much of my time on administrative issues,

education of students and faculty boards, I now enjoy being closer to instrumentation and observational issues. For me there is a very fruitful interplay between excellent science and expert knowledge of instruments. Most of my research projects focus on galaxy formation and evolution within a cosmological context. The projects provide strong constraints for models like the cold dark matter (CDM) based hierarchical build-up of cosmic structure by measuring the mass evolution, star-formation history and chemical enrichment of galaxies. The observations are mainly achieved with optical spectroscopy, using ESO's very efficient instruments, of distant galaxies out to redshift unity, combined with deep optical/NIR photometry and spatially highly-resolved Hubble Space Telescope imaging. For the interpretation of the results we compare the observational data with N-body/Smoothed Particle Hydrodynamics (SPH) simulations of galaxy evolution considering various interaction phenomena. Targeting not only field galaxies but also groups and clusters, we explore the environmental dependence of galaxy evolution.

Now in the lively community of ESO, I'm looking forward to many fruitful discussions of both scientific and observatory-related issues.



Photo: H. Heyer, ESO

Exploring the Cold Universe – A Planetarium Show for the IYA 2009

Henri Boffin¹
Agnès Acker^{2,3}

¹ ESO

² Observatoire de Strasbourg, France

³ Association des Planétariums
de Langue Française (APLF)

A planetarium show highlighting the ALMA project is being jointly prepared by ESO and the *Association des Planétariums de Langue Française*.

As part of a wide range of education and public outreach activities for the International Year of Astronomy 2009 (IYA 2009), ESO is collaborating with the *Association des Planétariums de Langue Française* (APLF, the association of French-speaking planetaria) and other partners in Europe to produce a new 30-minute long planetarium show centred on the ALMA project.

This show builds on the experience already gained by the APLF to produce unique planetarium shows at the European level. The APLF, born in 1984 but officially created in 1989, coordinates the operations of about 50 French planetaria

with a total annual visitorship of about 1.3 million. As member of the International Planetarium Society, the APLF has also established close links with planetaria from many other countries.

In 2001, the APLF, in collaboration with the French space agency CNES, produced a show about the Earth seen from space. In 2002, in collaboration with ESO, a very successful show was produced for the 40th anniversary of ESO, entitled “Mysteries of the Southern Sky”, celebrating the performance of the VLT. In both cases, the shows were presented in around 40 planetaria in France, Germany, Belgium, Italy, and Spain and other countries.

About 30 planetaria in several countries have already agreed to present the new show which will be available for viewing from autumn 2008 – in order to be included in school programmes – and officially inaugurated early in 2009. It is a unique chance for planetaria to be directly involved with the IYA 2009.

A fruitful collaboration

The emphasis of the new planetarium show is the incomparable scientific en-

deavour that the ALMA project represents. The unique setting of ALMA in the Atacama Desert at an altitude of 5 000 m is also emphasised, as well as the difficulty of building something in such a remote, inhospitable place. An astronomer will act as the primary guide through the show. The aim is to have a spectacle that is attractive to all members of the public, from young to old.

ESO provides the scientific expertise, validates the story-board, supplies images, computer simulations and videos, and financially supports the project. ESO will also produce a Chilean version and help provide associated documents for visitors. The APLF will make the story-board, produce the show in five languages, and is responsible for the promotion, duplication and distribution both in France and in Europe.

The show shall be available in three different formats: full dome video; All-Sky projection and video windows; image projection and video windows for smaller planetaria. It will be available to all planetaria worldwide for a very small fee, dependent on the type of planetarium, to cover basic costs.

Photo: H. H. Heyer, 3D Computer Rendering; L. Calcada and H. Zodet (all ESO)



Left: A photograph of the Chajnantor plateau with superposed 3D computer rendering of some ALMA antennas as they might appear when ALMA is operational.

Right: A view towards the VLT and the summit of Cerro Paranal with the VISTA dome in the foreground.

Personnel Movements

Arrivals (1 April–30 June 2008)

Europe	
Biggs, Andrew (GB)	Astronomer
Brucker, Cordula (D)	Secretary/Assistant
Checucci, Alessio (I)	Software Engineer
Forchi, Vincenzo (I)	Software Engineer
Galametz, Audrey (F)	Student
Heymann, Frank (D)	Student
Jalali, Behrang (IR)	Student
Kern, Lothar (D)	Electrical/Electronics Engineer
Larsen, Jonas (DK)	Software Engineer
Lilley, Paul (GB)	Electronic Engineer
Rose, Elke (D)	Secretary
Yagoubov, Pavel (NL)	System Engineer
Chile	
Ahumada, Andrea Veronica (RA)	Fellow
Bourget, Pierre (F)	Instrumentation Engineer
Caceres, Francisco (RCH)	Telescope Instruments Operator
de Graauw, Mattheus Thijs (NL)	ALMA Director (Interim)
Gallegos, Leonardo (RCH)	Telescope Instruments Operator
Kuo, Caterina (RCH)	Procurement Clerk
Ma, Qiao Yun (RCH)	Accountant
Merand, Antoine (F)	Operations Astronomer
O'Neal, Jared (USA)	Instrumentation Engineer
Reinero, Claudio (RCH)	Software Engineer
Rivas, Leonel (RCH)	Telescope Instruments Operator
Romero, Cristian (RCH)	Telescope Instruments Operator
Slusarenko, Nicolas (RCH)	Software Engineer

Departures (1 April–30 June 2008)

Europe	
Dolensky, Markus (A)	Software Engineer
Kotzlowski, Heinz E. (D)	Mechanical Engineer
Madrid Pariente, Silvia (E)	Secretary/Assistant
Muradore, Riccardo (I)	System Engineer
Pedicelli, Silvia (I)	Student
Teimoorinia, Hossein (IR)	Student
Wallander, Anders (S)	Software Engineer
Chile	
Duran, Domingo (RCH)	Electrical Assistant
Gardiazabal, Jose (RCH)	Software Engineer
Herrera, Leonardo (RCH)	Electronic Engineer
Jimenez, Jorge (RCH)	Instrument Technician
Reveret, Vincent (F)	Operations Astronomer
Robinson, William (RCH)	Mechanical Engineer
Salinas, Alejandro (RCH)	Network Specialist
Vanzi, Leonardo (I)	Operations Astronomer

Photo: H. H. Heyer, ESO



ESO is the European Organisation for Astronomical Research in the Southern Hemisphere. Whilst the Headquarters (comprising the scientific, technical and administrative centre of the organisation) are located in Garching near Munich, Germany, ESO operates three observational sites in the Chilean Atacama desert. The Very Large Telescope (VLT), is located on Paranal, a 2 600 m high mountain south of Antofagasta. At La Silla, 600 km north of Santiago de Chile at 2 400 m altitude, ESO operates several medium-sized optical telescopes. The third site is the 5 000 m high Llano de Chajnantor, near San Pedro de Atacama. Here a new submillimetre telescope (APEX) is in operation, and a giant array of 12-m submillimetre antennas (ALMA) is under development. Over 2 000 proposals are made each year for the use of the ESO telescopes.

The ESO Messenger is published four times a year: normally in March, June, September and December. ESO also publishes Conference Proceedings and other material connected to its activities. Press Releases inform the media about particular events. For further information, contact the ESO Public Affairs Department at the following address:

ESO Headquarters
Karl-Schwarzschild-Straße 2
85748 Garching bei München
Germany
Phone +49 89 320 06-0
Fax +49 89 320 23 62
information@eso.org
www.eso.org

The ESO Messenger:
Editor: Jeremy R. Walsh
Technical editor: Jutta Boxheimer
Technical assistant: Mafalda Martins
www.eso.org/messenger/

Printed by
Peschke Druck
Schatzbogen 35
81805 München
Germany

© ESO 2008
ISSN 0722-6691

Contents

The Organisation

T. de Zeeuw – The Perfect Machine	2
10th Anniversary of First Light of the VLT	4
Austria Declares Intent to Join ESO	5

Telescopes and Instrumentation

M. Kissler-Patig et al. – Hawk-I – First Results from Science Verification	7
M. Sarazin et al. – Seeing is Believing: New Facts about the Evolution of Seeing on Paranal	11
C. Snodgrass et al. – EFOSC2 Episode IV: A New Hope	18
I. Saviane, L. Monaco – Two Volume-phased Holographic Grisms Now Available for EFOSC2	20
M. Kraus et al. – The ALMA Antenna Transporter	23
R. Laing – Recent Progress at the ALMA Test Facility	28
H. Vázquez Ramió et al. – Cute-SCIDAR at Paranal for E-ELT Site Characterisation	29

Astronomical Science

D. Reimers et al. – The Antares Emission Nebula and Mass Loss of α Sco A	33
M. Matsuura et al. – SINFONI Observations of Comet-shaped Knots in the Planetary Nebula NGC 7293 (the Helix Nebula)	37
M. G. Haehnelt et al. – Hunting for the Building Blocks of Galaxies like our own Milky Way with FORS	41

Astronomical News

N. Delmotte – News from the ESO Science Archive Facility	47
R. Gilmozzi, G. Monnet, M. Robinson – FP7 E-ELT Preparation – Grant Agreement Funded by the European Commission is Underway	48
M. Sterzik, J. Melnick, C. Melo – Report on the International Workshop on Star Formation Across the Milky Way Galaxy	49
Announcement of the ESO Workshop on Large Programmes	50
Announcement of the Topical Symposium “Science with the E-ELT” at JENAM 2008	51
Fellows at ESO – M. Doherty, R. Gilmour	51
ESO Fellowship Programme 2008/2009	52
New Staff at ESO – G. Van Belle, B. Ziegler	53
H. Boffin, A. Acker – Exploring the Cold Universe – A Planetarium Show for the IYA 2009	54
Personnel Movements	55

Front Cover Picture: Ten years since VLT First Light: a view of Paranal and the Galactic Plane before sunrise. Photograph by Hans Hermann Heyer (ESO).